Biosynthesis of the Nitrogenase FeMo-cofactor from *Azotobacter vinelandii*: Involvement of the NifEN complex, NifX and the Fe protein

By

Paul J. Goodwin

Dissertation submitted to the faculty of the Virginia Polytechnic Institute and State University in partial fulfillment of the requirements for the degreee of

Doctor of Philosophy

In

Biochemistry

D.R. Dean, Chairman
D.R. Bevan
J.S. Chen
G.W. Claus
W.E. Newton

May 20, 1999
Blacksburg, VA

Biosynthesis of the Nitrogenase FeMo-cofactor from *Azotobacter vinelandii*: Involvement of the NifEN complex, NifX and the Fe protein

By

Paul J. Goodwin

ABSTRACT

The iron-molybdenum cofactor (FeMo-cofactor) of nitrogenase is the subject of one the most intensive biochemical/genetic detective cases of modern science. At the active site of nitrogenase, the FeMo-cofactor not only represents the heart of biological nitrogen fixation, but its synthesis also serves as a model for complex metallocluster biosynthesis. Research in the Dean Lab is focused on furthering the understanding of Fe-S cluster biosynthesis in the nitrogenase enzyme system.

Throughout the years, scientists from a broad range of disciplines have focused their intellectual might on deciphering not only the chemistry of the FeMo-cofactor, but also the biosynthesis of this unique metallocluster. Recent advances in the study of FeMo-cofactor biosynthesis have produced considerable insight regarding the complex series of biological reactions necessary for the synthesis of this metallocluster. The work contained within this dissertation represents my efforts to further the understanding of FeMo-cofactor biosynthesis.

The concept of a molecular scaffold in FeMo-cofactor biosynthesis is generally accepted in the field of nitrogenase. Previous work has implicated the products of *nif*E and *nif*N as providing the assembly site for FeMo-cofactor synthesis. Researchers were able to purify this molecular scaffold, commonly referred to as the NifEN complex,

however, detailed characterization was precluded by the inability to obtain sufficient quantities of NifEN. In an effort to fully characterize the NifEN complex, we initiated a gene fusion approach for the high level production NifEN. In addition to gene fusion, a poly-histidine tag was incorporated into NifEN, allowing purification through the application of immobilized metal-affinity chromatography (IMAC). NifEN obtained in this way was characterized using a variety of biophysical techniques and found to contain two [4Fe-4S] clusters in each NifEN tetramer. These clusters were also shown to be completely ligated by cysteine residues. With the information obtained from this study, it is concluded that the [4Fe-4S] clusters of the NifEN complex are likely to play either a structural or a redox role rather than being transferred and becoming incorporated into the FeMo-cofactor.

In addition to the biophysical characterization of the NifEN complex, a separate study was started to characterize the apo-MoFe protein. In this study we used IMAC to purify a poly-histidine-tagged apo-MoFe protein produced by a *nif*B-deletion mutant of *A. vinelandii*. Using the poly-histidine fusion approach, apo-MoFe protein was obtained in sufficient quantities for detailed catalytic, kinetic and spectroscopic analyses. This multidisciplinary approach confirmed that apo-MoFe protein contained intact P clusters and P cluster environments, as well as the ability to interact with the Fe protein. It was also shown for the first time that this tetrameric form of purified apo-MoFe protein could be activated by the addition of preformed FeMo-cofactor.

The NifEN complex was further characterized to investigate the presence of bound FeMo-cofactor intermediates. NifEN purified by IMAC is produced in the absence of the nitrogenase structural genes (*nif*HDK). In this genetic background, it is

believed that the FeMo-cofactor biosynthetic machinery will become obstructed with unprocessed FeMo-cofactor intermediates, such as the Fe-S precursors of FeMo-cofactor, NifB-cofactor. Previous work indicated that NifEN can exist in either a charged or discharged form, based on the presence or absence of the FeMo-cofactor precursor, NifB-cofactor. EPR and VTMCD spectroscopies showed the presence of a new paramagnetic signal associated with NifEN that is believed to be in the charged or precursor bound state. This represents the first spectroscopic evidence for a precursor to the FeMo-cofactor. Furthermore, an interaction of NifEN and NifX was examined by size exclusion chromatography. From this study, NifX exhibited the capacity to bind a chromophore, presumably an FeMo-cofactor precursor, from the NifEN complex. NifX was also capable of binding to isolated FeMo-cofactor and the FeMo-cofactor precursor, NifB-cofactor.

Finally, preliminary investigations involving interaction between the Fe protein and NifEN were initiated. Recent findings indicate that NifEN and the Fe protein have the capacity to interact specifically with one another. The interaction of NifEN and Fe protein appears to be dependent on the association of FeMo-cofactor precursor with NifEN. The NifEN complex also has the capacity to accept electrons from the Fe protein in a MgATP dependent manner. The ability of NifEN to accept electrons from the Fe protein may be involved in the role of Fe protein in FeMo-cofactor biosynthesis.

ACKNOWLEDGMENTS

I like to first thank Prof. Dennis R. Dean for giving me the opportunity to work in his laboratory. He has not only been a mentor in my scientific training but also a friend through the rough times of my career. Dennis was never afraid to be honest with me and for that I am thankful.

My sincere gratitude is also extended to the past and present members of Prof. Dean's research group, Dr. Jason Christiansen, Dr. Limin Zheng, Dr. Richard Jack, Prof. John Peters, Valerie Cash, Len Comaratta, Pramvadee Yuvaniyama and Amr Ragab. I thank you all for your assistance, friendship and patience throughout my years at Virginia Tech.

I also thank individuals with whom I have collaborated with during the course of my graduate studies. Prof. Michael K. Johnson and Jeff Agar at the University of Georgia have been fundamental in my understanding of biophysical characterization of metalloenzymes. Prof. Paul W. Ludden, Prof. Gary P. Roberts, Dr. Vinod Shah, and Dr. Jon T. Roll at the University of Wisconsin for their aid with biosynthetic assay development. I also thank Prof. Lance C. Seefeldt and Dr. William N. Lanzilotta for their assistance and helpful comments.

Dr. David Bevan, Dr. J.S. Chen, Dr. G. William Claus and Dr. William Newton have been very gracious and helpful committee members. I have often benefited from their knowledge and guidance.

My family has been there for me throughout my life. I take this opportunity to thank them for their kind support and encouragement, especially my father, Paul, my mother, Geraldine, and my brother, Justin. Thank you.

And last, but certainly not least, I thank my wife Nicole. I do not have enough room in this dissertation to begin to scratch the surface of what Nicole has done for me. She has been there for me at everyome of life's turns, whether good or bad. You are my best and dearest friend, and without you I would never have gotten this far. With love, I thank you.

TABLE OF CONTENTS

LIST OF ILLUSTRATIONS

LIST OF TABLES

ABBREVIATIONS

ADP	Adenosine 5^1 diphosphate
ATP	Adenosine 5^1 triphosphate
DEAE	Diethylaminoethyl cellulose
DTT	Dithiothreitol
ΔL127	Deletion of amino acid leucine 127
EDTA	Ethylene diamine tetraacetic acid
EPR	Electron paramagnetic resonance spectroscopy
FeMo-cofactor	Iron molybdenum cofactor
G	Gauss
GHz	Gigahertz
HEPES	N-[2-Hydroxylethyl]piperazine-N^1-[2-ethanesulfonic acid]
HPLC	High performance liquid chromatography
I-AEDANS	N-iodoacetyl-N^1-[5-sulfo-1-naphtyl]ethylenediamine
IDS	Indigo disulfonate
IMAC	Immobilized metal-affinity chromatography
k	Rate constant
K	Kelvin
kD	Kilodalton(s)
K_m	Michaelis Menten constant
Km^r	Kanamycin resistance
k_{obs}	Observed rate constant
MgADP	Magnesium adenosine 5^1 diphosphate

MgATP	Magnesium adenosine 5^1 triphosphate
M_r	Relative molecular mass
mV	Millivolt(s)
mW	Milliwatts(s)
nif	Nitrogen fixation gene
NHE	Normal hydrogen electrode
NifB-cofactor	Fe/S precursor of the FeMo-cofactor
Nif^-	Inability to grow on N_2
Nif^+	Ability to grow on N_2; diazotrophic growth
Nif^{slow}	Slow growth on N_2
NMF	N-methylformamide
PAGE	Polyacrylamide gel electrophoresis
P_I	Inorganic phosphate
PMSF	Phenylmethyl sulfonyl fluoride
P cluster	[8Fe-7S] cluster of the molybdenum-iron protein
P^N	P cluster in the as-isolated all-ferrous state
P^{1+}	P cluster that is oxidized by one electron relative to the P^N state
P^{2+}	P cluster that is oxidized by two electrons relative to the P^N state
RR	Resonance Raman
S	Electron paramagnetic spin state
SDS	Sodium dodecyl sulfate

T	Tesla
Tris-HCl	Tris (hydroxymethyl) aminomethane hydrochloride
UV	Ultraviolet
Vis	Visible
VTMCD	Variable-temperature magnetic circular dichroism

LITERATURE REVIEW

Introduction

The reduction of dinitrogen gas (N_2) to ammonia (NH_3) is called nitrogen fixation. Because ammonia is necessary for the formation of biologically essential, nitrogen-containing compounds, such as amino acids and nucleic acids, the availability of a source of "fixed" nitrogen is therefore necessary to sustain life on earth. Also, because ammonia that is necessary to support essential biosynthetic reactions is continually sequestered into sediments or is reconverted to N_2 through the combined biological processes of nitrification and denitrification, the pool of fixed nitrogen within the biosphere must be constantly replenished. Nitrogen fixation is necessary to maintain the diversity of life on earth because most organisms cannot metabolize the abundant, but relatively inert, N_2 molecule, but must assimilate nitrogen in a "fixed" form, such as ammonia or nitrate (NO_3^-). The three ways that nitrogen fixation occurs in the biosphere are: (i) lightning and natural combustion processes, (ii) the industrial Haber-Bosch process, and (iii) biological nitrogen fixation. Of these three, biological nitrogen fixation is the most significant contributor accounting for about 65% of the total annual fixation [1, 2].

Although most organisms cannot fix nitrogen there is a select group of microorganisms that can. These organisms are called diazotrophs, a term which means "nitrogen eaters", and they are widely distributed among, but restricted to, the Archaea and Eubacterial kingdoms. Examples of bacterial species that fix nitrogen and that have been extensively studied include *Azotobacter vinelandii* (an obligate aerobe), *Clostridium pasteurianum* (an obligate anaerobe), *Klebsiella pneumoniae* (a facultative anaerobe), *Rhodospirillum rubrum* (a photosynthetic bacterium), *Anabaena sp.* 7120 (a heterocyst forming cyanobacterium) and *Bradyrhizobium japonicum* (a symbiotic bacterium). Despite the differing physiological conditions in which

these various diazotrophs have evolved, almost all organisms examined contain the molybdenum (Mo) dependent nitrogenase encoded by the nitrogen fixation (*nif*) regulon. There is, however, another class of nitrogenases that do not contain Mo and these have been designated alternative nitrogenases [3, 4]. Two types of alternative nitrogenases have been identified thus far, the vanadium (V) dependent and the iron (Fe) dependent systems. Also, a recent report has identified the existence of a Mo-dependent nitrogenase from *Streptomyces thermoautotrophicus* that is unlike any Mo-dependent system studies so far [5].

Nitrogenase

Biological nitrogen fixation involves the reduction of atmospheric dinitrogen (N_2) to ammonia (NH_3) by the metalloenzyme nitrogenase [6, 7]. The minimal stoichiometry of the nitrogenase-catalyzed reaction is typically depicted as:

$$N_2 + 8H^+ + 8e^- + 16MgATP \Rightarrow 2NH_3 + H_2 + 16MgADP + 16Pi$$

Nitrogenase is a complex metalloenzyme composed of two component proteins, shown in Figure 1. The individual nitrogenase component proteins have been designated as the iron (Fe) protein and the molybdenum-iron (MoFe) protein; names derived from the complement of metal atoms within the individual proteins. The Fe protein is a γ_2 homodimer ($M_r \approx 64{,}000$; encoded by *nif*H) that contains two MgATP binding sites and a single [4Fe-4S] cluster [8, 9]. The MoFe protein is an $\alpha_2\beta_2$ heterotetramer ($M_r \approx 250{,}000$; encoded by *nif*D and *nif*K) that contains two pairs of metalloclusters, called P-clusters and iron-molybdenum cofactors (FeMo-cofactors) [10-12]. The Fe protein serves as the obligate electron donor to the MoFe protein, which in turn harbors the site of substrate binding and reduction. During catalysis, the Fe protein transfers electrons, one at a time, to the MoFe protein in a process that involves component protein

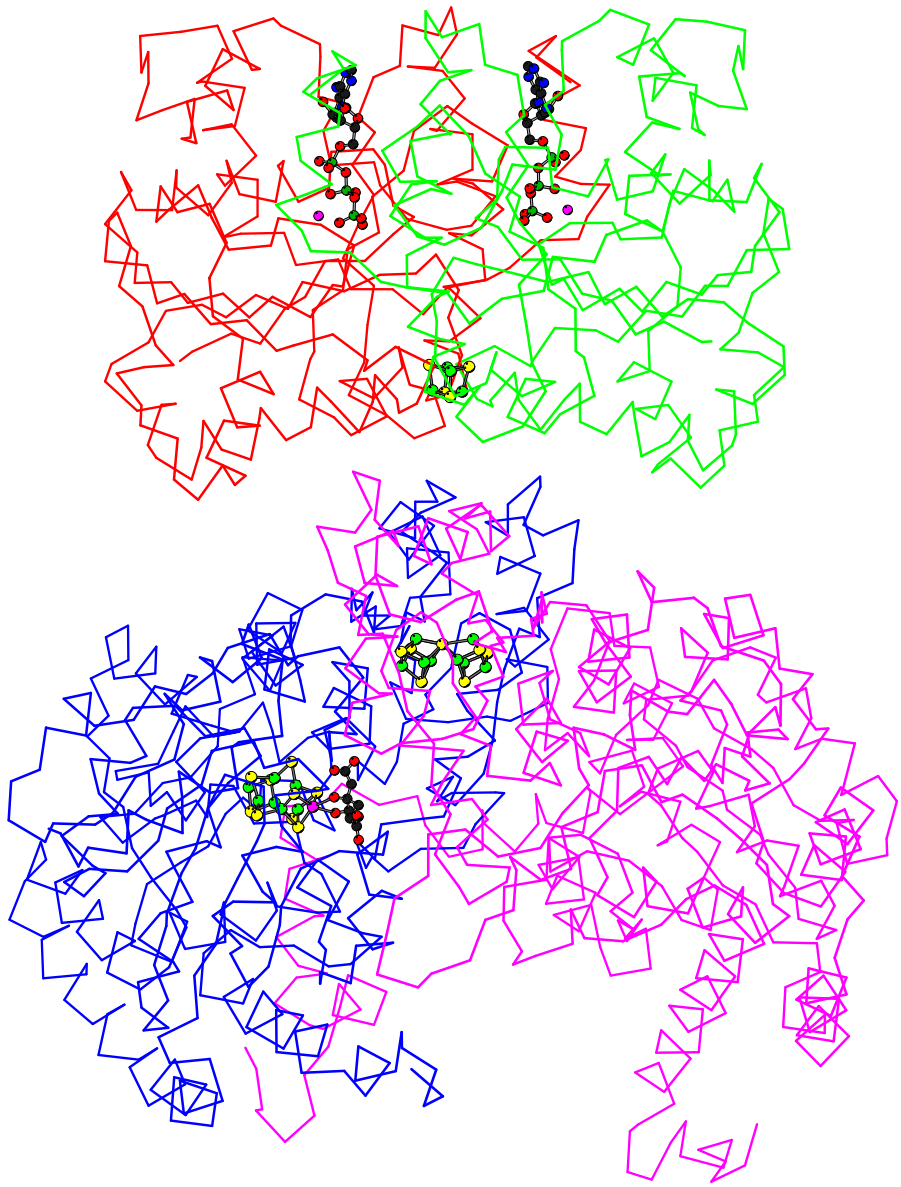

Figure 1. Wireframe diagram of the three-dimensional structures of the nitrogenase Fe protein and the MoFe protein. The view shows the MgATP bound Fe protein (top) poised for interaction with a single αβ-unit of the MoFe protein.

association and dissociation and the hydrolysis of MgATP. Because the Fe protein serves as a specific reductant of the MoFe protein, which in turn provides the site of substrate reduction, some investigators refer to the Fe protein as dinitrogenase reductase and the MoFe protein as dinitrogenase [13]. The work described within this dissertation involves the study of nitrogenase from *A. vinelandii*, particularly the biosynthesis of the FeMo-cofactor. The following sections will introduce both the Fe protein and the MoFe protein, describing key structural and functional aspects of these nitrogenase component proteins. Additional sections will discuss nitrogenase catalysis and substrate reduction, protein-protein interaction between the Fe protein and the MoFe protein and finally the maturation of the nitrogenase component proteins.

Fe Protein The crystallographic model of the Fe protein from *A. vinelandii* has been determined to 2.9 angstrom resolution [9]. A wireframe diagram of the Fe protein is shown in Figure 1. The [4Fe-4S] cluster of the Fe protein (Figure 2) is ligated by four cysteine residues, two from each subunit (Cys-97; Cys-132), and is bridged in the cleft between the two subunits of the homodimer [9, 14]. The nucleotide binding sites within the Fe protein are defined by two nucleotide-binding consensus motifs, the Walker A-type and the Walker B-type [15, 16]. Each subunit of the Fe protein contains a pair of these binding motifs and has the ability to bind a molecule of MgATP [16].

To serve its function in nitrogenase catalysis, the Fe protein must be able to integrate nucleotide binding and MgATP hydrolysis with electron transfer to the MoFe protein. Both cluster binding and nucleotide binding are located at the interface between the two subunits of the Fe protein dimer. The [4Fe-4S] cluster and the nucleotide binding sites are separated by a span of approximately 20 Å [9]. Upon binding of MgATP, the Fe protein undergoes a

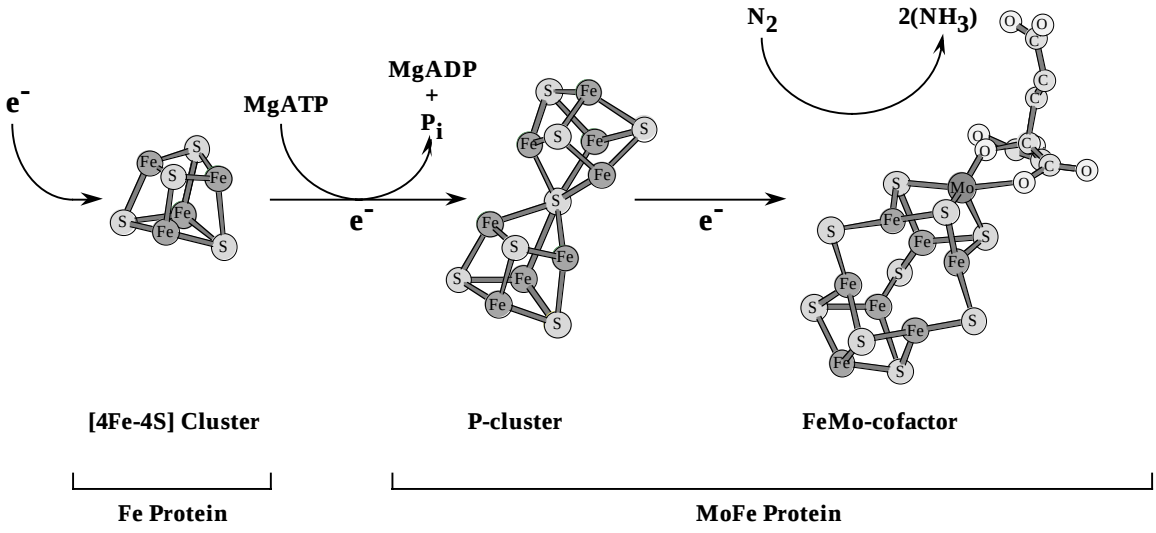

Figure 2. Organization and structures of the nitrogenase metalloclusters. The path of electrons is most likely from the [4Fe-4S] cluster of the Fe protein to the MoFe protein's P cluster and then to the FeMo-cofactor. Transfer of an electron from the Fe protein to the MoFe protein is coupled to MgATP hydrolysis. The FeMo-cofactor provides the N_2 binding and reduction site.

conformational change that results in a number of changes in the [4Fe-4S] cluster. This separation of the cluster and the nucleotide binding site suggests that the changes are not associated with direct interaction of nucleotide and cluster, but rather transmission of a structural signal through polypeptide conformational change. Changes associated with the binding of MgATP to the Fe protein include: (i) increased solvent exposure of the cluster, resulting in an increased susceptibility to Fe-specific chelators [17], (ii) a lowering of the mid-point potential of the cluster [18], and (iii) changes in the line shape of the cluster's characteristic electron paramagnetic resonance (EPR) spectrum [19]. These characteristics of Fe protein in the MgATP bound state are necessary to facilitate electron transfer during nitrogenase turnover. It should be noted that MgADP also induces the mid-point potential drop associated with nucleotide binding [20]. Also, Fe protein with bound MgADP cannot function in electron transfer, which lends to the inhibitory effect that MgADP has on nitrogenase catalysis [21].

The Fe protein also plays a role in the maturation of the MoFe protein [22]. The action of the Fe protein in MoFe protein maturation is discussed later in the section detailing nitrogenase component protein maturation. Also, the Fe protein has an undetermined role in biosynthesis of the FeMo-cofactor of nitrogenase. Investigations on the Fe protein's role in FeMo-cofactor synthesis are examined in Chapter IV of this dissertation.

MoFe Protein The crystallographic model for the MoFe protein was originally solved at 2.7 Å resolution in 1992 [12], and more recently refined to 2.0 Å resolution [23]. Since the MoFe protein tetramer has a two-fold axis of symmetry, it is often viewed as a dimer of $\alpha\beta$ dimers (Figure 1). The overall function of the MoFe protein is to mediate electron transfer from the Fe

protein and to serve as the site of substrate binding and reduction. To perform these tasks, the MoFe protein utilizes two specific metalloclusters, the P cluster and the FeMo-cofactor.

The P cluster functions as an electron mediator between the [4Fe-4S] cluster of the Fe protein and the FeMo-cofactor. The P cluster is located at the αβ interface of the MoFe protein subunits and, in its fully reduced form, is constructed from two [4Fe-4S] sub-clusters that share a central six-coordinate sulfide (Figure 2). Upon oxidation of the P cluster, a structural rearrangement occurs involving movement of two Fe atoms and a change in the ligand arrangement around the cluster [23]. Such redox-dependent structural changes within the P-cluster might be mechanistically related to its role in accepting electrons from the Fe protein and delivering them to the FeMo-cofactor [24]. Several lines of evidence support the P cluster as an intermediate in electron transfer from the Fe protein to the nitrogenase active site FeMo-cofactor. First, site directed mutagenesis in the region between the P cluster and the FeMo-cofactor acts to slow the reduction of substrate [25]. Second, two independent crystallographic models show that the P cluster is between the [4Fe-4S] cluster of the Fe protein and the FeMo-cofactor active site [23, 26]. And third, mutagenesis of the P cluster ligands has implicated that the P cluster has a redox role during nitrogenase turnover [27].

The FeMo-cofactor serves as the active site for nitrogenase. FeMo-cofactor consists of a metal-sulfur framework ($MoFe_7S_9$) and one molecule of (R)-homocitrate (Figure 2) and is located approximately 10Å from the surface of the MoFe protein. FeMo-cofactor is bound to the MoFe protein by α-Cys 275 and α-His 442 [28]. The former serves as a thiolate ligand to an Fe atom at one end of the cofactor, and the latter binds through a side chain nitrogen atom to the Mo atom at the opposite end of the cofactor. Homocitrate is coordinated to the Mo atom through its β-hydroxy and β-carboxy groups and interacts with the protein through a number of direct and

water-bridged hydrogen bonds [28]. There are several lines of evidence that the FeMo-cofactor provides the substrate binding and reduction site. Mutant strains that are unable to synthesize the FeMo-cofactor are also unable to catalyze nitrogen fixation [11]. When isolated FeMo-cofactor is added to crude extracts prepared from such mutant strains the *in vitro* ability to fix nitrogen is restored. Second, a MoFe protein that contains an altered form of the FeMo-cofactor, where citrate replaces homocitrate as its organic constituent, exhibits altered catalytic properties [29, 30]. When this altered FeMo-cofactor containing citrate is used to reconstitute apo-MoFe protein (MoFe protein containing P clusters, but lacking FeMo-cofactor), the same altered catalytic characteristics are exhibited. Finally, altered MoFe proteins that have amino acid substitutions located within FeMo-cofactor's polypeptide environment also exhibit altered catalytic properties [31]. Although it is not yet known how substrates interact with FeMo-cofactor during turnover, the presence of six coordinately unsaturated Fe atoms, as well as the attachment of homocitrate to the Mo atom has invited speculation about the nature of substrate binding [32]. For example, in one model it has been proposed that the carboxylate group coordinated to the Mo atom might serve as a leaving group in a mechanism that activates Mo to provide a substrate coordination site [33].

Nitrogenase Catalysis and Substrate Reduction

In order for nitrogen fixation to occur, the nitrogenase component proteins must be able to interact with one another to facilitate productive electron transfer. For complex formation to take place, the Fe protein must be in the MgATP bound state. Additionally, MgATP hydrolysis and intermolecular electron transfer only takes place in the Fe protein-MoFe protein complex [13, 34]. Early investigations as to the nature of component protein interaction involved the

effect of salt inhibition on nitrogenase activity [35] and chemical crosslinking experiments [36]. After the availability of the crystallographic models of the Fe protein and MoFe protein, a component protein docking model was devised by Howard and Rees [26, 37]. In the Howard-Rees model (Figure 1) the two-fold symmetric surface of the Fe protein that surrounds its [4Fe-4S] cluster is paired with the exposed surface of the MoFe protein's pseudosymmetric αβ interface. This model was used to suggest the probable pathway of electron transfer from component proteins and is shown in Figure 2.

Since the proposal of the individual structural models for the Fe protein and MoFe protein, a crystallographic model for the docked complex has been determined [38]. Experiments that illustrated the inhibition of nitrogenase with AlF_4^-, by the formation of a tight complex between the Fe protein and the MoFe protein, made it an ideal candidate for structural analysis [39, 40]. In this model, docking occurs so that the 2-fold symmetric axis surrounding the [4Fe-4S] cluster of the Fe protein becomes paired with the surface of the MoFe protein's pseudosymmetrical αβ-interface and supports the Howard-Rees model. This situation places the [4Fe-4S] cluster in close proximity (≈ 14 Å) to the P-cluster of the MoFe protein, and places the P cluster between the Fe protein [4Fe-4S] cluster and FeMo-cofactor. This arrangement is consistent with the electron transfer such that the role of the P cluster is to mediate electron transfer between the Fe protein and the substrate reduction site provided by FeMo-cofactor.

For nitrogenase to function, it requires the Fe protein, the MoFe protein, a source of low potential electrons (usually sodium dithionite *in vitro*), MgATP and an anoxic environment. The physiological substrate for nitrogenase is N_2. Six electrons reduce N_2 to two molecules of ammonia, and until 1966, N_2 was the only known substrate for nitrogenase. Although the product of N_2 reduction was known to be ammonia, repeated attempts to find an intermediate

between N_2 and ammonia were unsuccessful. Despite the lack of direct evidence, the reaction was assumed to take place in three distinct two-electron reduction steps with diazene and hydrazine as the probable intermediates. There is no evidence for the existence of the diazene-like intermediate, but hydrazine can be released from the functioning enzyme by acid or alkali treatment [41]. The N_2 reduction reaction is irreversible and is always accompanied by H_2 evolution. Even at high N_2 pressure (50 atm.), a minimum of 25% of the available electrons go into H_2 evolution [42]. This has led to the suggestion that N_2 binds to the MoFe protein by displacing a dihydride from the substrate-binding site [41].

Certain analogues of N_2, such as acetylene, are capable of inhibiting the N_2 fixation reaction. These analogues are not only inhibitors of nitrogenase but are substrates that can be reduced by the enzyme. The reduction of acetylene to ethylene was particularly advantageous for researchers because its K_m for reduction is less than that of N_2 (acetylene-0.005 atm versus dinitrogen-0.1 atm) and ethylene detection could be achieved quickly, cheaply and with great sensitivity using a gas chromatograph equipped with a flame ionization detector [43]. The reduction of acetylene remains a standard method for measuring nitrogenase activity both *in vivo* and *in vitro,* using purified protein or crude extract samples. Fortunately, no other known biological system has acquired the ability to reduce acetylene. In general, acetylene can only be reduced as far as ethylene, however a number of altered MoFe proteins produced by site directed mutagenesis and the V-dependent nitrogenase can reduce acetylene through to ethane [44-46].

Substrates are bound to and products released from the free nitrogenase MoFe protein, but substrate reduction is a function of the active complex [47]. MoFe protein is supplied with electrons by the Fe protein which, in turn, is reduced by an appropriate electron donor. The reaction mechanism for nitrogenase can therefore conveniently be considered in terms of an

electron flow from reductant to Fe protein to MoFe protein to substrate. The reduced Fe protein with 2MgATP bound forms a complex with the MoFe protein. After this association the Fe protein delivers an electron to the MoFe protein and the MgATP molecules are subsequently hydrolyzed. The oxidized Fe protein then dissociates from the MoFe protein in what is considered to be the rate-limiting step in the process. Slow dissociation of the Fe protein-MoFe protein complex may be necessary to ensure efficient transfer of electrons to substrate rather than H^+. The Fe protein becomes recharged with an electron from the supplied source (flavodoxin or ferredoxin *in vivo*, sodium dithionite *in vitro*) and undergoes a nucleotide exchange reaction to replace the existing MgADP with MgATP. This Fe protein is then primed and ready to participate in another protein-protein association event. No one product can be obtained from a single electron transfer reaction and so multiple cycles, eight in the case of N_2 reduction, are necessary before product release occurs. The transfer of more than one electron means that the MoFe protein may exist in a number of different redox states. Such redox states likely have a role in determining which substrates bind to the active site. It has been proposed that N_2 binds to the three electron reduced state and that after four electrons have been transferred, N_2 is committed to being reduced to ammonia [41]. Acetylene on the other hand has been proposed to bind to the one and two electron reduced states and ethylene is released from the three electron reduced state [48]. Using these parameters it has been possible to successfully simulate pre-steady-state substrate reduction data. Although in the future we will undoubtedly see modifications of and additions to this scheme, it does offer the most complete description of nitrogenase action currently available and also provides a useful model upon which to base future work.

Maturation of the Nitrogenase Component Proteins

The primary translational products of the nitrogenase structural genes (*nif*HDK) are not active. Rather, a consortium of *nif*-specific gene products is required for the maturation of the immature nitrogenase structural components to active forms. Therefore, an important avenue of research is to understand how the metalloclusters for electron transfer and substrate reduction are synthesized and inserted into their respective component proteins.

In the case of the Fe protein, the *nif*M, *nif*U and *nif*S gene products are specifically required for its maturation [7, 49]. The *nif*M gene product has not yet been isolated in an active form, but it is a member of a family of peptidyl-prolyl *cis/trans* isomerases [50]. Such enzymes are thought to assist protein folding by catalyzing the *cis/trans* isomerization of certain prolyl peptide bonds in proteins. The requirement for such an activity in maturation of the Fe protein is not obvious but it could relate to the appropriate organization of the cysteine ligands needed for correctly inserting the [4Fe-4S] cluster [7]. The catalytic action of NifS is involved in the synthesis of the [4Fe-4S] cluster of the Fe protein [51]. Both NifU and NifS are described in later sections of this review.

Maturation of the MoFe protein, particularly the formation and insertion of the FeMo-cofactor, is much more complicated. The investigators who began this work in the early 1970's had a daunting task in store for them. In spite of this, a number of features worked in their favor. First, because the physiological requirement for nitrogenase activity can be circumvented by the addition of a fixed nitrogen source to the growth medium, it was relatively easy to identify mutants impaired in nitrogenase activity [52]. Second, FeMo-cofactor can be chemically extruded [11], and it possesses a unique spectroscopic signature that can be used to monitor the reconstitution of cofactorless forms of the MoFe protein (apo-MoFe protein) that are produced in

certain mutant strains. Third, the reduction of acetylene to ethylene is a simple and convenient way to measure nitrogenase activity in both crude extracts and whole cells. Taking advantage of these key features, extracts from two different mutants, both of which are individually impaired in nitrogenase activity, can be mixed and examined for nitrogenase activity. With this complementation approach, it was possible to purify factors with complementary biochemical functions. In addition to this biochemical complementation approach, a related strategy involving the reconstitution of inactive nitrogenase with isolated FeMo-cofactor was launched. Using these two approaches, investigators were able to screen a large number of nitrogenase mutants and discern among those that are impaired in the nitrogenase structural genes (*nif*HDK) and those impaired with the maturation process of nitrogenase.

A problem associated with the biochemical-genetic approach is that it is unable to discriminate between two separate mutations which are impaired in the identical biochemical function, but which have mutations in different genes. Due to this limitation, it was essential that traditional genetic mapping strategies, involving genetic complementation, were used in parallel with biochemical complementation experiments [53, 54]. *K. pneumoniae* was used in the development of the first genetic map of the nitrogen fixation genes (*nif* genes), and was later followed by *A. vinelandii* and *R. capsulatus.* Among the most fascinating and most impressive aspects of nitrogenase research is the remarkable accuracy of the insights provided by the application of traditional genetic and biochemical complementation experiments when viewed in the present context of the available DNA sequences and the structural models for the component proteins and their associated metalloclusters.

Examination of the structural model of the FeMo-cofactor, as discussed above, brings to light a number of salient questions concerning its biosynthesis. How are the Fe and S mobilized

and targeted for metallocluster synthesis? What is the source of homocitrate, and how does homocitrate become coupled to Mo? Are the two subcluster fragments of the FeMo-cofactor synthesized separately or together? Is FeMo-cofactor synthesized step-wise into apo-MoFe protein, or is it synthesized separately and then inserted into apo-MoFe protein? Are there proteins that aid in the insertion of the FeMo-cofactor into apo-MoFe protein? Though the biochemical-genetic approach was unable to answer these questions, it was able to identify the key players involved in FeMo-co biosynthesis. In *A. vinelandii,* genes that have been found essential for the biosynthesis of FeMo-co are: *nif*B, *nif*E, *nif*N, *nif*H and *nif*V. Other non-essential genes involved with FeMo-cofactor biosynthesis are: *nif*Y, *nif*X, *nif*Q, *nif*U, *nif*S, *nif*W, and *nif*Z. Organization of the *nif*-specific genes from *A. vinelandii* is shown in Figure 3. The remainder of this chapter will focus on the current state of knowledge regarding these genes and their products.

NifB Extracts with a deficiency in *nif*B have been shown to accumulate apo-MoFe protein which can be activated by the addition of FeMo-cofactor [55-57]. The FeMo-cofactor biosynthetic assay developed by Shah and coworkers [11] has allowed the purification of a cofactor related to the NifB protein[58], however the NifB protein has not yet been isolated. It is thought that NifB provides a scaffold or an assembly site for the biosynthesis of an Fe/S precursor to the FeMo-cofactor that has been termed NifB-cofactor. During FeMo-cofactor biosynthesis, NifB-cofactor is first formed on NifB, with Fe and S provided by NifU and NifS, respectively. This Fe/S precursor is then donated to further stages in the biosynthesis of the FeMo-cofactor [59, 60]. Some evidence exists to support this hypothesis: (i) a cysteine-rich region contained within the NifB primary sequence may provide a nucleation site for cluster

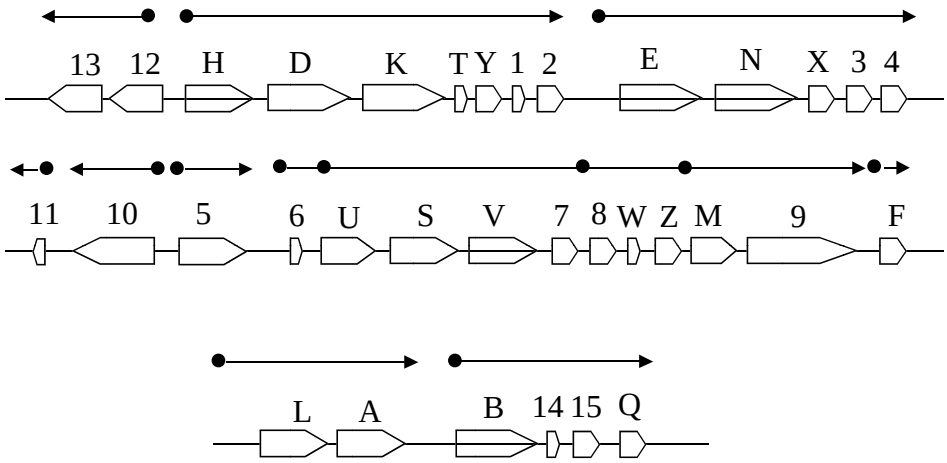

Figure 3. Organization of the nitrogen fixation specific (*nif*) genes of *Azotobacter vinelandii*. Black arrows indicate transcriptional units and the direction of their transcription. The genes encoding products essential for FeMo-cofactor biosyntheis are shaded. Functions of the *nif* gene products involved with FeMo-cofactor biosynthesis are described in the text.

formation, (ii) the number of hydrophilic residues in proximity to the cysteine-rich region imply a processing site for Fe/S cluster formation near the protein's surface [61], and (iii) the *nif*B and *nif*N genes in *C. pasteurianum* are fused [62], suggesting that NifB may form a complex with NifEN during the biosynthesis of FeMo-cofactor. This point will be discussed further in the section describing the role of NifE and NifN in FeMo-cofactor biosynthesis.

The most current work involving NifB-cofactor has involved the use of ^{55}Fe and ^{35}S labeled NifB-cofactor to trace this metallocluster during FeMo-cofactor biosynthesis by the application of anoxic native gel electrophoresis and phosphor-imaging techniques. Using this approach a number of *nif*-specific gene products have been implicated in the processing of the FeMo-cofactor precursors and synthesis of FeMo-cofactor. Among these are: NifEN, NifH (Fe protein), and NifX.

NifE AND NifN Similar to *nif*B mutant extracts, strains harboring mutations in the *nif*E and *nif*N genes produce apo-MoFe protein. This apo-MoFe protein can then be activated by the addition of purified FeMo-cofactor. These reconstitution experiments spurred investigators to ask whether or not FeMo-cofactor was synthesized step-wise into apo-MoFe protein or if it was synthesized separately and then inserted into apo-MoFe protein. Experiments in which crude extract from a *nif*DK deletion strain was able to reconstitute nitrogenase activity in crude extracts containing apo-MoFe protein showed that the FeMo-cofactor is synthesized prior to insertion into apo-MoFe protein [63]. Because the source of the FeMo-cofactor must come from the extract deleted for *nif*D and *nif*K, which does not produce the MoFe protein subunits, the step-wise insertion into apo-MoFe protein is not required for FeMo-cofactor formation. These experiments suggested that FeMo-cofactor is separately synthesized, perhaps on a molecular

scaffold, prior to insertion into apo-MoFe protein. A likely candidate for this scaffold was believed to be another *nif* specific gene product that shared significant primary sequence conservation to the nitrogenase structural genes [64]. Comparison of the primary sequences of the *nif*D and *nif*K gene products to those *nif* genes essential for FeMo-cofactor biosynthesis indicated a high degree of primary sequence conservation between the *nif*E and *nif*N gene products, respectively [65]. The primary sequence conservation and the mutual stability requirements for NifE and NifN [55] led to the concept that NifE and NifN might form a macromolecular complex on which FeMo-cofactor could be synthesized. Also, based on primary sequence conservation, it was thought that this NifEN complex might contain Fe/S clusters similar to the P-clusters of the MoFe protein [65].

Using the *in vitro* FeMo-cofactor synthesis assay [63] investigators were able to purify small quantities of NifEN complex [66]. NifEN complex purified in this manner was shown to be an $\alpha_2\beta_2$ heterotetramer ($M_r \approx 200{,}000$) containing iron and inorganic sulfur presumably organized into a single Fe_4S_4 cluster per NifEN tetramer. This purified NifEN could reconstitute nitrogenase activity in a *nif*E deletion strain and NifEN activity was sensitive to air and heat-labile, suggesting the activity was dependent on a redox active protein[66]. More recently, NifEN has been shown to accumulate in different forms, these forms being dependent on the source of the mutant extract [60]. The different forms of NifEN are thought to be different global conformations, contingent on the presence or absence of FeMo-cofactor precursors [60]. The ability of NifEN to shift from one form to another upon the addition of NifB-cofactor supports the scaffold role of NifEN in FeMo-cofactor biosynthesis.

If NifEN does provide a platform on which FeMo-cofactor is synthesized a number of interesting questions arise. How does the NifEN scaffold site compare to the FeMo-cofactor

binding site within the MoFe protein? What are the conserved amino acids, if any? Does NifEN contain a similar structure to that of the P-cluster in the MoFe protein? If so, what are the ligands and what is the role of such a cluster in FeMo-cofactor biosynthesis. In light of the MoFe protein crystal structure, the structural models for the MoFe protein metal centers, and the primary sequence conservation between the NifEN complex and the MoFe protein, a homology model has been generated for NifEN [62]. Though this model provides a great tool to increase the understanding of the NifEN complex, there are some drawbacks. Because it is a model based upon homology with the MoFe structure, and not based on crystal diffraction data of the NifEN complex, one must be careful when making assumptions as to the structure of NifEN. Also, because the model is based on the crystallographic solution of the MoFe protein, it is biased toward a NifEN complex that can bind or synthesize a mature form of the FeMo-cofactor. The model also suggests an overall polypeptide-fold for NifEN similar to that of the MoFe protein. The conservation of polypeptide conformation between NifEN and the MoFe protein suggests a possible interaction of NifEN with the Fe protein. Whether or not the Fe protein binds to the NifEN complex remains to be seen, however a number of residues required for the docking model by Howard and Rees [37] are conserved in NifEN. These include NifE residues 132-138, and NifN residues 78, 108, 110, and 111 [62]. The true test of the NifEN model will come from direct analysis of purified NifEN. To this end, the inability to obtain sufficient NifEN in concentrations amenable to detailed biophysical and biochemical characterization has slowed progress in this area of research. Because NifEN is a metallocluster biosynthetic enzyme and is only required in very low intracellular amounts, only small quantities have been purified[66]. It is believed that during FeMo-co biosynthesis NifEN binds the FeMo-co precursor, NifB-cofactor, and presumably processes it along the path to FeMo-cofactor. It is not certain if FeMo-

cofactor biosynthesis is completed on NifEN, but it is at least partially completed [60]. Whether or not Mo and homocitrate react at the point of NifEN involvement remains to be determined. There is evidence that supports the involvement of the Fe protein with NifEN during FeMo-cofactor biosynthesis and will be discussed in the body of this dissertation. Work included within this dissertation has made it possible to purify quantities of NifEN such that characterization of this FeMo-cofactor scaffold protein can be investigated in detail.

NifV Homocitrate is the organic acid constituent of the FeMo-cofactor, which is produced by the action of NifV. NifV is a homocitrate synthase that catalyzes the condensation of acetyl-CoA and α-ketoglutarate to produce homocitrate[67]. *K. pneumoniae* and *A. vinelandii* strains deficient in *nif*V produce MoFe proteins that have altered catalytic characteristics. These altered proteins are capable of the reduction of acetylene to ethylene, but are poor nitrogen fixers [68, 69]. The first direct evidence that FeMo-cofactor was the substrate reduction site was shown by experiments where apo-MoFe protein reconstituted by FeMo-cofactor isolated from MoFe protein produced by a *nif*V$^-$ mutant exhibited the altered catalytic properties associated with the n*if*V phenotype [29]. In *K. pneumoniae,* FeMo-cofactor produced by nifV$^-$ mutants accumulate citrate rather than homocitrate as its organic acid component [30]. In the case of *A. vinelandii*, it appears as if no organic acid is associated with the FeMo-cofactor in the absence of *nif*V (Commaratta, L.M., and Dean, D.R. unpublished results). The mechanism of homocitrate incorporation into FeMo-cofactor is unknown. Whether homocitrate is added at the stage of NifEN or at a later stage is currently under investigation. However, the involvement of NifW and NifZ may be involved in homocitrate processing and incorporation into active FeMo-cofactor [62] .

NifH The involvement of *nif*H in FeMo-cofactor biosynthesis is one of the most puzzling aspects of nitrogenase maturation. The Fe protein, encoded by *nif*H, is the obligate electron donor to the MoFe protein during nitrogenase catalysis [47]. Extracts from certain *nif*H mutant strains produce apo-MoFe protein [70, 71]. The reconstitution of these apo-MoFe proteins requires the presence of both MgATP and Fe protein [22, 72]. However, reconstitution of apo-MoFe protein produced by *nif*E or *nif*B mutants does not require the addition of Fe protein or MgATP [22, 56, 73, 74]. Studies involving the application of anoxic native gel electrophoresis have shown that apo-MoFe protein produced by *nif*B or *nif*E mutant strains are different from the apo-MoFe protein produced by a *nif*H mutant strains [22, 74]. These results have been interpreted as the Fe protein having two distinct functions in FeMo-cofactor biosynthesis, the direct involvement of Fe protein in the biosynthesis of FeMo-cofactor, and the active participation in the maturation of the apo-MoFe protein such that it is in a form that is amenable to FeMo-cofactor insertion.

The active participation of the Fe protein and MgATP in FeMo-cofactor biosynthesis is very reasonable based on the apparent structural similarities between the MoFe protein and the NifEN complex. It was first thought that the role of Fe protein in FeMo-cofactor biosynthesis was similar to its role in nitrogenase catalysis, such that NifEN replaced MoFe protein as the Fe protein's substrate [71]. This idea is very intriguing, based on the conservation of a number of residues within NifEN that are thought to be involved in the MoFe protein-Fe protein docking model. Three possible roles of the Fe protein binding to the NifEN complex are: (i) an electron transfer event required for the activation of a FeMo-cofactor precursor (NifB-cofactor) bound to NifEN, (ii) an Fe protein binding induced conformational change on the NifEN complex which

is required for the accessibility of a metallocluster assembly site that is otherwise buried within NifEN, and (iii) Fe protein induced redox or conformational change required for the release of FeMo-cofactor or precursor from the NifEN complex [62]. Though these possible interactions are intriguing, there is little evidence to support the involvement of Fe protein with NifEN. A number of studies have shown that altered Fe proteins that can no longer function in nitrogenase catalysis are still capable of the biosynthesis of FeMo-cofactor. For example, Fe protein produced from a *nif*M mutant strain is inactive in substrate reduction, however functions in the synthesis of FeMo-cofactor [55, 75]. Additionally, a number of mutant strains that produce Fe proteins that are defective in electron transfer, or MgATP binding or hydrolysis accumulate MoFe protein that contains FeMo-cofactor [76, 77].

The involvement of Fe protein and MgATP with apo-MoFe protein maturation is just as perplexing as its role in FeMo-cofactor synthesis. There are two main theories about FeMo-cofactor insertion into apo-MoFe protein. One theory involves a molecular prop that is necessary to keep the apo-MoFe protein in a conformation amenable for FeMo-cofactor insertion. In *K. pneumoniae* this molecular prop is encoded by *nif*Y [78], and in *A. vinelandii* it is encoded by a non-*nif* regulated protein designated gamma (γ) [79]. The association of this prop (NifY or gamma) converts the apo-MoFe protein from an $\alpha_2\beta_2$ tetrameric conformation to an $\alpha_2\beta_2\gamma_2$ hexameric conformation, and is dependent on Fe protein and MgATP. There is, however, a case in which the tetrameric apo-MoFe protein produced by a *nif*B-deletion in *A. vinelandii* can be activated by addition of FeMo-cofactor alone [56]. This data suggests that gamma, in the case of *A. vinelandii*, is not necessary for FeMo-cofactor insertion into apo-MoFe protein. Perhaps the role of gamma is to kinetically enhance this process or perhaps gamma is required *in vivo* for some aspect of FeMo-cofactor insertion.

NifY Different forms of the apo-MoFe protein accumulate under different genetic backgrounds. These forms have been characterized by their electrophoretic mobilities under non-denaturing conditions [22, 74, 78, 80]. When extracts deficient in the products of *nif*B, *nif*E, or *nif*N are examined, the apo-MoFe proteins produced all have the same electrophoretic mobility. This mobility is different from that of apo-MoFe proteins produced by a *nif*H deletion. The difference in these forms of the apo-MoFe protein is the presence or absence of a small molecular weight protein. In *K. pneumoniae*, the small molecular weight protein was identified as the *nif*Y gene product [78, 80]. In *A. vinelandii*, the small molecular weight protein (termed γ) was shown to be a non-*nif* encoded protein [78]. Addition of FeMo-cofactor to apo-MoFe protein associated with either NifY (*K. pneumoniae*) or γ (*A. vinelandii*), results in the reconstitution of apo-MoFe protein and the release of either NifY or γ [78, 80]. However, the apo-MoFe protein produced by a *nif*H deletion does not have the γ subunits associated with it, and is not activated with the addition of FeMo-cofactor. However, the addition of Fe protein and MgATP to such extracts results in the association of γ [22]. The γ subunits attached in this way can subsequently be released from the complex by the addition of FeMo-cofactor [62].

These results indicate that the apo-MoFe protein must be processed in order to be competent to accept FeMo-cofactor. This processing event involves the Fe protein and MgATP dependent association of the small molecular weight protein (NifY or γ) to the apo-MoFe protein. The role of this small molecular weight protein is thought to be as a molecular prop, which facilitates the insertion of FeMo-cofactor into apo-MoFe protein [80]. Its action may be to maintain a conformation of the apo-MoFe protein where the FeMo-cofactor-binding site either remains accessible for FeMo-cofactor attachment or is protected from reactivity with other

cellular constituents [62]. There is evidence supporting these ideas from two independent studies by Homer *et al*. [78], and Christiansen *et al.* (see Chapter II). The study by Homer *et al.* showed that in a *K. pneumonia nif*B-*nif*Y double mutant apo-MoFe protein is only partially activated upon addition of FeMo-cofactor. Christiansen *et al.* [56] showed that in an *A. vinelandii nif*B deletion, apo-MoFe protein containing a poly-histidine fusion did not associate with the γ subunit, rendering it susceptible to alkylation at the exposed active site cysteine (α275). It is believed that after insertion of FeMo-cofactor the reconstituted apo-MoFe protein undergoes a conformational change, resulting from a dissociation of the molecular prop, which is evidenced by a change in electrophoretic mobility under nondenaturing conditions.

NifX Inspection of the *nif*-specific gene organization (Figure 3) reveals that *nif*Y is contained within the same transcriptional unit and downstream from the genes encoding the MoFe protein subunits. The *nif*EN transcription unit contains *nif*X downstream from the *nif*EN genes. NifY and NifX bear significant primary sequence identity when compared to each other [81]. Based on these considerations, and on the likely structural similarity between the MoFe protein and the NifEN complex, it is inferred that NifY and NifX probably have related functions in processing FeMo-cofactor or FeMo-cofactor precursors, respectively. This proposed model is also attractive based on primary sequence conservation between NifX and NifB in *R. capsulatus* [82], as well as in *K. pneumoniae* and *A. vinelandii*. Cysteine residues that are conserved within NifX proteins from the above mentioned organisms may provide the ligands necessary to bind a FeMo-cofactor precursor. Recent work utilizing a purified FeMo-cofactor synthesis system, lacking the presence of crude extract, has shown that NifX activity is required for FeMo-cofactor formation [83]. Despite this result, the activity and function of NifX has not yet been

determined. Work present in Chapter III of this dissertation examines the involvement of NifX in metallocluster binding.

NifQ The precise role of *nif*Q in FeMo-cofactor biosynthesis is not known, however it is believed to be involved in molybdenum processing and insertion into the FeMo-cofactor [84]. In *nif*Q$^-$ mutants of both *K. pneumoniae* and *A. vinelandii,* a Nif$^-$ phenotype is observed under low molybdenum (nanomolar) conditions [84, 85]. However, this phenotype can be overcome by the simple addition of molybdenum (micromolar) to the growth medium [84]. Although *nif*Q mutations are not defective in the uptake of Mo, they accumulate lower levels of intracellular molybdenum than wild type [84]. Malfunctions in *nif*Q can be overcome by the addition of cysteine as a sulfur source in the medium [86]. The fact that *nif*Q is not involved in the synthesis of molybdenum cofactor (the cofactor of other molybdoenzymes) suggests it has a specific role in FeMo-cofactor biosynthesis [87]. In spite of these results, NifQ has neither been purified to date, nor is there any known activity for NifQ. Inspection of the NifQ primary sequence revealed a cluster of four conserved cysteine residues at the C-terminus of the protein [61]. These cysteine residues may provide the ligands for a redox site within NifQ, or perhaps provide a nucleation site for the formation of a Mo-containing precursor of the FeMo-cofactor. The location of this cysteine-rich region near the surface of the protein is indicated by the relatively high number of hydrophilic residues in this region [61]. If this Mo-containing precursor were to be transferred to an additional protein on the FeMo-cofactor assembly line, an ideal location within NifQ would be near the surface of the protein.

NifU and NifS In addition to the gene products that are specifically involved in nitrogenase metallocluster biosynthesis there are two other *nif*-genes, *nif*S and *nif*U, whose products catalyze reactions that are involved in the mobilization of Fe and S for metallocluster assembly [51, 88]. The *nif*S gene product is a cysteine desulfurase that activates S for Fe-S cluster formation, whereas the *nif*U gene product probably has a complementary role as an Fe carrier [89]. The catalytic role of NifS in Fe-S cluster synthesis was demonstrated by the ability of NifS to reconstitute the [4Fe-4S] cluster of the Fe protein, providing a source of Fe and reductant was present [51]. Homologues to *nif*U and *nif*S whose expression is not under *nif*-specific control are present in many organisms. The products of these genes probably have general functions in [Fe-S] cluster formation and repair [90].

Current research in this area involves the formation of Fe-S clusters *in vitro,* by the action of NifU and NifS. NifU is a modular protein containing distinct functional domains, which has permitted the purification of these specific polypeptide domains. NifU-1 encompasses the N-terminal region of NifU containing three conserved cysteine residues that are required for NifU activity. NifU-2 contains the region of NifU that has a bound [2Fe-2S] cluster. The ability to purify the functional domains of NifU has permitted the study of Fe-S cluster synthesis *in vitro* by monitoring cluster formation over time by UV-VIS spectroscopy. The interferring signal from the [2Fe-2S] cluster of NifU can be excluded by purifying NifU-1 and using it in the Fe-S synthesis reactions. NifU-1 has the ability to bind Fe, and when incubated with catalytic amounts of NifS, cysteine and β-mercaptoethanol will catalyze the formation of [2Fe-2S] clusters (P. Yuvaniyama, and D.R. Dean, personal communication).

NifW and NifZ The functions of NifW and NifZ in FeMo-cofactor biosynthesis are not fully understood. During FeMo-cofactor synthesis homocitrate formed by NifV must be coordinated to Mo. It is not clear whether this process requires an enzymatic activity, or if this process occurs on the NifEN complex or at a later step during FeMo-cofactor biosynthesis. Deletion of either *nif*W or *nif*Z results in a slower diazotrophic growth rate than a wild type strain and a slight decrease in MoFe protein activity, but no apparent effect on Fe protein activity [75, 91]. It has been suggested that NifW and NifZ may form a macromolecular complex, owing to their similar biochemical and growth phenotypes as well as the fact that *nif*W and *nif*Z are co-transcribed in *K. pneumoniae* [92] and *A. vinelandii* [75]. Study of a *nif*W-*nif*Z double mutant in *R. capsulatus* has shed more light on the possible involvement of these proteins with homocitrate processing. The *nif*W-*nif*Z double mutant has a more pronounced effect on the diazotrophic growth rate when compared to wild type, however, this phenotype can be rescued by the addition of homocitrate to the growth medium [Masepohl, 1989 #4550]. This effect is also seen in an *A. vinelandii nif*W-*nif*V double mutant, which alludes to the involvement of NifW and NifZ in a common processing event requiring homocitrate [62].

Proposed Model for FeMo-cofactor Biosynthesis

The current model for FeMo-cofactor synthesis is illustrated in Figure 4. NifU and NifS most likely mobilize Fe and S, respectively. Fe and S recruited in this manner are then donated to NifB. Using this donated Fe and S, NifB catalyzes the formation of an Fe/S precursor to the FeMo-cofactor, termed NifB-cofactor. NifB then donates NifB-cofactor to the NifEN complex. Whether or not NifB directly interacts with NifEN is not known. Perhaps NifB-cofactor association with NifEN requires specific proteins that act to transport metalloclusters. A possible

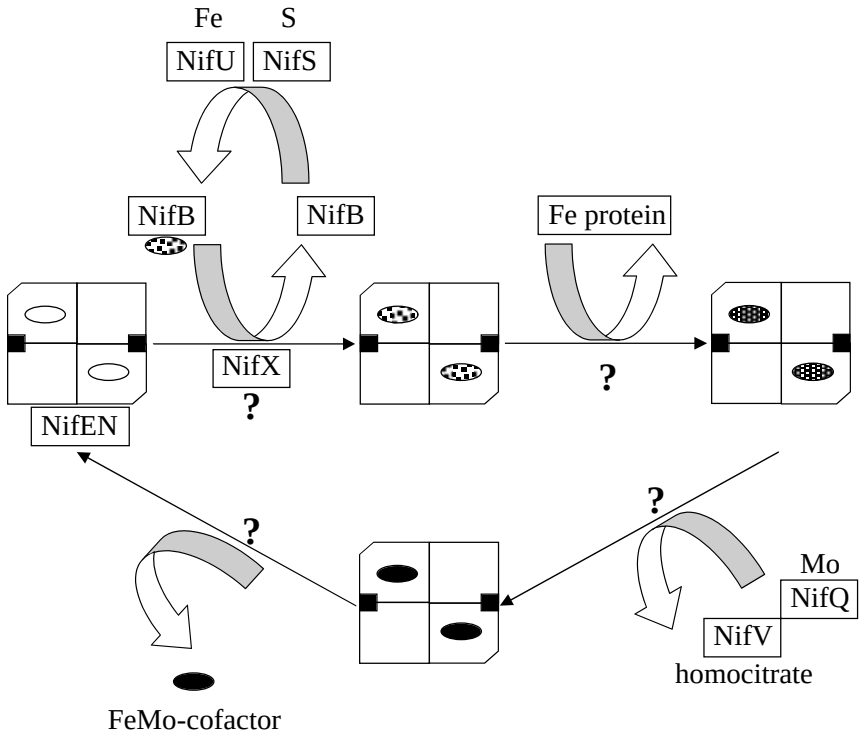

Figure 4. Schematic model for FeMo-cofactor biosynthesis in *A. vinelandii*. The following features of FeMo-cofactor biosynthesis are summarized: (i) NifU and NifS are probably involved in mobilization of Fe and S, respectively; (ii) NifB promotes the formation of an FeMo-cofactor precursor using the Fe and S provided by NifU and NifS; (iii) The FeMo-cofactor precursor provided by NifB, NifB-cofactor, is donated to the NifEN complex. This process may involve direct association of NifB and NifEN or the involvement of a metallocluster transport protein, such as NifX; (iv) NifEN with bound NifB-cofactor interacts with the Fe protein in an unknown manner; (v) After NifEN interacts with Fe protein, it is possible that NifEN is capable of incorporating Mo and homocitrate into FeMo-cofactor synthesis; (vi) Finally, fully formed FeMo-cofactor is released from NifEN and is available for the maturation of the apo-MoFe protein. Question marks indicate areas of synthesis that are not fully understood. Also, it is not known whether FeMo-cofactor is directly released to the apo-MoFe protein from NifEN or whether there is an intermediate carrier.

candidate for such a trafficking role is the NifX protein. The NifEN complex acts as a processing point for FeMo-cofactor biosynthesis. NifEN binds NifB-cofactor and processes it along the path of FeMo-cofactor synthesis. Whether or not a structural rearrangement of NifB-cofactor occurs upon NifEN is not known. It is thought that after NifEN binds, and perhaps processes, NifB-cofactor, the Fe protein interacts with the NifEN in some manner. The next few steps are unclear. It is not known if the Mo and homocitrate are incorporated at the stage of NifEN or at a later stage in synthesis. Organic acid and metal analysis of NifEN have not indicated the presence of homocitrate or Mo. Also, it is not certain how fully formed FeMo-cofactor is mobilized for the activation of apo-MoFe protein. It is thought that γ, a non-*nif* protein, is involved with mobilization of FeMo-cofactor and subsequent insertion into apo-MoFe protein. However, conflicting reports exist of the matter of γ involvement. The most interesting holes concerning the process of FeMo-cofactor biosynthesis, as it pertains to the research contained within this dissertation, pertain to the involvement of the Fe protein and the transport of metalloclusters such as NifB-cofactor and FeMo-cofactor.

The dissertation in hand is focussed on increasing the understanding of FeMo-cofactor biosynthesis in *A. vinelandii*. Chapter I deals with the development of a gene fusion approach for NifEN overproduction and the application of immobilized metal-affinity chromatography for the purification of a poly-histidine tagged NifEN complex. Within this chapter the initial biophysical characterization of the NifEN complex metal centers were completed. Chapter II involves the poly-histidine fusion approach for the purification of apo-MoFe protein from a *nif*B-deletion in *A. vinelandii*. Also contained within this chapter is the detailed biophysical characterization of the P-cluster associated with the apo-MoFe protein. Chapter III constitutes an initial study of an FeMo-cofactor precursor bound to the NifEN complex. Additional work

includes the involvement of NifX in processing NifB-cofactor, FeMo-cofactor and precursor bound on NifEN. Finally, chapter IV probes at the interaction of the Fe protein of nitrogenase with the NifEN complex. Aspects of this study involve the use of altered forms of the Fe protein to probe protein-protein interaction with NifEN and the use of biophysical techniques to investigate electron transfer from the Fe protein to the NifEN complex.

CHAPTER I

The *Azotobacter vinelandii* NifEN Complex Contains Two Identical [4Fe-4S] Clusters

This Chapter was written by the combined efforts of myself, Jeffrey N. Agar,[§] Jon T. Roll,[¶] Gary P. Roberts,[¶] Michael K. Johnson,[§] and Dennis R. Dean* and was published in the journal *Biochemistry* (Goodwin *et al.*,1998). I was involved in all aspects of the experiments performed for the preparation of this manuscript. Experiments pertaining to recombinant DNA technology, bacterial strain construction , protein purification and protein characterization were performed in the laboratory of Dennis Dean at Virginia Tech. Plasmids used in strain construction were prepared by technician Valerie Cash of Dennis Dean's laboratory. Experiments involving biophysical characterization techniques were performed under the supervision of Jeff Agar in the laboratory of Michael Johnson at the Center for Metalloenzyme studies located at the University of Georgia.

[‡] Department of Biochemistry, Virginia Tech, Blacksburg, VA 24061

[§] Department of Chemistry and Center for Metalloenzyme Studies, University of Georgia, Athens, GA 30602

[¶] Department of Bacteriology, University of Wisconsin, Madison, WI 53706

Summary

The nifE and nifN gene products from *Azotobacter vinelandii* form an $\alpha_2\beta_2$ tetramer (NifEN complex) that is required for the biosynthesis of the nitrogenase FeMo-cofactor. The current model for NifEN complex organization and function is that it is structurally analogous to the nitrogenase MoFe protein and that it provides an assembly site for a portion of FeMo-cofactor biosynthesis. In the present work, gene fusion and immobilized metal-affinity chromatography strategies were used to elevate the *in vivo* production of NifEN complex and to facilitate its rapid and efficient purification. The NifEN complex produced and purified in this way exhibits a similar FeMo-cofactor biosynthetic activity to that previously described for NifEN complex purified by traditional chromatography methods. UV-visible, EPR, variable-temperature magnetic circular dichroism, and resonance Raman spectroscopies were used to show that the NifEN complex contains two identical $[4Fe\text{-}4S]^{2+,+}$ clusters. These clusters have a predominantly $S = 1/2$ ground state in the reduced form, exhibit a reduction potential of -350 mV, and are likely to be coordinated entirely by cysteinyl residues based on spectroscopic properties and sequence comparisons. A model is proposed where each NifEN complex [4Fe-4S] cluster is bridged between a NifE-NifN subunit interface at a position analogous to that occupied by the P clusters in the nitrogenase MoFe protein. In contrast to the MoFe protein P clusters, the NifEN complex [4Fe-4S] clusters are proposed to be asymmetrically coordinated to the NifEN complex where NifE cysteines-37, -62, and -124 and NifN cysteine-44 are the coordinating ligands. Based on a homology model of the three dimensional structure of the NifEN complex, the [4Fe-4S] cluster sites are likely to be remote from the proposed FeMo-cofactor assembly site and are unlikely to become incorporated into FeMo-cofactor during its assembly.

Introduction

Biological nitrogen fixation is catalyzed by nitrogenase, a metalloenzyme composed of two-component proteins called the Fe protein and MoFe protein (reviewed in [6, 26, 93]). The Fe protein (also called dinitrogenase reductase [13]) is a homodimer that contains a single [4Fe-4S] cluster bridged between its identical subunits [14]. The MoFe protein (also called dinitrogenase) is an $\alpha_2\beta_2$ tetramer that contains two pairs of novel metalloclusters called the P-cluster (Fe_8S_7) and the iron-molybdenum cofactor (FeMo-cofactor [Fe_7S_9Mo:homocitrate]). Each αβ-unit of the MoFe protein is believed to comprise a single catalytic unit that contains one P-cluster and one FeMo-cofactor that are separated by approximately 17 Å [12]. During catalysis the Fe protein delivers electrons to the MoFe protein in a process that involves association-dissociation of the component proteins, MgATP binding, and nucleotide hydrolysis [13]. The nucleotide binding sites are located on the Fe protein and a minimum of two MgATP are hydrolysed for each electron transfer event. The P-cluster is located at the αβ-interface of the MoFe protein and appears to function as an intermediate electron carrier site that accepts electrons from the Fe protein and subsequently effects their intramolecular delivery to FeMo-cofactor [25, 94, 95] - the site of substrate binding and reduction [11, 29, 31].

Because FeMo-cofactor provides the site of substrate binding and reduction, its structure and assembly have attracted considerable attention. X-ray crystallographic analyses have shown that FeMo-cofactor consists of a metal sulfur core (Fe_7S_9Mo) and one molecule of (R)-homocitrate [28]. The metal-sulfur core is constructed from Fe_3S_3Mo and Fe_4S_3 fragments that are connected by three inorganic sulfide bridges located between pairs of Fe atoms from

opposing fragments. Homocitrate is coordinated to the Mo atom through its 2-hydroxy and 2-carboxyl groups.

Biochemical and genetic studies using both *Azotobacter vinelandii* and *Klebsiella pneumoniae* have revealed that at least six *nif*-specific gene products, including NifB, NifE, NifN, NifV, NifQ, and NifH, are directly involved in the biosynthesis of FeMo-cofactor [96]. NifB catalyzes the formation of an FeMo-cofactor precursor called B-cofactor which is composed of an iron-sulfur core that does not include Mo or homocitrate [58]. NifE and NifN form an $\alpha_2\beta_2$ tetramer [66] that is able to bind B-cofactor [59, 60], and in doing so provide a scaffold for one or more steps in FeMo-cofactor biosynthesis. NifQ appears to have a role in the activation of Mo for FeMo-cofactor assembly [84], and NifV is a homocitrate synthase that provides the organic constituent of FeMo-cofactor [67, 97]. The role of NifH (Fe protein) in FeMo-cofactor assembly is not yet understood but its role does not appear to involve either electron transfer or MgATP hydrolysis [62, 76, 98]. The Fe protein and the product of another gene (NifY in the case of *K. pneumoniae* [78, 80] and a protein called gamma in the case of *A. vinelandii* [73, 79]) also appear to have some role in the incorporation of FeMo-cofactor into the apo-MoFe protein.

Most of what is known about the assembly of FeMo-cofactor has involved the application of *in vitro* reconstitution [11] and *in vitro* biosynthetic assays [99] developed by Shah and coworkers. For example, *in vitro* reconstitution assays were used to show that FeMo-cofactor is separately synthesized and then inserted into the apo-MoFe protein rather than being assembled stepwise into the apo-MoFe protein [63]. This observation, primary sequence comparisons [65, 100], and the two-dimensional electrophoretic properties of NifE and NifN ultimately led to the hypothesis that the NifEN complex provides a molecular scaffold for at least a portion of FeMo-

cofactor biosynthesis [100]. In related experiments it was found that NifB- and NifE- or NifN-deficient extracts could be mixed to achieve FeMo-cofactor formation, providing that Mo and MgATP were also added to the reaction mixture [99]. Experiments of this sort provided an assay that permitted the isolation of small amounts of the NifEN complex [66], which was shown to be an $\alpha_2\beta_2$ tetramer that contains Fe-S cluster(s). One problem encountered in the isolation and characterization of FeMo-cofactor biosynthetic enzymes is that they are only present in very low intracellular amounts. To date, this feature has precluded the purification of the NifEN complex in the quantities necessary for detailed biophysical characterization of its associated Fe-S cluster(s). In the present work a gene fusion approach for overproduction of the NifEN complex in *A. vinelandii* and the application of immobilized metal-affinity chromatography for NifEN complex purification are described. These procedures have permitted purification of active NifEN complex in sufficient quantities for biophysical characterization.

Experimental Procedures

DNA biochemistry and strain constructions. Transformation of *A. vinelandii* was performed as previously described by Page & von Tigerstrom [101]. Strain DJ1061 (Figure 1) was constructed in several steps. In the first step, polymerase-chain-reaction (PCR) -directed DNA amplification and mutagenesis was used to obtain an approximately 0.9-Kb *Msc*I-*Sal*I fragment of *A. vinelandii* genomic DNA [100] that was incorporated into *Sma*I-*Sal*I-digested pUC119 vector DNA. This plasmid was designated pDB902 and it contains the *A. vinelandii nifE* promoter, as well as upstream and downstream sequences extending approximately 450 base-pairs in each direction. Plasmid pDB902 was also constructed so that a unique *Nde*I restriction enzyme site overlaps the *nifE* translation initiation site. Plasmid pDB904 was constructed by

digesting pDB902 with *Nde*I and incorporating a kanamycin-resistance cartridge derived from pUC4-KAPA [102] at the *Nde*I site of pDB902. Plasmid pDB906 was constructed by digesting pDB902 with *Nde*I and then ligating a synthetic DNA cartridge into this site. The sense strand of the synthetic cartridge has the sequence: 5'TATGCATCACCACCATCACCACCA3'. The triplet that corresponds to the *nifE* translation initiation codon is underlined in the synthetic DNA cartridge shown above. This construction places seven in-frame histidine codons between the initiating methionine-codon and the second codon of the cloned portion of *nifE* carried on pDB906. Restriction enzyme mapping and DNA sequence analyses were used to confirm all plasmid constructions. Wild-type *A. vinelandii* cells were transformed using pDB904 DNA as the donor and then selecting for kanamycin resistance and scoring for ampicillin sensitivity. One transformant that resulted from double-reciprocal crossover events, and which is Nif-minus, kanamycin^R, and ampicillin^S, was designated DJ1057. Strain DJ1061 was constructed by transformation of DJ1057, using pDB906 DNA as the donor, resulting in a Nif-plus, kanamycin^S phenotype. Strain DJ1061 is genotypically identical to the wild-type except that there are seven histidine codons immediately following the initiating methionine codon at the N-terminus of *nifE*. It should be noted that none of the plasmids used for strain constructions described in the present work are capable of autonomous replication in *A. vinelandii*.

Strain DJ1041 (Figure 1) was also constructed in several steps. In the first step a DNA cartridge, extending from the *nifH* translation initiation site to approximately 500 base-pairs upstream, was generated by PCR amplification. This cartridge was constructed so that an *Nde*I restriction enzyme site was located at the *nifH* translation initiation site, and a *Bgl*II site was located approximately 500 base-pairs upstream of the *nifH* translation initiation site. This cartridge was digested by *Nde*I and *Bgl*II and ligated into *Nde*I-*Bgl*II-digested pT_7-7 plasmid

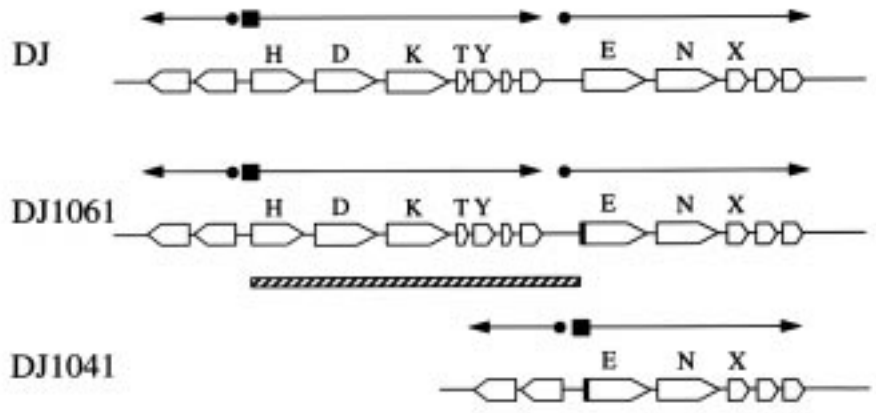

Figure 1. Organization of *nif*-specific genes in various strains relevant to the present work. Horizontal arrows indicate the direction of transcription. The approximate position of the *nif*H promoter is indicated by a filled box, and filled circles indicate the approximate positions of promoters for other transcription units. The cross-hatched bar indicates the region deleted from the chromosome in construction of DJ1041. The filled portion at the beginning of the *nif*E gene for DJ1061 and DJ1041 indicates the position of the sequence encoding the respective polyhistidine tags.

vector DNA [103] to form plasmid pDB591. In the second step a *nifE* -gene cartridge was generated by PCR amplification so that an *Nde*I site was located at the *nifE*-initiation codon and a *Bam*HI site was located shortly downstream of the *nifE*-coding sequence. This cartridge was ligated into *Nde*I-*Bam*HI-digested pT_7-7 vector DNA to form pDB558. In the next step pDB558 was digested with *Nde*I and *Bam*HI and the resulting *nifE*-cartridge purified and ligated into *Nde*I-*Bam*HI-digested pDB591 to form pDB597. Construction of pDB597 results in a fusion of the *nifH*-transcriptional and -translational elements to the coding portion of the *nifE* gene. In the final step of plasmid constructions pDB597 was digested with *Nde*I and ligated with the same synthetic DNA cartridge described above to form plasmid pDB867. This construction places seven in-frame histidine codons between the initiating methionine-codon and the second codon of the *nifE* -coding sequence. The fusion of the *nifH* promoter sequence with the *nifE*-coding sequence carried by pDB867 was then transferred to the *A. vinelandii* chromosome to yield strain DJ1041. This construction was accomplished by transformation using congression (coincident transfer of unlinked genetic markers) where the rifampicin-resistance marker contained in pDB303 [64] was used as the selected marker. The phenotype of DJ1041 is Nif^- and Rif^R.

Cell growth, purification of the NifEN complex, and assays. *A. vinelandii* cells were grown at 30°C in a 150-L custom-built fermenter (W. B. Moore, Inc. Easton , PA) in modified Burk medium containing 10 μM Na_2MoO_4 and 10 mM urea[104]. Cultures were sparged with pressurized air (80 l/min at 5 psi) and agitated at 125 rpm. When the cell density reached 180 Klett units (red filter) they were derepressed for *nif* expression by concentration and resuspension in Burk medium with no added nitrogen source [44]. Harvested cells were stored at

-80°C until used. Crude extracts were prepared by the osmotic shock method [105] in degassed buffer containing 25 mM Tris-HCl (pH 7.9) and 1 mM Na dithionite. Prior to NifEN complex purification, the extracts were made 500 mM in NaCl by the addition of degassed, granular NaCl. All biochemical manipulations were performed under an Argon atmosphere using a Schlenk apparatus. Approximately 120 g of cells (wet weight) were processed for each purification yielding approximately 10 g of total protein in the crude extract. The NifEN complex was purified using immobilized metal-affinity chromatography (IMAC) and DEAE-sepharose anion-exchange chromatography (Amersham-Pharmacia, Piscataway, NJ). Cell extracts were loaded on an IMAC Zn(II)-charged column (30 ml of resin in a 1.5 cm x 15 cm column) using a peristaltic pump. After loading the extract, the column was washed with three column volumes of the above buffer containing 20 mM imidazole-HCl. The protein that remained bound to the column was then eluted using the above buffer containing 250 mM imidazole-HCl. The eluted protein was collected and diluted 7 x in a degassed buffer (25 mM Tris-HCl, pH 7.9) containing 1 mM Na dithionite. The diluted protein was then loaded onto a DEAE-sepharose column (30 ml of resin in a 1.5 cm x 15 cm column) and eluted using a linear NaCl gradient (100 mM to 300 mM NaCl over 5 column volumes). The NifEN fraction, which eluted at approximately 250 mM NaCl, was collected and concentrated using an Amicon concentrator (Beverly, MA) fitted with a YM100 filter. Concentrated protein was pelleted and stored in liquid nitrogen until used. Protein purity was monitored by SDS-PAGE electrophoresis as previously described [44]. Protein was quantitated by the BCA method using bovine serum albumin as the standard [106].

NifEN activity was determined by slight modifications of previously described procedures [60, 66]. Each degassed 9-ml reaction vial included 0 to 60 μg of isolated NifEN,

100 μl of 25 mM Tris-HCl (pH 7.4, 1.0 mM Na dithionite), 20 μl of 5 mM homocitrate, 10 μl of 1.0 mM Na_2MoO_4, 200 μl of an ATP-regenerating system (containing 3.6 mM ATP, 6.3 mM $MgCl_2$, 51 mM phosphocreatine, 20 unit/ml creatine phosphokinase, and 6.3 mM Na dithionite), and 200 μl of DJ1007 (Δ*nifE*) crude extract. The reaction vial also included an excess of B-cofactor, which is necessary for FeMo-cofactor biosynthesis (20 μl of an isolated B-cofactor preparation (60 mg of Fe/L) provided by V. K. Shah was used [58]). Vials were incubated at 30 °C for 30 min to allow FeMo-cofactor biosynthesis and insertion into apo-MoFe protein present in the DJ1007 crude extract. An additional 800 μl of the ATP-regenerating system was then added, the vials brought to 1 atm, and a 30 min acetylene reduction assay was performed under a 10% acetylene atm at 30 °C. Ethylene formation was monitored using a Hewlett Packard 5890A gas chromatograph equipped with an FID detector. The amount of apo-MoFe protein present in the DJ1007 extract was estimated by the reconstitution system using isolated FeMo-cofactor (100 mg of Fe/L) as previously described [11]. FeMo-cofactor used in the present work was a gift from V. K. Shah.

Metal analysis. Fe was quantitated by the α,α' bipyridyl method [107], and Mo was quantitated by inductively coupled plasma emission (Utah State University, Soil Testing Laboratory).

Preparation of Antisera Against NifN. For the preparation of antibodies against NifN for use in western analyses, NifN was produced at a high level in *E. coli* and purified. For this purpose a PCR-generated *nifN* gene cartridge was cloned into the *Nde*I-*Bam*HI sites of the cloning vector pT_7-7 to form pDB560. This construct places expression of *nifN* under the T_7 control elements. Plasmid pDB560 was then transformed into the *E. coli* host strain BL21(DE3). NifN was then

produced at a high level and purified by using essentially the same procedures previously described for the high level of expression and purification of NifU [88]. Purified NifN was then sent to Cocalico Biologicals Inc., Reamstown, PA, for commercial production of Rabbit anti-NifN antisera. Chemicals for western analysis were obtained from ICN Biomedicals (Costa Mesa, CA) and the procedures recommended by the supplier were followed.

Spectroscopic Characterization of NifEN. The sample concentrations given in the figure captions are based on the quantitation of the purified protein solution by the BCA method [106]. Spectroscopic results were quantified per αβ–heterodimer. UV-Visible absorption spectra were recorded under anaerobic conditions in septum-sealed 1-mm cuvettes using a Shimadzu 3101PC scanning spectrophotom[1]eter. Variable-temperature magnetic circular dichroism (VTMCD) spectra were recorded on samples containing 55% (v/v) glycerol in 1-mm cuvettes using an Oxford Instruments Spectromag 4000 (0-7 T) split coil superconducting magnet (1.5-300 K) mated to a Jasco J-715C spectropolarimeter. Experimental protocols used for VTMCD studies were performed as previously described [108, 109]. X-band (~9.6 GHz) Electron Paramagnetic Resonance (EPR) spectra were recorded on a Bruker ESP-300E EPR spectrometer equipped with a dual mode ER-4116 cavity and an Oxford Instruments ESR-9 flow cryostat. Frequencies were measured with a Systron-Donner 6054B frequency counter, while the magnetic field was calibrated with a Bruker ER035M gaussmeter. Spin quantitations were carried out under non

[1] Abbreviations: VTMCD, variable-temperature magnetic circular dichroism; RR, resonance Raman; NHE, normal hydrogen electrode

saturating conditions with 1mM Cu(II)EDTA as the standard, using the procedures outlined by Aasa and Vänngård [110].

Resonance Raman spectra were recorded using an Instruments SA Ramanor U1000 spectrometer fitted with a cooled RCA 31034 photomultiplier tube with 90° scattering geometry. Spectra were recorded digitally using photon-counting electronics, and signal-to-noise was improved by signal averaging of multiple scans. Band positions were calibrated using the excitation frequency and CCl_4 and are accurate to $\pm 1 cm^{-1}$. Laser excitation lines were from a Coherent Innova 100 10-W argon ion laser, with plasma lines removed using a Pellin Broca Prism premonochromater. Resonance Raman samples were placed in a specially designed sample cell [111] at the end of an Air Products Displex Model CSA-202E closed-cycle refrigerator and remained at 28 K and under an atmosphere of argon throughout scanning. The low sample temperature facilitates improved spectral resolution and prevents laser-induced sample degradation. Scattering was collected from the surface of a frozen 12 μL droplet.

EPR redox titration was performed at ambient temperature (25-27° C) within a glovebox under anaerobic conditions, using 20 mM Tris-HCl buffer (pH 7.9) and 300 mM NaCl. The concentration of the NifEN complex was 140 μM. Each mediator dye was added to a concentration of 50 μM in order to cover the range of -500 through -100 mV (vs NHE). The mediator dyes used were methyl viologen, benzyl viologen, neutral red, safranin O, anthraquinone-2-sulfonate, phenosafranin, and anthraquinone-1-5-disulfonate. Samples were first reduced by addition of excess sodium dithionite followed by oxidative titration with potassium ferricyanide. Potentials were measured with a platinum working electrode and a saturated Ag/AgCl reference electrode. After equilibration at the desired potential, a 250 μL

aliquot was transferred to a calibrated EPR tube and frozen immediately in liquid nitrogen. Redox potentials are reported relative to the NHE.

Results

Expression and Purification of the NifEN complex. Figure 1 shows a schematic of the relevant genomic *nif* region for the wild type (DJ) and the two strains (DJ1061 & DJ1041) that were constructed by gene-directed mutagenesis and gene-replacement techniques. Strain DJ1041 was designed for: (a) the elevated production of the *nifEN* gene products and, (b) the facile purification of the NifEN complex by using IMAC. The first of these goals was achieved by deleting the intervening region between the relatively strong *nifH* promoter and the *nifEN* structural genes, thereby placing the expression of *nifEN* under the direction of the *nifH* transcriptional and translational control elements. The second goal was made possible by placing seven histidine codons between the methionine initiation codon and the second codon of the *nifE*-coding sequence. Strain DJ1061 was constructed to: (a) determine whether or not insertion of the polyhistidine coding sequence at the N-terminus of *nifE* alters the *in vivo* activity of the NifEN complex and, (b) permit the comparison of the relative amounts of the NifEN complex that accumulate when *nifEN* expression is driven by either the *nifE*- or the *nifH*-control elements. Both the wild type and DJ1061 grow at the same rate (doubling-time of 2.2 - 2.4 hours) when cultured under diazotrophic growth conditions. Thus, because strains deleted for *nifE* are unable to grow diazotrophically [65], this result indicates that placement of the poly-histidine tail at the N-terminal region of NifE does not impair the NifEN complex to an extent that can be detected *in vivo*. Figure 2A and 2B show SDS-PAGE profiles for fractions obtained

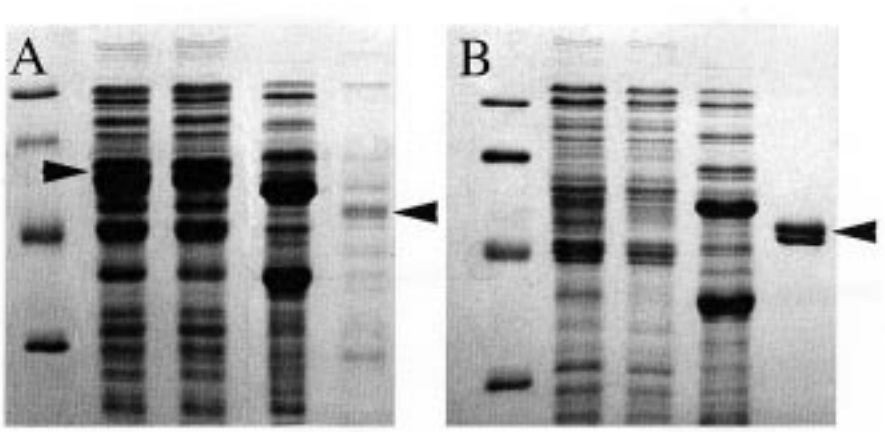

Figure 2. Gel electrophoresis of various stages during the IMAC purification of the NifEN complex from DJ1061 (panel A) and DJ1041 (panel B). The proteins were separated by 12% SDS-PAGE and stained with Coomassie brilliant blue. Lane 1, M_r standards (phosphorylase b, bovine serum albumin, carbonic anhydrase, and soybean trypsin inhibitor); Lane 2, crude extract; Lane 3, column flow through; Lane 4, 20 mM imidazole-HCl wash fraction; Lane 5, purified NifEN complex. Arrows pointing left indicate the position of NifE (upper band) and NifN (lower band). The arrow pointing right in panel A indicates the position of the MoFe protein α- and β-subunits. Corresponding MoFe protein subunit bands are not seen in panel B because *nifDK* are deleted in strain DJ1041.

during the purification of the NifEN complex from DJ1061 and DJ1041, respectively. The simple four-step purification procedure involves: (i) passing a crude extract prepared from *nif*-derepressed cells over a Zn(II) charged IMAC column, (ii) washing the column with a 20 mM imidazole-HCl buffer, (iii) eluting the bound protein with 250 mM imidazole-HCl buffer, and (iv) anion-exchange column chromatography. The relative amounts of NifEN complex purified from DJ1061 and DJ1041 shown in Figure 2, which represent different purifications performed on different days, cannot be quantitatively compared. Nevertheless, examination of the individual panels in Figure 2, which compare individual fractions at different stages of purification, clearly indicates that the amount of NifEN complex that can be purified from DJ1041 is much higher than from DJ1061. About 70 mg of pure NifEN complex can be routinely obtained from 10 gm of DJ1041 crude extract protein whereas only about 7 mg of NifEN complex can be obtained from the same amount of DJ1061 crude extract protein. Also, the estimated amount of NifEN complex obtained from DJ1061 crude extracts is probably an overestimation because there is a significant amount of contaminating proteins in the purified sample from DJ1061, as can be seen by inspection of lane 5 in Figure 2A. Identification of the protein bands indicated as NifEN in Figure 2 was confirmed in two different ways. First, bands at a similar location were not recognized when crude extract from the wild-type strain was processed in the same way. This result is consistent with the fact that NifE from the parental wild-type strain does not have a polyhistidine tail. Second, the bands corresponding to NifN in Figure 2 were identified by western analysis (data not shown) using rabbit antibodies raised against purified NifN protein that was heterologously expressed in *E. coli*. Although the amount of NifEN complex accumulated by DJ1041 is much greater than that accumulated by DJ1061, the yield is still lower than might be expected for proteins whose synthesis is directed by the

nifH-control elements. For example, in related studies we have also placed a polyhistidine tag near the N-terminus of *nifD*, which encodes the α-subunit of the MoFe protein, and whose synthesis is naturally directed by the *nifH*-promoter. By using the same IMAC approach described here for NifEN purification, 350 mg of polyhistidine tagged MoFe protein, having full catalytic activity (≈ 2,000 nmoles H_2 evolved · min^{-1} · mg^{-1} protein), can be routinely isolated from 10 g of nitrogenase-derepressed crude extract (Christiansen, Goodwin, Zheng & Dean, unpublished). Although it is not known why NifEN from DJ1041 accumulates to levels lower than might be expected, it was found that the amount of NifEN that can be detected in crude extracts by western analysis drops dramatically after about three hours of nitrogenase derepression (data not shown). This result indicates that the NifEN complex might have a relatively short *in vivo* half-life. Roll *et al* [60] have also reported that the yield of NifEN complex obtained by using other purification methods is dependent upon the genetic background from which the complex is isolated.

IMAC-Purified NifEN Complex Activity. Previous work has shown that the NifEN complex isolated from a *nifB*-deficient *A. vinelandii* strain can be added to a *nifEN*-deficient crude extract to achieve activation of the apo-MoFe protein, providing other factors necessary for FeMo-cofactor biosynthesis (MgATP, Mo, and homocitrate) are also included [60, 66]. Furthermore, FeMo-cofactor biosynthetic activity is maximized in this system when an excess of B-cofactor, product of NifB activity, is also added to the reaction mixture. In the present work it was important to establish that the NifEN complex isolated by the IMAC method has the same composition and a similar ability to participate in FeMo-cofactor biosynthesis as previously reported for NifEN complex isolated by other methods. These features were demonstrated in the

following ways. The ability of IMAC-purified NifEN complex to activate apo-MoFe protein in extracts prepared from a *nifE*-deletion mutant was shown to be almost identical to that described for NifEN complex that was purified using the original purification scheme reported by Paustian *et al*. (Figure 3B; see Figure 5 in ref. [66]). The maximum amount of activation of apo-MoFe protein effected by IMAC-purified NifEN complex (Figure 3B) also corresponds to the maximum amount of reconstitution that can be achieved by addition of isolated FeMo-cofactor to the same extract (Figure 3A). IMAC-purified NifEN complex was shown to be an $\alpha_2\beta_2$ tetramer by its mobility on a gel exclusion chromotography column (data not shown). It was also found that, like the NifEN complex previously characterized [66], IMAC-purified NifEN is oxygen-labile, contains Fe, and exhibits a characteristic UV-Visible spectrum in its oxidized and reduced states (Figure 4).

Biophysical Characterization of the NifEN Complex Fe-S Clusters: UV-visible Absorption. Figure 4 shows the UV-Visible absorption of oxidized and reduced NifEN. The oxidized spectrum with its pronounced shoulder at 410 nm is characteristic of proteins containing [4Fe-4S]$^{2+}$ clusters [112]. Upon reduction with dithionite, the peak at 410 nm diminishes and a broad featureless spectrum indicative of a [4Fe-4S]$^{+}$ cluster appears. The molar extinction coefficients for oxidized (ε_{410}=13,500 $M^{-1}cm^{-1}$) and reduced (ε_{390}= 9,500 $M^{-1}cm^{-1}$) NifEN (expressed per αβ-dimer) indicate two [4Fe-4S]$^{2+,+}$ clusters per NifEN $\alpha_2\beta_2$-tetramer. These results are also in good agreement with iron analyses of NifEN, which indicate 9.5 ± 0.5 iron atoms per $\alpha_2\beta_2$-tetramer, with no Mo detected.

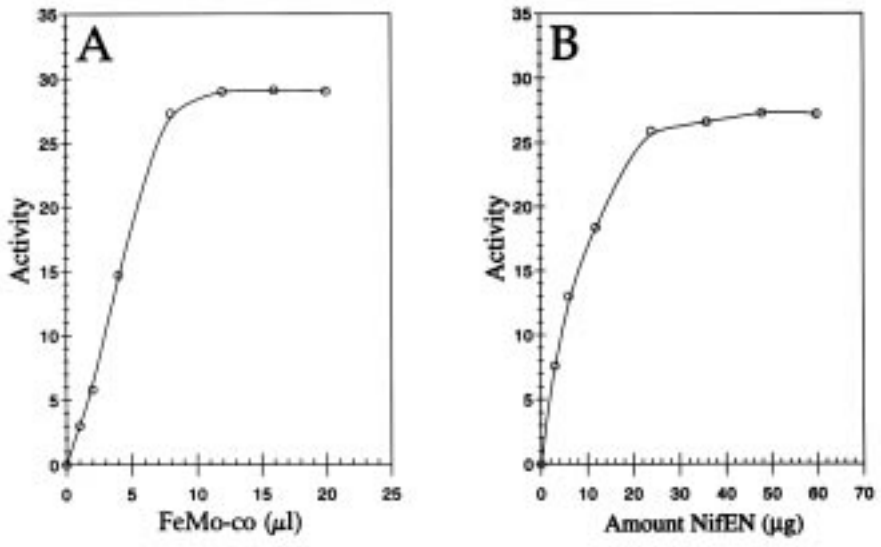

Figure 3. Reconstitution of apo-MoFe protein using either isolated FeMo-cofactor (panel A) or the FeMo-cofactor biosynthesis system (panel B), as described in *Experimental Procedures*. MoFe protein activity is expressed as nanomoles of ethylene produced per min. Assay conditions are described in Experimental Procedures. For the biosynthetic assay shown in panel B all known components required for FeMo-cofactor biosynthesis are present in excess except for the NifEN complex. The same crude extract (9.0 mg for each assay) was used for all reconstitution assays shown in panel A and panel B. Data points represent the average of two independent assays.

EPR and EPR-monitored Redox Titration. X-band EPR spectra of dithionite-reduced NifEN were recorded at temperatures in the range 4.2-100 K with microwave powers between 0.001 and 100 mW. A less extensive series of experiments were conducted on NifEN samples containing 55% (v/v) glycerol (i.e. the same samples used for VTMCD studies), and the EPR properties were found to be unperturbed by the presence of glycerol. A representative EPR spectra of dithionite-reduced NifEN is shown in Figure 5. The protein exhibits a rhombic spectrum, g = 2.10, 1.92, 1.85, that is only discernible at temperatures below 30 K. This resonance accounts for 1.1 spins per αβ-dimer and except for a minor adventitious Fe^{3+} ion signal centered at g = 4.3, there was no evidence for any $S > 1/2$ resonances in the low field region. Taken together, the spin quantitation, g-values and the relaxation properties indicate two $S = 1/2$ $[4Fe\text{-}4S]^{+}$ clusters per $\alpha_2\beta_2$-tetramer. In order to assess the midpoint potential of the $[4Fe\text{-}4S]^{2+,+}$ couple, a dye-mediated EPR-monitored redox titration of purified NifEN was carried out at pH 7.9. Figure 6 shows a plot of the intensity of the $S = 1/2$ resonance as a function of the potential. A one-electron Nernst plot overlays the individual data points to a good approximation, indicating a midpoint potential of -350 ± 20 mV.

VTMCD. Temperature-dependant MCD bands are observed throughout the 300-800 nm region in the VTMCD spectra of reduced NIFEN (Figure 7). The pattern of these bands is characteristic of a $[4Fe\text{-}4S]^{+}$ cluster [112-115], with the derivative feature centered around 410 nm arising at least in part from a very minor heme contaminant. While the absence of a pronounced negative feature centered around 650 nm is generally indicative of a $S = 3/2$ $[4Fe\text{-}4S]^{+}$ cluster [113, 114],

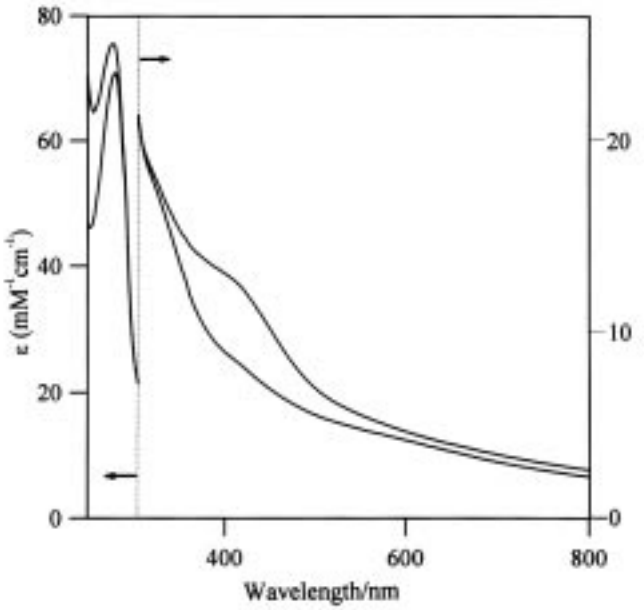

Figure 4. UV-visible absorption spectra for oxidized and reduced NifEN. Excess sodium dithionite was removed from reduced NifEN (lower spectrum) by anaerobic buffer exchange. NifEN was oxidized with thionine (upper spectrum) and the excess was removed by anaerobic buffer exchange.

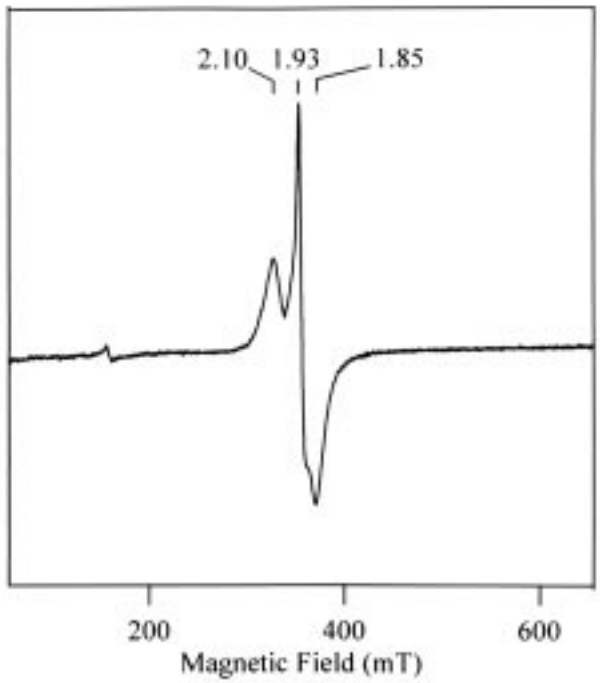

Figure 5. X-band EPR spectrum of dithionite-reduced NifEN. The sample (0.4 mM) was in 20 mM Tris-HCl buffer, pH 7.9, with 1 mM sodium dithionite. Conditions of measurement: microwave frequency, 9.6 GHz; modulation amplitude, 0.64 mT: microwave power, 20 mW; temperature 10 K.

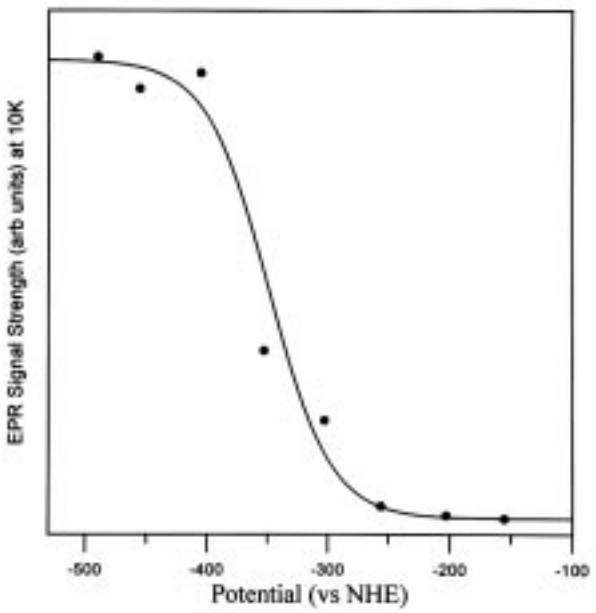

Figure 6. EPR signal intensity (arbitrary units) for NifEN (0.15 mM) as a function of poised potential. Dye-mediated redox titrations were carried out as described in the Experimental section. Data points correspond to the peak-to-trough intensity (g = 1.93 - 1.85) at 10 K. Solid line represents a plot of a one-electron Nernst equation with a midpoint potential (vs NHE) of -350 mV. EPR conditions: temperature 10 K; microwave power, 20 mW; modulation amplitude, 1.02 mT; microwave frequency, 9.60 GHz.

MCD magnetization data collected at 536 nm (Figure 9) indicate that the cluster ground state is predominantly $S = 1/2$, in accord with the EPR results. The magnetization data collected at three fixed temperatures (1.8 K, 4.2 K and 10.0 K) are fit to first approximation by theoretical data constructed using the EPR-determined g-values, $g_{\|} = 2.10$ and $g_{\perp} = 1.89$. The intensities of the low-temperature MCD spectra of paramagnetic Fe-S clusters, compared under equivalent conditions after normalizing for concentration and path length, and correcting for sample depolarization [108, 109], provide an approximate estimation of cluster concentration. Synthetic and biological $S = 1/2$ $[4Fe\text{-}4S]^{+}$ clusters have $\Delta\varepsilon$ values for the positive band at 520 nm in the range of 60-90 $M^{-1}\ cm^{-1}$ at 4.5 T and 2 K [112, 113]. The 2 K MCD spectrum of NifEN, which has $\Delta\varepsilon = 76\ M^{-1}\ cm^{-1}$ when quantified per αβ-heterodimer, complements the UV-visible molar extinction coefficients and the EPR spin quantitation in suggesting that there is one $[4Fe\text{-}4S]^{+}$ cluster per NifEN αβ-heterodimer.

Resonance Raman. Resonance Raman spectra in the Fe-S stretching region, 200-450 cm^{-1} provide a means for identifying both Fe-S type in diamagnetic redox states [116, 117] and assessing the cluster ligation [114, 118]. The RR spectrum of thionine-oxidized NifEN complex obtained with 457.9-nm laser excitation is shown in Figure 9. The vibrational frequencies and relative intensities of the Fe-S stretching modes are characteristic of those established for $[4Fe\text{-}4S]^{2+}$ clusters [119, 120] and can be assigned by direct analogy under idealized tetrahedral symmetry for the $Fe_4S_4{}^{b}S_4{}^{t}$ unit (b = bridging and t = terminal), i.e. (T_2) $Fe\text{-}S^{b}$, 251 cm^{-1}; (T_1) $Fe\text{-}S^{b}$, 265 cm^{-1}; (E) $Fe\text{-}S^{b}$, 280 cm^{-1}; (A_1) $Fe\text{-}S^{b}$, 340 cm^{-1}; (T_2) $Fe\text{-}S^{t}$, 356 cm^{-1}, (T_2) $Fe\text{-}S^{b}$, 383

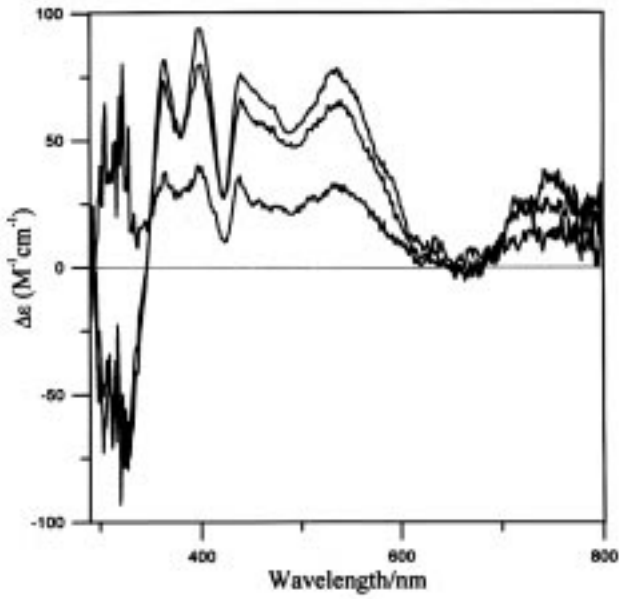

Figure 7. VTMCD spectra of dithionite-reduced NifEN. The sample (0.1 mM) was in 20 mM Tris-HCl buffer, pH 7.9, with 1 mM sodium dithionite and 55% (v/v) glycerol. The MCD spectra were recorded in a 1-mm cuvette with a magnetic field of 6.0 T, at 1.8, 4.2, and 10.0 K. All bands increase in intensity with decreasing temperature.

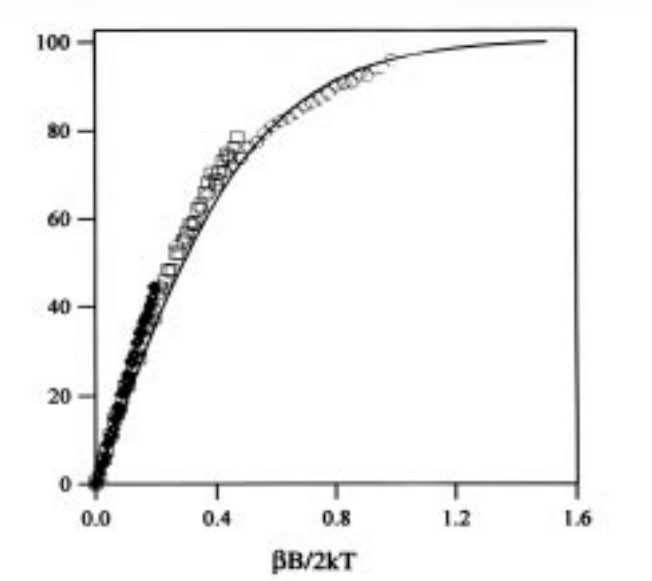

Figure 8. MCD magnetization data for dithionite-reduced NifEN. Sample description is given in Fig. 7. NifEN magnetization collected at 536 nm using magnetic fields between 0 and 6 T and fixed temperatures of: 10.0 K (◊), 4.2 K, ([]) 1.8 K (O). Solid line is theoretical magnetization data for a S = 1/2 ground state using EPR-determined g-values $g_{||}$= 2.098 and g =1.888 and with $m_{z/xy}$ = 1.1.

cm^{-1}, (A_1) Fe-S^t, 390 cm^{-1}. For example, resonance Raman spectra having similar relative band intensities and frequencies are observed for the $[4Fe\text{-}4S]^{2+}$ cluster contained in the nitrogenase Fe protein [120] and in synthetic analog complexes having benzyl thiolate ligands [119]. The frequency of the most intense band, which corresponds to the totally symmetric breathing mode of the Fe_4S_4 cubane, has been found to a be a useful indicator of non-cysteinyl coordination at a specific Fe [114]. This band occurs at 340 cm^{-1} in NifEN, just outside the range established for $[4Fe\text{-}4S]^{2+}$ clusters with complete cysteinyl ligation (333-339 cm^{-1} [114]) and within the range established for clusters with oxygenic ligation at a specific Fe site (339-342 cm^{-1} [114, 121]). Although this raises the possibility of an oxygenic cluster ligand, the slightly higher (A_1) Fe-S^b frequency could equally well be the result of a hitherto uninvestigated arrangement of coordinating cysteine residues. For example, sequence comparisons with the MoFe protein suggest cluster ligation by three cysteines from the NifE subunit and one from the NifN subunit, see below. This type of subunit bridging arrangement would be unique among Fe-S proteins and hence could account for a slightly higher frequency for the totally symmetric breathing mode.

Discussion

It was previously shown [65, 100] that the products of the FeMo-cofactor biosynthetic genes, *nifE* and *nifN*, bear sequence identity when respectively compared to the α- and β-subunits of the MoFe protein. In other words, NifE has a primary sequence similar to NifD (MoFe protein α-subunit), and NifN has a primary sequence similar to NifK (MoFe protein β-subunit). Such primary sequence comparisons, the relative migration patterns of NifD, NifK, NifE and NifN on two-dimensional electrophoretic gels [122], the *in vivo* mutual stability requirements for

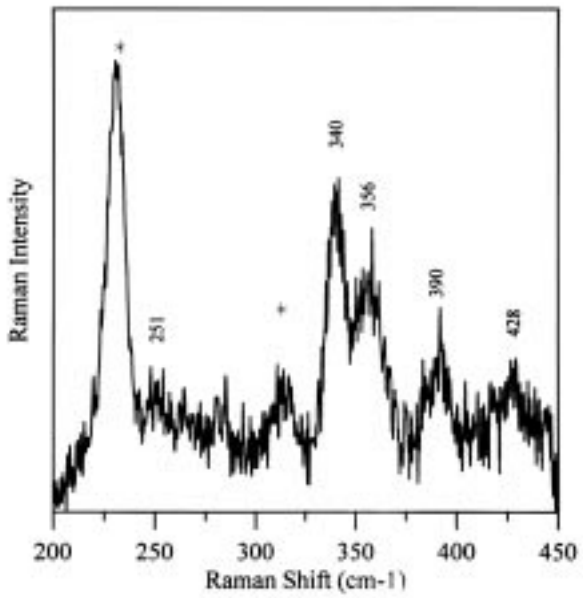

Figure 9. Low-temperature resonance Raman spectrum of thoinin-oxidized NifEN. Protein concentration was ~3 mM, and the buffering medium was 20 mM Tris HCl, pH 7.9. The spectrum was obtained at 28 K using 457.9-nm argon laser excitation and is the sum of 103 scans. Each scan involved advancing the spectrometer in 0.5 cm^{-1} increments, and photon counting for 1s/point with 6 cm^{-1} spectral resolution. A linear ramp was subtracted to correct for background fluorescence and lattice modes of ice are indicated by an asterisk.

NifE and NifN [122], and the observation that FeMo-cofactor biosynthesis is completed prior to its insertion into apo-MoFe protein [63], led to the hypothesis that NifE and NifN form a complex [122] that is structurally homologous to the MoFe protein and which provides a scaffold for one or more steps in FeMo-cofactor biosynthesis [65]. This hypothesis was supported by Paustian *et al.* [66] who purified a tetrameric form of NifEN from *A. vinelandii*, and reported evidence that the as-isolated NifEN complex contains an Fe-S cluster. In the case of the MoFe protein there are two different types of metalloclusters, the P-cluster and the FeMo-cofactor [6, 26, 93]. Thus, by analogy to the MoFe protein, it is reasonable to expect that the NifEN complex could also have two types of metalloclusters. One such site within the NifEN complex could be analogous to the MoFe protein P-cluster site, while the other provides an FeMo-cofactor intermediate assembly site. In this model the NifEN complex is expected to cycle between a "charged" form that contains an FeMo-cofactor intermediate and a "discharged" form that has released the FeMo-cofactor intermediate during maturation of the apo-MoFe protein [7]. Strong evidence supporting this possibility was reported by Roll *et al*. [60] who found that the native electrophoretic mobility of the NifEN complex is different in crude extracts prepared from different genetic backgrounds. For example, the native electrophoretic mobility of the NifEN complex present in a NifB-deficient crude extract is different than the native electrophoretic mobility of NifEN complex present in a crude extract prepared from a strain deleted for *nifHDK* . Importantly, the addition of B-cofactor to a NifB-deficient crude extract alters the native electrophoretic mobility of the NifEN complex so that it assumes the same native electrophoretic mobility as NifEN complex produced from the *nifHDK* deletion strain. Because the originally purified NifEN complex was obtained from a NifB-deficient background, and therefore can not contain B-cofactor, the question arises about the nature and function of the Fe-S cluster

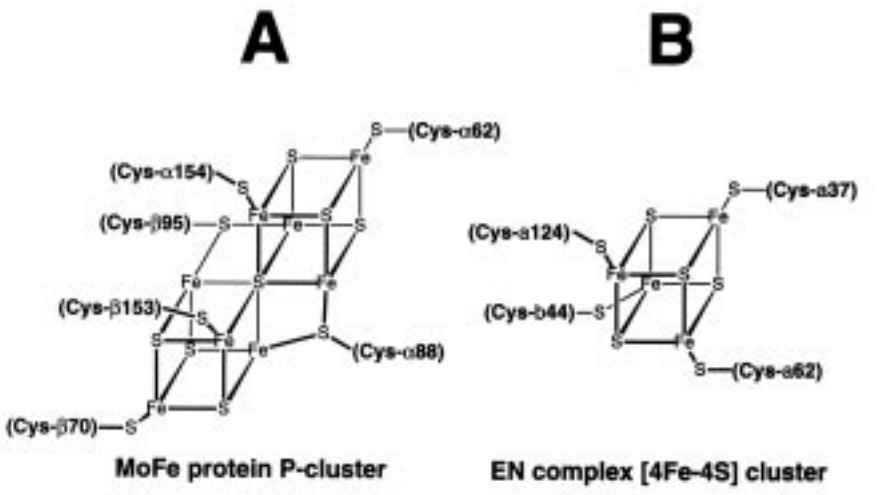

Figure 10. Comparison of the structural model for the P-cluster (62) in its as-isolated P^N state (A) and the proposed structure and organization of the NifEN complex [4Fe-4S] cluster (B). In the above schematic the NifEN complex residues from the NifE subunit are indicated as (a) and the residue from the NifN subunit is indicated as (b). Primary sequence comparisons (21, 33) indicate that MoFe protein residues α-62, α-88, α-154, and β-70 are located at equivalent positions to residues a-37, a-62, a-124, and b-44, respectively, in the primary sequence of the NifEN complex.

contained in the as-isolated NifEN complex. It should be noted that, although it appears that B-cofactor is attached to the NifEN complex in the early stages of its purification from a NifHDK deficient background, NifEN complex isolated from either a NifB-deficient or a NifHDK-deficient background appear to be identical [66]. In other words, B-cofactor is lost from the NifEN complex during its purification from a MoFe protein-deficient background.

In order to purify enough NifEN complex for rigorous biophysical analyses, gene fusion and affinity purification methods were respectively used to elevate the *in vivo* level of NifEN complex and to facilitate its rapid and efficient purification. The NifEN complex produced and purified in this way is apparently unaltered in either its *in vivo* or *in vitro* activities. In the present study a combination of UV-Visible, EPR, VTMCD, and resonance Raman spectroscopies have been used to show that the Fe contained in the as-isolated NifEN complex is organized into two identical $[4Fe\text{-}4S]^{2+,+}$ clusters. These clusters are ligated to the protein complex for the most part or entirely by cysteine residues, have predominantly $S=1/2$ ground in the reduced form, and exhibit a midpoint potential of -350 mV. What then is the function of the [4Fe-4S] clusters contained within the as-isolated NifEN complex? Among the obvious possibilities are: (i) they play a structural role in formation or stabilization of the tetrameric complex, (ii) they have a redox function that is necessary for FeMo-cofactor formation, (iii) they are FeMo-cofactor precursors, or (iv) some combination of these possibilities.

Muchmore *et al.* [62] have previously developed a homology model for the three-dimensional structure of the NifEN complex that is based on the crystallographically solved MoFe protein structure [26]. This model places four cysteine residues (three from NifE - residues-37, -62 and -124; and one from NifN - residue-44) in the appropriate geometry to form a [4Fe-4S] cluster that is located at the NifE-NifN interface at a position analogous to the MoFe

protein P cluster site (Figure10). We favor this model because the four proposed [4Fe-4S] cysteine ligands, and the proposed FeMo-cofactor assembly site cysteine (residue-250 [65, 100]), are the only conserved cysteines among all known NifE and NifN primary sequences [61]. This model indicates that the NifEN complex [4Fe-4S] clusters are most likely to play structural or redox roles rather than becoming incorporated into FeMo-cofactor during its assembly because it places the proposed [4Fe-4S] cluster sites at positions that are remote from the proposed FeMo-cofactor assembly sites [62]. Site-directed mutagenesis and gene-replacement experiments similar to those used to alter the functional properties of the P cluster [123] should be useful in clarifying the functional role of the [4Fe-4S] clusters contained within the NifEN complex. This approach, and the availability of relatively large amounts of purified NifEN complex, should also help extend the experimental strategy described Roll *et al.* [60] to clarify the nature of the interaction of B-cofactor with the NifEN complex and to determine if the B-cofactor Fe-S core is rearranged or further processed upon its binding to the NifEN complex.

Acknowledgements

We thank Dr. Vinod Shah for supplying samples of B-cofactor and FeMo-cofactor and for providing invaluable advice and Paul Ludden for permitting a portion of this work to be completed in his laboratory. We thank Shannon Garton and Chris Staples for help with the spectroscopic measurements and Amr Ragab for expert technical assistance. We also thank Dr. Jason Christiansen for helpful discussion throughout the preparation of this manuscript.

CHAPTER II

Catalytic and Biophysical Properties of a Nitrogenase apo-MoFe protein produced by a *nifB*-deletion mutant of *Azotobacter vinelandii.*

This Chapter was written by the combined efforts of myself, Jason Christiansen[‡], William N. Lanzilotta[§], Lance C. Seefeldt[§*] and Dennis R. Dean[‡] and was published in the journal *Biochemistry* (Christiansen *et al.*,1998). I was involved in all aspects of the experiments performed for the preparation of this manuscript. Experiments pertaining to recombinant DNA technology, bacterial strain construction , protein purification and protein characterization were performed with Jason Christiansen in the laboratory of Dennis Dean at Virginia Tech. Plasmids used in strain construction were prepared by technician Valerie Cash of Dennis Dean's laboratory. Experiments involving electron paramagnetic resonance spectroscopy and stopped-flow spectrophotometry were performed by the combined efforts of myself, Jason Christiansen and William Lanzilotta in the laboratory of Lance Seefeldt at Utah State University.

[‡] Department of Biochemistry - Fralin Biotechnology Center, Virginia Tech, Blacksburg, VA 24061

[§] Department of Chemistry and Biochemistry, Utah State University, Logan, UT 84322

Summary

A Zn immobilized metal-affinity chromatography technique was used to purify an FeMo-cofactorless MoFe protein (apo-MoFe protein) from a *nifB* deletion mutant of *Azotobacter vinelandii*. Apo-MoFe protein prepared in this way was obtained in sufficient concentrations for detailed catalytic, kinetic, and spectroscopic analyses. Metal analysis and electron paramagnetic resonance spectroscopy (EPR) was used to show that the apo-MoFe protein does not contain FeMo-cofactor. The EPR of the as-isolated apo-MoFe protein is featureless except for a minor *S*=1/2 signal probably arising from the presence of either a damaged P cluster or a P cluster precursor. The apo-MoFe protein has an $\alpha_2\beta_2$ subunit composition and can be activated to 80% of the theoretical MoFe protein value by the addition of isolated FeMo-cofactor. Oxidation of the as-isolated apo-MoFe protein by indigodisulfonate was used to elicit the parallel mode EPR signal indicative of the two-electron oxidized form of the P cluster (P^{2+}). The midpoint potential of the P^N/P^{2+} redox couple for the apo-MoFe protein was shown to be shifted by -63 mV when compared to the same redox couple for the intact MoFe protein. Although the apo-MoFe protein is not able to catalyze the reduction of substrates under turnover conditions, it does support the hydrolysis of MgATP at 60% of the rate supported by the MoFe protein when incubated in the presence of Fe protein. The ability of the apo-MoFe protein to specifically interact with the Fe protein was also shown by stopped-flow techniques and by formation of an apo-MoFe protein-Fe protein complex. Finally, the two-electron oxidized form of the apo-MoFe protein could be reduced to the one-electron oxidized form (P^{1+}) in a reaction that required Fe protein and MgATP. These results are interpreted to indicate that the apo-MoFe protein produced in a *nifB*-deficient genetic backround contains intact P clusters and P cluster polypeptide environments.

Small changes in the electronic properties of P clusters contained within the apo-MoFe protein are most likely caused by slight perturbations in their polypeptide environments.

Introduction

Nitrogenase is a complex, two-component metalloprotein composed of the iron (Fe) protein and the molybdenum-iron (MoFe) protein [7]. The Fe protein is a 64 kD homodimer that contains two MgATP binding sites and a single [4Fe-4S] cluster [9]. The MoFe protein is a 240 kD $\alpha_2\beta_2$ tetramer that contains two pairs of novel metalloclusters, called P clusters and FeMo-cofactors [28, 124]. The structures of the two nitrogenase component proteins, together with models of their associated metalloclusters, have been determined by x-ray crystallography [9, 23, 28]. During catalysis the Fe protein serves as a specific reductant of the MoFe protein, which in turn provides the site of substrate reduction [47]. The most probable direction of electron flow in this process is shown in Scheme 1.

Scheme 1

Fe protein [4Fe-4S] cluster → MoFe protein [P cluster] → MoFe protein [FeMo-cofactor] → substrate

A major challenge of nitrogen fixation research is to understand how the mutliple electrons required for substrate reduction are delivered by the Fe protein and accumulated within the MoFe protein. How P clusters might accept electrons from the Fe protein during intercomponent electron transfer is currently enigmatic because they are believed to be already fully reduced in the as-isolated resting state [125]. Two approaches that should be useful to probe the function of the P cluster include substitution of amino acids that provide the coordination shell that surrounds the P cluster, and alteration of P cluster function by treatment with small molecule inhibitors of nitrogenase catalysis, such as NO, CN^-, and CO. In the case of nitrogenase there are several caveats to these approaches that, so far, have denied an unambiguous assignment of the role of P clusters in the nitrogenase catalytic mechanism. First,

it is not possible to treat the P clusters with small molecule inhibitors of nitrogenase catalysis without also affecting the function of FeMo-cofactor. For this same reason, evaluation of perturbations in the P cluster environment caused by amino acid substitutions cannot be made with complete confidence that new spectroscopic or catalytic features have not been elicited by an attendant alteration in FeMo-cofactor or its polypeptide environment. Finally, we have found that many of the potentially most interesting MoFe proteins altered by site-directed mutagenesis can not be characterized owing to their lability during the standard purification procedure, which involves a heat step and strong ion-exchange chromatography [126, 127].

One possible way to circumvent these problems would be to isolate an FeMo-cofactorless form of the MoFe protein that contains intact P clusters and can be activated by the simple addition of isolated FeMo-cofactor. To be useful for the approaches described above, it is necessary that such a protein be amenable to isolation in sufficient quantities for detailed catalytic, kinetic and spectroscopic analyses. In the present work, site-directed mutagenesis and gene-replacement techniques were used to construct MoFe proteins that respectively contain poly-histidine sequences near the N- or C-terminus regions of their α-subunits. An immobilized metal-afinity chromatography (IMAC)-based technique was developed for the rapid and gentle purification of these MoFe proteins. Gene-directed mutagenesis was also used to construct derivatives of these strains which are inactivated for *nifB* gene function. It has previously been shown that MoFe protein from *nifB*-deficient mutants do not contain FeMo-cofactor but do contain other metal clusters, presumably P clusters [57, 73]. The same IMAC-based method described above was also used to purify “apo-MoFe protein” from these *nifB*-deficient strains. The catalytic and biophysical properties of the MoFe proteins produced in the present work are described.

Experimental Procedures

Strain Constructions and DNA Biochemistry. Five different *A. vinelandii* strains were used in the present work (Table 1). These include: (i) the high-frequency transforming *A. vinelandii* wild-type strain designated DJ (the strain from which all other mutants were ultimately derived); (ii) a strain that has eight histidine codons placed between the third and fourth codons of the *A. vinelandii* wild-type *nifD* gene (DJ1141). The *nifD* gene encodes the MoFe protein α-subunit [128]; (iii) a strain derived from DJ1141 that also contains an insertion and deletion mutation within the *nifB* gene (DJ1143); (iv) a strain that has seven histidine codons placed between codons 481 and 482 of the wild-type *nifD* gene (DJ995) and; (v) a strain derived from DJ995 that also contains an insertion and deletion mutation within the *nifB* gene (DJ1003).

The plasmid used for initiating construction of DJ1141 was designated pDB280. This plasmid contains a 1.1 kb *Kpn*I restriction enzyme fragment that includes portions of the *A. vinelandii nifH* and *nifD* genes [128] cloned into the pUC19 vector [102]. Plasmid pDB280 DNA was digested with *Age*I and a DNA cartridge encoding eight histidine codons was inserted into this site to form pDB944. The unique *Age*I restriction enzyme site within pDB280 spans the third and fourth codons of *nifD*. The synthetic DNA fragments used to form the cartridge that was inserted into pDB280 to construct pDB944 have the sequences: 5'CGGTCATCACCATCACCACCATCACCACT3' and 5'CCGGAGTGGTGATGGTGGTGATGGTGATGA3'. The gene cartridge contained within the *nifD* coding region of pDB944 was then transferred to the *A. vinelandii* chromosome by double-reciprocal recombination events that occured during transformation using pDB944 as the donor DNA. Procedures for transformation [101] and gene replacement [64, 75] were performed as previously described. Strain DJ1143 was constructed by transformation of DJ1141 to Km^R using pDB218 as the donor DNA. Plasmid pDB218 contains a portion of the *A. vinelandii nifB* gene cloned into the pUC7 vector. Plasmid pDB218 also has an internal portion of the *nifB* gene sequence deleted and replaced by a Km^R gene cartridge. The

Table 1: Strains used in this study

Strain	Features
DJ	Wild type *A. vinelandii* parental strain.
DJ995	Produces MoFe protein that contains seven tandem histidines within the C-terminal region of the α-subun
DJ1141	Produces MoFe protein that contains eight tandem histic within the N-terminal region of the α-subunit.
DJ1003	Same as DJ995 but also contains an insertion and deletion mutation within *nifB.*
DJ1143	Same as DJ1141 but also contains an insertion and deletion mutation within *nifB.*

portion of the *nifB* gene deleted in pDB218 is flanked by *Sph*I restriction enzyme sites [85]. The plasmid used for initiating construction of strain DJ995 was designated pDB875. It contains a 2.9 kb *Sal*I restriction enzyme fragment that includes all of *nifD*, as well as portions of the flanking *nifH* and *nifK* genes [128], cloned into the pUC119 cloning vector [129]. Plasmid pDB875 was digested with *Hind*III and a DNA cartridge encoding seven histidine codons was inserted into this site to form pDB827. The unique *Hind*III site within pDB875 spans *nifD* codons 481 and 482. The synthetic DNA fragments used to form the cartridge had the sequences: 5'AGCTCACCACCATCACCACCACCATGC3' and 5'AGCTGCATGGTGGTGGTGATGGTGGTG3'. The gene cartridge contained within the *nifD* coding region of pDB827 was then transferred to the *A.vinelandii* chromosome by double-reciprocal recombination events that occured during transformation using pDB944 as the donor DNA. Strain DJ1003 was constructed by transforming DJ995 to Km^R using pDB218 as the donor DNA.

Cell Growth and Protein Purification. *A. vinelandii* cells were grown at 30˚C in a 150-L custom-built fermenter (W. B. Moore, Inc. Easton, PA) in modified Burk medium [104] containing 10 μM Na_2MoO_4 and 10 mM urea as a nitrogen source. Cultures were sparged with pressurized air (80 L/min at 5 psi) and agitated at 125 rpm. When the cell density reached ≈220 Klett units (red filter) cells were derepressed for *nif* gene expression by concentration (6-fold) using a custom-built AG Technologies tangential-flow concentrator and resuspension in Burk medium with no added nitrogen source [44]. Harvested cells were stored at -80˚C until used. All protein manipulations were performed under anaerobic conditions maintained using either a Schlenk apparatus [126] or an anaerobic glovebox.

Crude extracts were prepared by the osmotic shock method [105] in a degassed buffer that contained 25 mM Tris-HCl (pH 7.9) and 1 mM Na dithionite. For crude extract preparation, the buffer also contained 0.2 mM PMSF to inhibit protease activity. Prior to purification, the extracts were brought to 500 mM in NaCl by the addition of degassed, granular NaCl. Approximately 360 g of cells (wet weight) were processed for each purification. Poly-histidine

tagged proteins were purified using immobilized metal-affinity chromatography (IMAC) and DEAE-Sepharose anion-exchange chromatography (Amersham-Pharmacia, Piscataway, NJ). Column eluents were monitored at A_{405} using a Pharmacia UV-1 optical detector and control unit (Amersham-Pharmacia, Piscataway, NJ).

Cell extracts were loaded onto a Zn(II)-charged IMAC column (90 mL of resin in a 2.5 cm x 30 cm column) using a peristaltic pump. After loading the extract, the column was washed with three column volumes of Buffer A (25 mM Tris-HCl, pH 7.9, 500 mM NaCl, 1 mM Na dithionite) containing 40 mM imidazole·HCl. The protein that remained bound to the column was then eluted using Buffer A containing 250 mM imidazole·HCl. The eluted protein was collected and diluted 8-fold in a degassed buffer (25 mM Tris·HCl, pH 8.0) containing 1 mM Na dithionite. The diluted protein was then loaded onto a DEAE-Sepharose column (30 mL of resin in a 1.5 cm x 15 cm column) and eluted using a linear NaCl gradient (100 mM to 300 mM NaCl over 5 column volumes). Proteins eluted and were collected at approximately 250 mM NaCl. Proteins were concentrated using an Amicon concentrator (Beverly, MA) fitted with a YM100 filter. Protein was quantitated by a modified biuret method using bovine serum albumin as the standard [130], and protein purity was monitored by SDS-PAGE electrophoresis [131]. The final purified product was pelleted and stored in liquid nitrogen until used.

Assays. Nitrogenase assays were performed as previously described [127, 132]. FeMo-cofactor was extracted into NMF and concentrated as previously described [11]. For apo-MoFe protein activation experiments, 5 μL of isolated FeMo-cofactor (0.31 mg/L in Fe, 0.05 mg/L in Mo) was added to 50 μg of purified apo-MoFe protein and allowed to incubate for 5 minutes with gentle shaking in a 30° C water bath. MoFe protein control samples followed the same steps with or without the addition of isolated FeMo-cofactor. FeMo-cofactor-treated protein was then assayed by the addition of 450 μg of purified Fe protein. Samples were incubated for 8 minutes with gentle shaking in a 30°C water bath and the reaction was terminated by addition of 250 μL of a 0.4 M EDTA solution. H_2 production was monitored by injection of 200 μL of the gas phase into a Shimadzu GC-14 equipped with a Supelco 80/100 molecular sieve 5A column and a TCD

detector. Acetylene reduction assays were performed under a 10% acetylene atmosphere and monitored using a Hewlett-Packard 5890A gas chromatograph equipped with an Al_2O_3 capillary column and a FID detector.

MgATP hydrolysis was determined by a colorimetric assay [133] that measures the rate of creatine produced from the MgATP regenerating system used in the gas chromatography assays described above.

Metal analysis. Fe was quantitated by the α,α' bipyridyl method [107], and Mo was quantitated by inductively coupled plasma emission (Utah State University, Soil Testing Laboratory).

Chemical modification of cysteines. The alkylating reagent, I-AEDANS, was used to determine if the apo-MoFe protein has solvent exposed sulfhydryl groups. For this analysis 130 μg of protein was brought up to a volume of 40 μL by the addition of 0.5 M Tris·HCl, pH 8.0, 1 mM Na dithionite. The alkylation reaction was initiated by addition of 10 μL of a 10 mM I-AEDANS solution to the protein sample followed by incubation at room temperature. The alkylation reaction was terminated at specific time points by the addition of 10 μL of a 1.0 M DTT solution to the sample. Approximately 10 μg of I-AEDANS-treated protein was then loaded onto an SDS-PAGE gel [131] to separate the individual protein bands and to remove excess I-AEDANS. Protein alkylation was visualized by UV illumination of the PAGE gel prior to staining with Coomassie brilliant blue.

UV/Visible absorption spectroscopy. UV/Visible spectra were collected on a Hewlett-Packard 8452A diode array spectrophotometer. Samples were prepared by passage over a Sephadex G-25 column to remove Na dithionite or a Dowex 1X8-100 ion exchange column (Sigma, St. Louis, MO) to remove IDS. Samples were sealed inside a 1 cm pathlength quartz cuvette under anoxic conditions [134]. Final protein concentration was 1.2 mg/mL for all samples.

EPR and Redox Titrations of MoFe protein and apo-MoFe Protein. EPR spectra were recorded on a Bruker ESP300E spectrometer equipped with a dual mode cavity and an Oxford ESR 900 liquid helium cryostat. Unless otherwise noted, all spectra were recorded as follows: Parallel mode spectra were recorded at 12 K with a microwave power of 10.1 mW, microwave frequency of 9.39 GHz, modulation amplitude of 7.969 G, modulation frequency of 100 kHz, and time constant and conversion time of 10.24 ms each. In each case, the final spectrum was the sum of 20 scans. EPR spectra acquired in perpendicular mode were recorded at 12 K with a microwave power of 6.36 mW, microwave frequency of 9.64 GHz, modulation amplitude of 7.969 G, modulation frequency of 100 kHz, and a time constant and conversion time of 10.24 ms. For each case, the final spectrum was the sum of 10 scans.

Potentiometric redox titrations were performed essentially as previously described [135]. Protein samples were prepared for redox titrations by first passing them over a Sephadex G-25 column equilibrated with the appropriate buffer and at the required pH value. For all redox titrations, the redox mediators flavin mononucleotide (E_m = -172 mV and -238 mV), benzyl viologen (E_m = -361 mV), and methyl viologen (E_m = -440 mV) were used at final concentrations of 50 μM each. The redox potential of the titration solution was adjusted by the addition of small aliquots of a 2 mM Na dithionite solution or an oxidized 25 mM IDS solution. At defined potentials, 250 μL aliquots were removed from the titration solution and were immediately frozen in calibrated quartz EPR tubes (Wilmad Co., Buena, NJ). The final concentration for each protein sample analyzed was approximately 75 μM. The reference electrode was a Ag/AgCl microelectrode calibrated against a standard calomel electrode. The electrode calibration was confirmed by performing a redox titration of MoFe protein at pH 8.0, which has a known E_m=-309 mV (vs. NHE) [136]. All potentials are reported relative to the normal hydrogen electrode (NHE).

For analysis of the titration data, the relative concentration of the P^{2+} state of the P cluster was quantified from the peak to baseline height of the $S \geq 3$ parallel mode EPR signal at g =11.8 [125, 136, 137]. Normalized signal intensities were determined by comparing each signal

intensity to the maximum intensity observed at positive potentials. The relative signal intensities were plotted against the applied potential and each data set was fit to the Nernst equation for a one electron transfer [138].

Activation of apo-MoFe protein as monitored by EPR. The same apo-MoFe protein:FeMo-cofactor ratio used in the activation assays described above (50 μg:5 μL) was used to examine the EPR of apo-MoFe protein activated by FeMoFeMo-cofactor. A 250 μL sample of 36.5 mg/mL apo-MoFe protein was diluted into 183 mL of 25 mM HEPES, pH 7.4, and 1 mM Na dithionite. Isolated FeMo-cofoactor (total volume 1.8 mL) was then slowly added to the solution with gentle mixing. After a 5 minute incubation at 30° C, the mixture was loaded onto a DEAE Sepharose column (10 mL resin, 0.5 x 20 cm column) equilibrated in 25 mM Tris·HCl, pH 8.0, and 1 mM Na dithionite. Excess FeMo-cofactor was removed by washing the column with 3 volumes of 100 mM NaCl, 25 mM Tris·HCl, pH 8.0, and 1 mM Na dithionite. FeMo-cofactor-treated MoFe protein was then eluted using a linear salt gradient of 100 mM NaCl to 300 mM NaCl over 4 column volumes. A 250 μL sample of the reconstituted protein (6 mg/mL) was loaded under anoxic conditions into a quartz EPR tube and the EPR spectrum was recorded as described above.

Stopped-Flow Spectrophotometry. The rate constant for the dissociation of Fe protein-MoFe protein complex was determined from stopped-flow experiments by measuring the decrease in A_{430} during the transition of Fe protein from an oxidized to a reduced state as it dissociates from the MoFe protein and is reduced by Na dithionite [139]. Rate constants were determined by fitting the data to a single exponential function. For these experiments, Na dithionite was removed from the reduced, as-isolated, proteins and exchanged into a 50 mM HEPES buffer, pH 7.4, by passage over a Sephadex G-25 column. Oxidized Fe protein was generated by treating the as-isolated Fe protein with increments of a 25 mM IDS solution until a persistent blue color

was observed. IDS was then removed by passing the sample over a Dowex anion exchange column. Experiments were performed using a Hi-Tech SF61 stopped flow spectrophotometer, equipped with a computer controlled data acquisition and analysis package (Hi-Tech, Salisbury, Wilts, UK). The SHU-61 sample handling/mixing unit was kept inside an anaerobic glovebox and temperature was maintained at 22.4 ± 0.1° C with a Techne C-85D closed cycle water circulator attached to a Techne FC-200 flow cooler (Techne Ltd., Duxford, Cambridge, UK). For each experiment, syringe A contained 40 μM IDS-oxidized Fe protein, 40 μM MoFe protein, 5 mM MgADP, and 200 mM NaCl in a 50 mM HEPES buffer, pH 7.4, and syringe B contained 200 μM reduced Fe protein, and 10 mM Na dithioninte in 50 mM HEPES buffer, pH 7.4. For those experiments involving apo-MoFe protein, identical experimental conditions were used except that MoFe protein was replaced with apo-MoFe protein.

The rate constant for primary electron transfer from the reduced Fe protein to the MoFe protein was also determined using stopped-flow and was monitored by an increase in A_{430} that occurs as the Fe protein becomes oxidized during turnover. For these conditions, the apparent first order rate constant of primary electron transfer can be determined by fitting the data to a single exponential function [140, 141]. In these experiments syringe A contained 20 μM MoFe protein, 10 mM MgATP, and 10 mM Na dithionite in 50 mM HEPES buffer, pH 7.4, and syringe B contained 80 μM Fe protein and 10 mM Na dithionite in 50 mM HEPES buffer, pH 7.4.

Complex Formation. Two different methods were used to assess complex formation between the Fe protein and different forms of the MoFe protein. One method involved the use of an altered Fe protein that is deleted for residue Leu^{127} (ΔL127 Fe protein) [95]. The second method involved the use of a phosphate analog, AlF_4^-, and MgATP to capture the Fe protein - MoFe

protein complex [39, 40]. In both types of experiments, a Superose-12 gel exclusion column (Pharmacia, Piscataway, NJ) equilibrated in 100 mM MOPS buffer, 25 mM Tris, pH 7.3, 100 mM NaCl, and 2 mM Na dithionite was used for chromatography. Column eluent was monitored using a Pharmacia UV-1 detector and control unit (see above). Fe protein and MoFe protein were added in a 4:1 molar ratio for both types of experiments.

Electron Transfer to the apo-MoFe protein. In order to determine if the Fe protein is able to transfer electrons to the oxidized P clusters of the apo-MoFe protein, EPR spectroscopy was used to monitor the signals from the nitrogenase metal clusters. For these experiments all proteins were exchanged into a 50 mM MOPS buffer, pH 7.0, that contained 2 mM Na dithionite. MoFe and apo-MoFe proteins were first oxidized with IDS which was then removed by passing the sample over a Dowex anion exchange column. Na dithionite was removed from the Fe protein by passage over a Sephadex G-25 column. Proteins were prepared in an Fe protein:MoFe protein ratio of 2:1 in the presence of either 2.5 mM MgATP or MgADP. Samples of the individual MoFe/apo-MoFe proteins, together with Fe protein and the appropriate nucleotide, were flash-frozen in a hexane/liquid nitrogen slurry and monitored by EPR. For parallel mode EPR, each plot shown is the sum of 40 scans collected at 17 K with a microwave frequency of 9.4 GHz, microwave power of 20.1 mW, modulation amplitude of 12.63 G at a frequency of 100 kHz, conversion and time constants of 20.48 ms. For perpendicular mode EPR, the spectra are the sum of 50 scans collected at 17 K with a microwave frequency of 9.64 Ghz, microwave power of 10.1 mW, modulation amplitude of 7.969 G at a frequency of 100 kHz, conversion and time constants of 20.48 ms.

Results

Purification and characterization of poly-histidine-tagged MoFe proteins. Two mutant strains were constructed for which IMAC-based methods could be applied to MoFe protein purification (Table I). One of these mutants (DJ1141) has eight histidine codons inserted between the third and fourth codons of the *nifD* gene and produces a modified MoFe protein that has a histidine-tag located near the N-terminus of each of its α-subunits. The other strain (DJ995) has seven histidine codons inserted between *nifD* codons 481 and 482 and produces a modified MoFe protein having a histidine-tag located near the C-terminus of each of its α-subunits. A third strain was constructed that produces a modified MoFe protein containing the same poly-histidine stretch within the C-terminal region of the MoFe protein α-subunits as DJ995, but it also contains a factor Xa cleavage site (Ile-Glu-Gly-Arg) preceding the poly-histidine tagged sequences. However, MoFe protein produced by this strain could not be cleaved by treatment with factor Xa protease under anaerobic conditions that included the presence of 1.0 mM Na dithionite in the buffer, so it was not studied further.

MoFe proteins that contained poly-histidine tags at either the N- or C- terminal regions of their respective α-subunits were isolated from crude extracts of nitrogenase-derepressed DJ1141 (N-tag) or DJ995 (C-tag) cells using a simple four step procedure that includes: (i) passing approximately 30 g of crude extract protein over a Zn(II)-charged IMAC column, (ii) washing the column with Buffer A containing 40 mM imidazole, (iii) eluting the bound protein with Buffer A containing 250 mM imidazole, and (iv) DEAE-Sepharose ion-exchange column chromatography. The entire procedure can be completed in about 12 h and routinely yields approximately 1.2 g of electrophoretically pure MoFe protein for each 30 g of crude extract protein processed. Also, the heme-containing protein that is often found as a persistent

contaminant in preparations of MoFe protein when traditional chromatography methods are used [142] is not found when MoFe protein is isolated using the IMAC-based method described here.

MoFe protein isolated from extracts of the wild-type DJ strain by using the traditional purification protocol [126, 127] was compared to poly-histidine-tagged MoFe proteins purified using the IMAC-based method. These comparisons include the following catalytic, kinetic and spectroscopic parameters: (i) proton reduction specific activity (2,000 - 2,400 nmoles H_2 formed min^{-1} mg MoFe $protein^{-1}$), (ii) acetylene reduction specific activity (1,800 - 2,100 nmoles acetylene reduced min^{-1} mg MoFe $protein^{-1}$), (iii) rate of MgATP hydrolysis observed in hydrogen- or acetylene-reduction assays (4.5 - 5.5 MgATP hydrolysed per each 2 e^- transferred to product), (iv) the amount of Fe protein needed to achieve half the maximum activity (2.5-3.2 μM of Fe protein per approximately 0.42 μM of MoFe protein used in a 1.0 mL assay), (v) rate constant of primary electron transfer from the Fe protein to the MoFe protein (120 to 160 s^{-1}), (vi) Fe protein-MoFe protein dissociation rate constant (4.4-6.5 s^{-1}), (vii) presence of the characteristic *S*=3/2 perpendicular mode EPR spectrum indicative of the FeMo-cofactor (g= 4.3, 3.7, 2.0, [[143]], see Figure 4), (viii) presence of the characteristic parallel mode EPR spectrum indicative of oxidized P clusters (P^{2+}, g≈11.8, [[125, 136, 137]], see Figure 5) and, (ix) all three MoFe proteins also exhibited the ability to form a tight complex when incubated with the Fe protein in the presence of MgATP and AlF_4^- or when incubated with ΔL127 Fe protein. There is some variation from certain published values determined by different investigators because most kinetic and catalytic parameters of nitrogenase depend upon the protein concentration, the assay pH, component protein ratios, and salt concentration [35, 144-146]. All three MoFe protein types characterized in the present work were examined under identical experimental conditions for each parameter tested. Thus, a lack of a substantial difference for any of the catalytic, kinetic

or spectroscopic features measured for the three forms of MoFe protein characterized here indicates that neither of the poly-histidine-tagged versions of the MoFe protein are appreciably different from the normal MoFe protein in terms of their catalytic or biophysical properties. This conclusion is further supported by the observation that strains DJ, DJ1141 (N-tag), and DJ995 (C-tag) all exhibit the same diazotrophic growth rates. Because strains DJ1141 (N-tag) and DJ995 (C-tag) produce proteins having nearly identical properties, only strain DJ1141 (N-tag), and derivatives thereof, were studied further in the present work.

IMAC purification of apo-MoFe protein. Strain DJ1141 (N-tag) was used as the parental strain to construct a mutant strain deleted for *nifB* (DJ1143). Previous work has shown that MoFe protein produced from this genetic background does not contain FeMoFeMo-cofactor, but does contain other metal centers, presumably P clusters [11, 57, 73] (MoFe protein that does not contain FeMo-cofactor is referred to as apo-MoFe protein[see footnote 1]). Hereafter, MoFe protein will refer to the poly-histidine modified form produced by strain DJ1141 (N-tag), and apo-MoFe protein will refer to the poly-histidine modified form produced by DJ1143. By using the same IMAC-based approach described above it was possible to purify approximately 400 mg of apo-MoFe protein per 30 gram of DJ1143 crude extract protein processed. Figure 1 shows an SDS-PAGE gel for a typical purification of apo-MoFe protein.

Time-dependent alkylation of MoFe protein and apo-MoFe protein. Figure 2 shows a comparison of the time course alkylation of MoFe protein and apo-MoFe protein. For the apo-MoFe protein, there is already some apparent alkylation after only 1 second of I-AEDANS treatment (Figure 2, panel B). However, even after a 30 second I-AEDANS treatment, intact

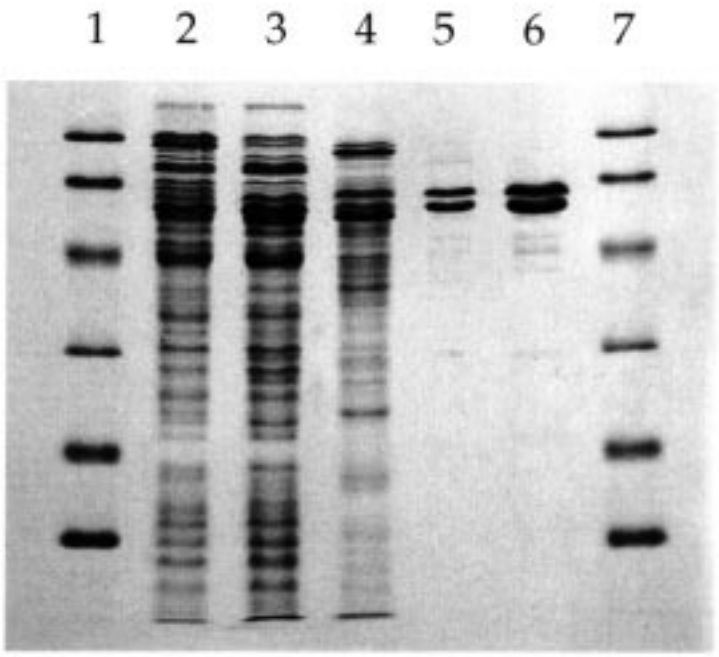

Figure 1: *SDS-PAGE for the IMAC purification of apo-MoFe protein (DJ1143).* Proteins were separated using SDS-PAGE with a 4% stacking gel and a 20% running gel and then stained with Coomassie brilliant blue. Lane 1 and 7, M_r standards, (from top: phosphorylase b, 97,400; serum albumin, 66,200; carbonic anhydrase, 31,000; soybean trypsin inhibitor, 21,500; lysozyme, 14,400); Lane 2, sample of crude extract that was loaded onto the IMAC column; Lane 3, IMAC column flow through; Lane 4, IMAC column eluent from Buffer A, 20 mM imidazole·HCl wash; Lane 5, protein collected from the Buffer A, 250 mM imidazole·HCl elution; Lane 6, purified apo-MoFe protein from DEAE column fraction. For lane 2 the amount of protein loaded was ~30 μg, and for lane 6 the amount of protein loaded was ~10 μg. For the other lanes the amount of protein loaded was not determined.

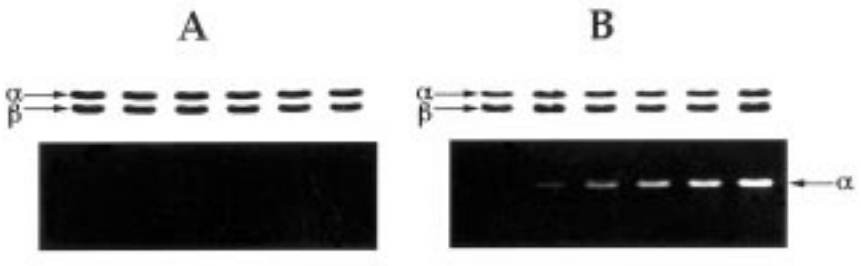

Figure 2: *Time course for the alkylation of the isolated MoFe protein and apo-MoFe protein.* Coomassie stained SDS-PAGE gels of MoFe protein (*Panel A, top*) and apo-MoFe protein (*Panel B, top*) treated with I-AEDANS as described in the experimental section. Each lane was loaded with ~10 μg of I-AEDANS treated protein. The leftmost lane in both gels is a control, where the MoFe protein or apo-MoFe protein was not treated with I-AEDANS, the lanes that follow correspond to 1, 5, 10, 15 and 30 second I-AEDANS incubation, respectively. The SDS-PAGE gel of MoFe protein (*Panel A, bottom*) and apo-MoFe protein (*Panel B, bottom*) visualized with UV light prior to Coomassie staining. The apo-MoFe protein alkylates rapidly, while the MoFe protein is not modified during the same time period. The locations of the α– and β– subunits of the MoFe and apo-MoFe protein are indicated by arrows for the SDS-PAGE gels in both panels.

MoFe protein does not show any modification (Figure 2, panel A). These results are consistent with those reported by Magnuson, *et al.* [147]who showed that apo-MoFe protein has two cysteines (residues α–Cys-45 andα–Cys-275) that are readily alkylated, whereas the intact MoFe protein is not susceptible to rapid alkylation. In a separate experiment, a 20 minute, anoxic incubation of isolated apo-MoFe protein (7.3 μM in 1 mL) with a 1 mM α,α' bipyridyl solution did not result in a change in the A_{520}. Thus, the iron contained within the intact apo-MoFe is not accessible to the metal-chelating reagent α,α' bipyridyl. However, upon exposing the same sample to air, the A_{520} showed a 7-fold increase within one minute.

UV-visible spectroscopic properties of apo-MoFe protein. Isolated apo-MoFe protein has a distinct maroon color that is readily distinquished from the greenish-brown color of purified MoFe protein. The UV/Visible spectra of the reduced, as-isolated-, and IDS-oxidized-, forms of the MoFe protein and the apo-MoFe protein are shown in Figure 3. The respective spectra of the MoFe protein and apo-MoFe protein are essentially featureless in the 350 nm to 700 nm range. For the apo-MoFe protein, the amplitude in the visible range is lower when compared to the MoFe protein. The inset to Figure 3 shows that at 400 nm, the reduced apo-MoFe protein has an ε_{400}=35.5 $mM^{-1}cm^{-1}$, whereas the reduced MoFe protein has an ε_{400}=62.3 $mM^{-1}cm^{-1}$[148]**.** Another property is that the respective ε_{400} values for neither the apo-MoFe protein nor the MoFe protein appreciably change upon their oxidation by IDS[149].

Activation of apo-MoFe protein. The as-isolated apo-MoFe protein does not exhibit the *S*=3/2 EPR signal that is characteristic of the MoFe protein or isolated FeMo-cofactor[143, 150], a

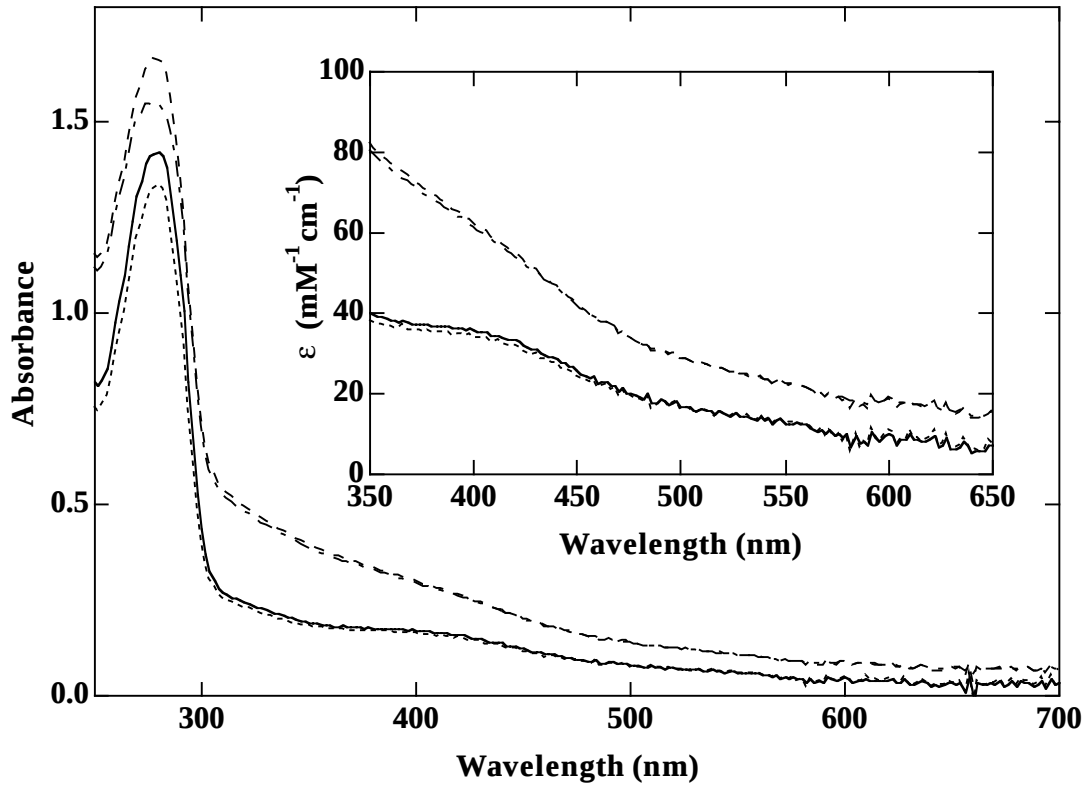

Figure 3: *UV/Visible spectra of the apo-MoFe protein and MoFe protein.* Spectra of the as-isolated (solid line) and IDS-oxidized (dotted line) apo-MoFe protein. Also shown is the UV/Visible spectrum of the MoFe protein in the as-isolated (dash-dot) and IDS-oxidized (dashed) forms. Before taking the spectra, Na dithionite or IDS were removed by anaerobic buffer exchange using either a G-25 column or a Dowex strong anion exchange column, respectively. Protein concentrations were maintained at 1.2 mg/mL for each spectrum. The inset shows the 350-700 nm visible region with the y-axis converted to units of absorption coefficient (ε).

result that is consistent with the expectation that apo-MoFe protein does not contain any FeMo-cofactor (Figure 4A). This result is also consistent with metal analyses that failed to detect any Mo associated with the as-isolated apo-MoFe protein. Although there is no *S*=3/2 EPR signal present in the as-isolated apo-MoFe protein, there is an *S*=1/2 signal that is recognized in the g=2 region and that disappears completely above 30 K. Spin quantitation of this species revealed that it is a very minor component representing less than 0.05 spins per apo-MoFe protein.

Apo-MoFe protein could be activated by the addition of isolated FeMo-cofactor to yield a MoFe protein that exhibits an *S*=3/2 EPR signal that is identical in lineshape and g-values to the isolated MoFe protein (Figure 4B) and does not exhibit the broad spectral features seen in the EPR of isolated FeMo-cofactor[150]. As discussed below, a small *S*=1/2 EPR signal that is present in the as-isolated apo-MoFe protein persists in the FeMo-cofactor-treated sample. The activated protein has a specific activity of 1600 nmoles H_2 formed min^{-1} mg apo-MoFe $protein^{-1}$. The apo-MoFe protein did not exhibit any proton- or acetylene-reduction activity prior to FeMo-cofactor addition. MoFe protein isolated from DJ1141 (N-tag) typically has a specific activity of 2,000 nmoles H_2 formed min^{-1} mg MoFe $protein^{-1}$, so the activation achieved by FeMo-cofactor addition represents about 80% of the theoretical activation value. Attempts to enhance the FeMo-cofactor-dependent activation of apo-MoFe protein by the addition of either dithiothreitol or Fe protein, with or without MgATP, were not successful. Similarly, the addition of crude extracts from a Δ*nifHDK* strain also failed to enhance the activation of apo-MoFe protein.

EPR spectroscopic properties of apo-MoFe protein. Two EPR signals have been reported that represent two different oxidation states of the P cluster. One of these signals arises from the one-electron oxidation of the P cluster (P^{1+} state) and can be recognized by a rhombic signal in

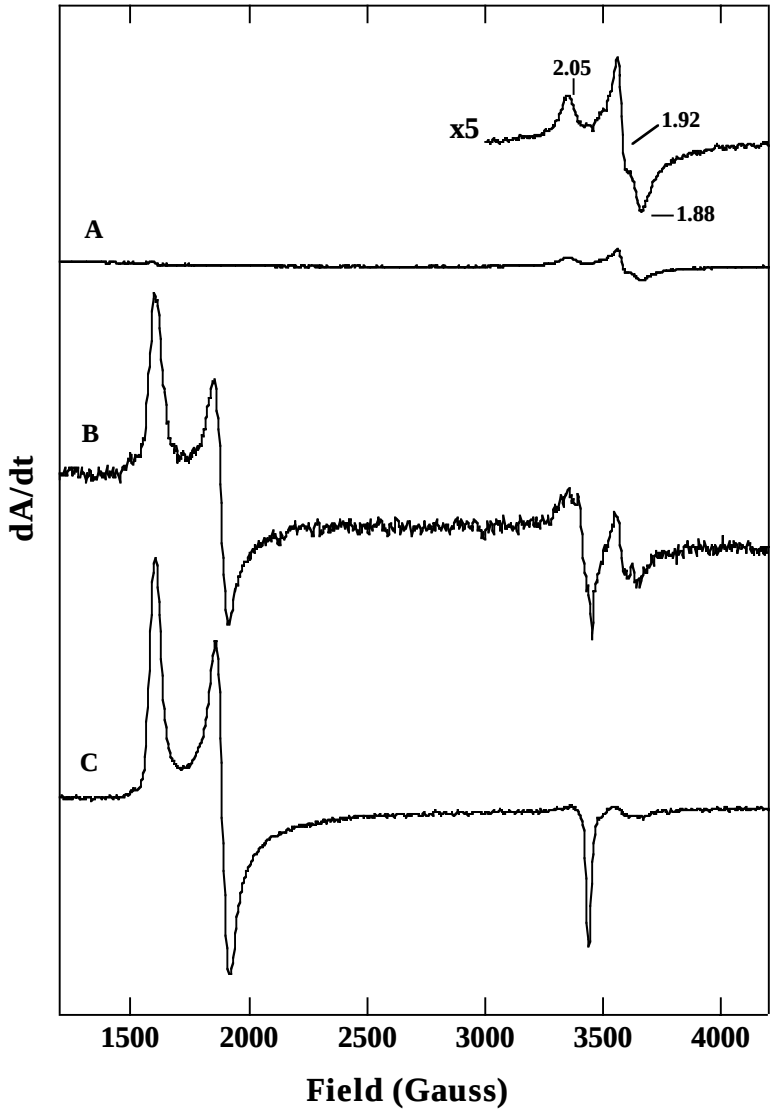

Figure 4: *Activation of apo-MoFe protein observed using EPR.* (*A*) Perpendicular mode EPR of the apo-MoFe protein (36.5 mg/mL, 10 scans). The inset in the upper right corner is a 5x blow-up of the g_{av}=1.95 signal with the associated g-values shown. (*B*) Perpendicular mode EPR spectrum of the activated apo-MoFe protein (6 mg/mL, 30 scans), activated as described in the text. (*C*) EPR of MoFe protein (62.7 mg/mL, 10 scans). All spectra have been amplitude corrected for protein concentration (and also for power in the case of the MoFe protein spectrum). Spectra were collected at 12 K and 9.64 GHz with the following parameters: power 6.36 mW (with the exception of the MoFe protein sample, which was at 0.201 mW), receiver gain $1x10^4$, modulation frequency 100 kHz, modulation amplitude 12.6 G.

perpendicular mode EPR with g-values of 2.05, 1.94, and 1.81[151]. The other signal arises from the two-electron oxidized form (P^{2+} state) and can be recognized by a g≈11.8 peak observed in parallel mode EPR[125, 136, 137]. At pH 8.0, the pH at which all the proteins were purified in the present work, the P^{1+} EPR signal cannot be observed because the P^{2+}/P^{N} and P^{2+}/P^{1+} redox couples exhibit the same midpoint potentials (-309 mV, [[136]]). The P^{1+} signal was initially observed for a MoFe protein sample prepared in a pH 7.4 buffer[151], and recent work has shown that the P^{2+}/P^{1+} redox couple is pH-dependent[24]. Thus, by exchanging the protein into a pH 7.4 buffer, and poising the sample at a defined potential, both forms of the oxidized P cluster from the MoFe protein can be observed (Figure 5 A & B, trace 2). For similarly treated apo-MoFe protein, both the P^{1+} and P^{2+} signals, having the same g-values and line-shape as the corresponding intact MoFe protein signals, can be recognized (Figure 5 A & B, trace 1). The spectra shown in Figure 5B represent the maximum observed intensity of the P^{1+} signal for the samples run. However, each sample had to be poised at a different potential for these spectra (see legend to Figure 5) which suggested that the midpoint potentials for the metal cluster in the apo-MoFe protein may be different from that observed in the MoFe protein. Differences between the spectra shown in Figure 5B are due to the contribution of the g=2 feature from the FeMo-cofactor S=3/2 signal in the MoFe protein sample, and the contribution of a mediator-derived radical signal at g=2 in the apo-MoFe protein sample. As discussed below, the P^{N}/P^{2+} redox couple for the apo-MoFe protein is shifted -63 mV relative to the intact MoFe protein. Thus, a corresponding mediator-derived radical signal is not recognized for intact MoFe protein because the respective samples were poised at different potentials.

By monitoring the amplitude of the P^{2+} EPR signal at pH 8.0, the midpoint potential for

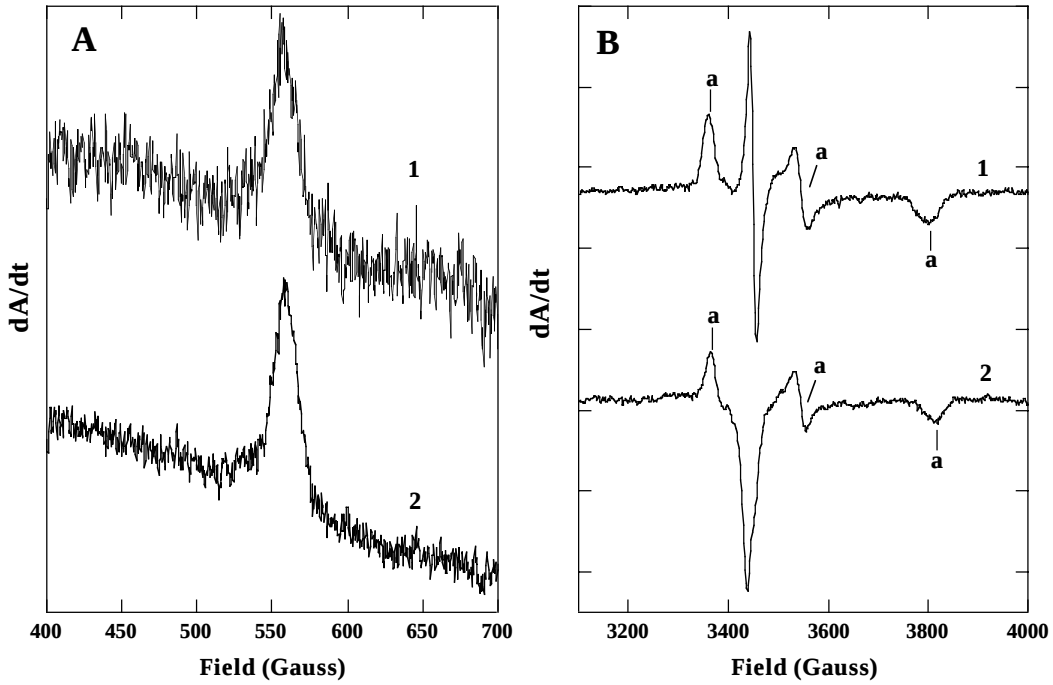

Figure 5: *EPR spectra of the P^{2+} and P^{1+} states of the P cluster in apo-MoFe and MoFe protein*. Representative spectra taken from the redox potential titrations performed as described under experimental methods. (*Panel A*) Spectra for IDS-oxidized apo-MoFe (*trace 1*) and IDS-oxidized MoFe proteins (*trace 2*) in parallel mode at pH 8.0. The MoFe protein P^{2+} signal intensity was adjusted for protein concentration. (*Panel B*) Spectra for the IDS-oxidized apo-MoFe protein (-306 mV) (*trace 1*) and MoFe protein (-230 mV) (*trace 2*) in perpendicular mode at pH 7.4. The P^{1+} signal is indicated by 'a' in the figure. The radical signal exhibited in the apo-MoFe protein at ~3450 G arises from the mediator solution (as described in results), while the dip observed for the MoFe protein in the same region is due to the FeMo-cofactor *S*=3/2 signal.

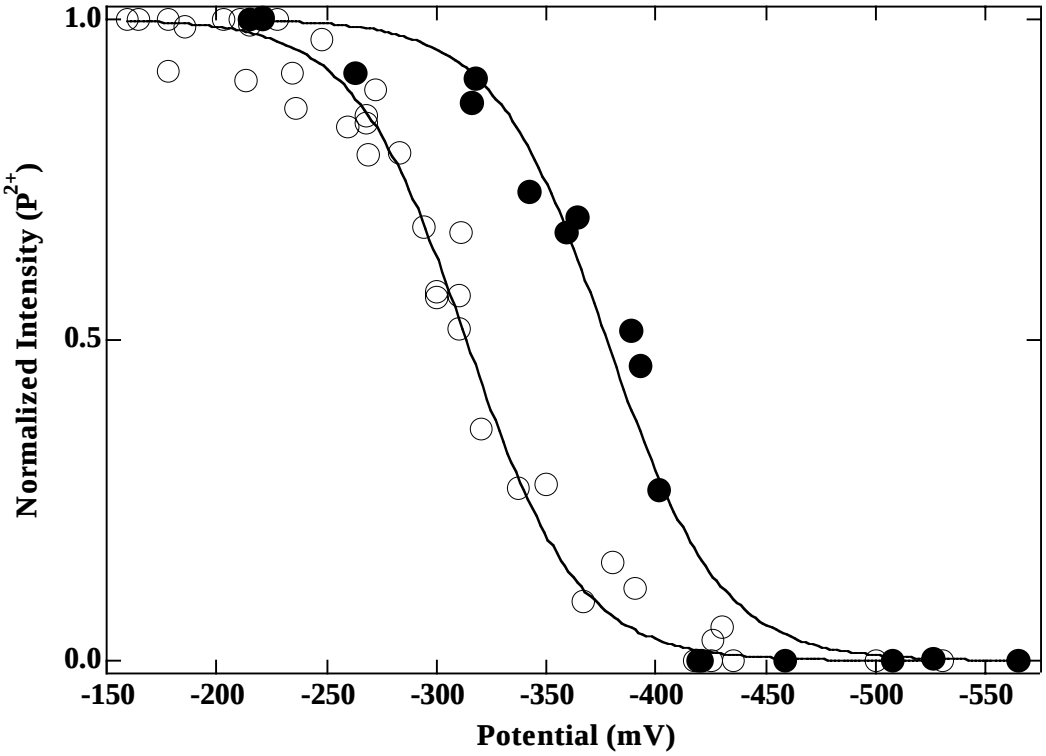

Figure 6: *Redox titration of the P^{2+} signal from apo-MoFe protein and the MoFe protein.* Redox titrations were performed as described in experimental procedures. Normalized intensities of the apo-MoFe protein (●) and MoFe protein (O) P^{2+} EPR signals are plotted against the applied potential (vs. NHE). Data has been fit to the Nernst equation for a one electron transfer event. Midpoint potentials are -377 mV and -314 mV for the apo-MoFe protein and the MoFe protein, respectively.

the P^N/P^{2+} redox couple can be measured by performing a mediated redox titration. Figure 6 shows titration data with corresponding fits to the Nernst equation for a single electron transfer. The MoFe protein Nernst fit yields a midpoint potential of -314 mV for the P^N/P^{2+} couple, a value that is consistent with previous reports [6]. In contrast, the apo-MoFe protein Nernst fit renders a midpoint potential of -377 mV, which represents a -63 mV shift relative to the MoFe protein.

Fe protein-apo-MoFe protein interactions. Incubation of the MoFe protein with Fe protein, Na dithionite and MgATP under an argon atmosphere results in the reduction of protons with approximately 4-5 MgATP hydrolysed for each H_2 evolved [146]. The maxium rate for H_2 evolution catalyzed by the isolated MoFe protein produced by strain DJ1141 (N-tag) was approximately 2,000 nmoles H_2 formed min^{-1} mg MoFe $protein^{-1}$ with a corresponding MgATP hydrolysis rate of 9800 nmoles MgATP hydrolyzed min^{-1} mg MoFe $protein^{-1}$ (4.9 MgATP/$2e^-$). Incubation of apo-MoFe protein under the same catalytic conditions resulted in no H_2 evolution, but MgATP hydrolysis occurred at a rate of 5,900 nmoles MgATP hydolyzed min^{-1} mg apo-MoFe $protein^{-1}$, which is about 60% that supported by the MoFe protein. No MgATP hydrolysis was catalyzed by the apo-MoFe protein in the absence of the Fe protein.

Another way to examine the interaction of the nitrogenase component proteins is to measure the apparent first order rate constant of dissociation using stopped flow spectroscopy. As described in the experimental section, the dissociation rate constant of the component proteins can be indirectly measured by determining the rate of Na dithionite-mediated reduction of the oxidized MgADP-bound Fe protein as it is released from the MoFe protein. The measured dissociation rate constant for the MoFe protein - Fe protein•MgADP complex is 3.6 s^{-1}, and the

dissociation rate constant for the apo-MoFe protein - Fe protein•MgADP complex is 4.5 s^{-1} (Figure 7). In similar experiments, where the ΔL127 Fe protein is used in place of the Fe protein, the rate of MoFe protein-ΔL127 Fe protein dissociation is too slow to be accurately measured. In contrast, the dissociation rate constant for the apo-MoFe protein - ΔL127 Fe protein could be measured and was found to be approximately 1.0 s^{-1}.

Finally, evidence for specific interaction between the apo-MoFe protein and the Fe protein was obtained by complex formation, as evaluated by gel exclusion chromatography, when apo-MoFe protein and Fe protein were incubated in the presence of MgATP and AlF_4^-. These results are similar to those previously reported for the intact MoFe protein [39, 40], except that trapping of all of the available apo-MoFe protein, even when incubated in the presence of a large excess of Fe protein, could not be achieved (data not shown). In contrast, incubation of a molar excess of Fe protein relative to the MoFe protein, together with MgATP and AlF_4^-, resulted in the capture of all the available MoFe protein into a tight complex composed of 2 bound Fe protein per each MoFe protein tetramer ([[38]], control experiments performed in the present work). Another difference observed between the intact MoFe protein and the apo-MoFe protein was that co-incubation of apo-MoFe protein and Fe protein in the presence of MgATP and AlF_4^- beyond 15 min resulted in precipitation of the sample. In related experiments, incubation of apo-MoFe protein with the ΔL127 Fe protein also resulted in formation of a complex that could be detected by gel exclusion chromatography. The ΔL127 Fe protein is known to adopt a nucleotide-bound conformation even in the absence of nucleotides [135], and it forms a tight 2:1 complex when incubated with the MoFe protein [95]. Incubation of an excess of the ΔL127 Fe protein with the apo-MoFe protein did result in the formation of a tight apo-

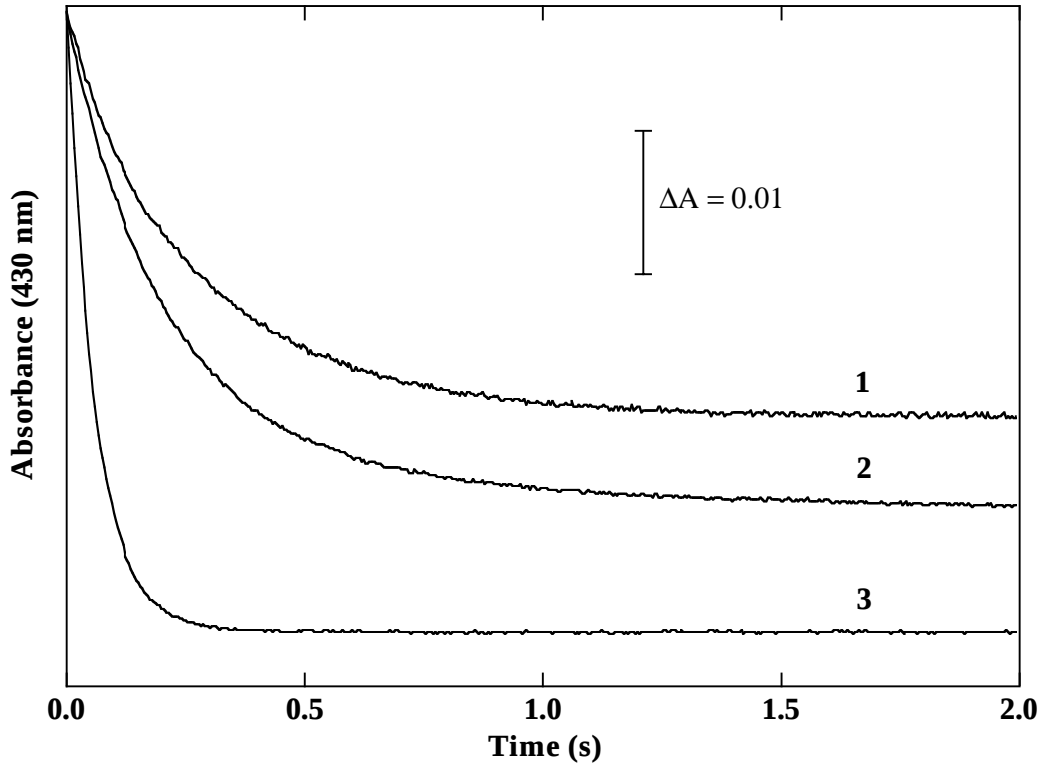

Figure 7: *Interaction of apo-MoFe protein with Fe protein monitored by stopped-flow spectrophotometry*. The interaction of the apo-MoFe and the Fe protein was measured using stopped-flow methods. The apparent first order rate constant, k, resulted from single exponential fits to the data. Each trace represents the change in A_{430} that occurred after mixing a solution containing 200 μM Fe protein and 10 mM Na dithionite in 50 mM HEPES, pH 7.4 with a solution containing: (*trace 1*) 20 μM reduced MoFe protein without Na dithionite, 20 μM oxidized Fe protein and 5 mM MgADP, k=3.6 s^{-1}, or (*trace 2*) 20 μM reduced apo-MoFe protein without Na dithionite, 20 μM oxidized Fe protein and 5 mM MgADP, k=4.5 s^{-1}. (*trace 3*) Change in A_{430} that occurred after mixing a 10 mM Na dithionite solution with a solution containing 20 mM oxidized Fe protein and 5 mM MgADP, k=17 s^{-1}. For all experiments, the oxidized Fe protein syringe contained 50 mM HEPES pH 7.4, 200 mM NaCl for buffer.

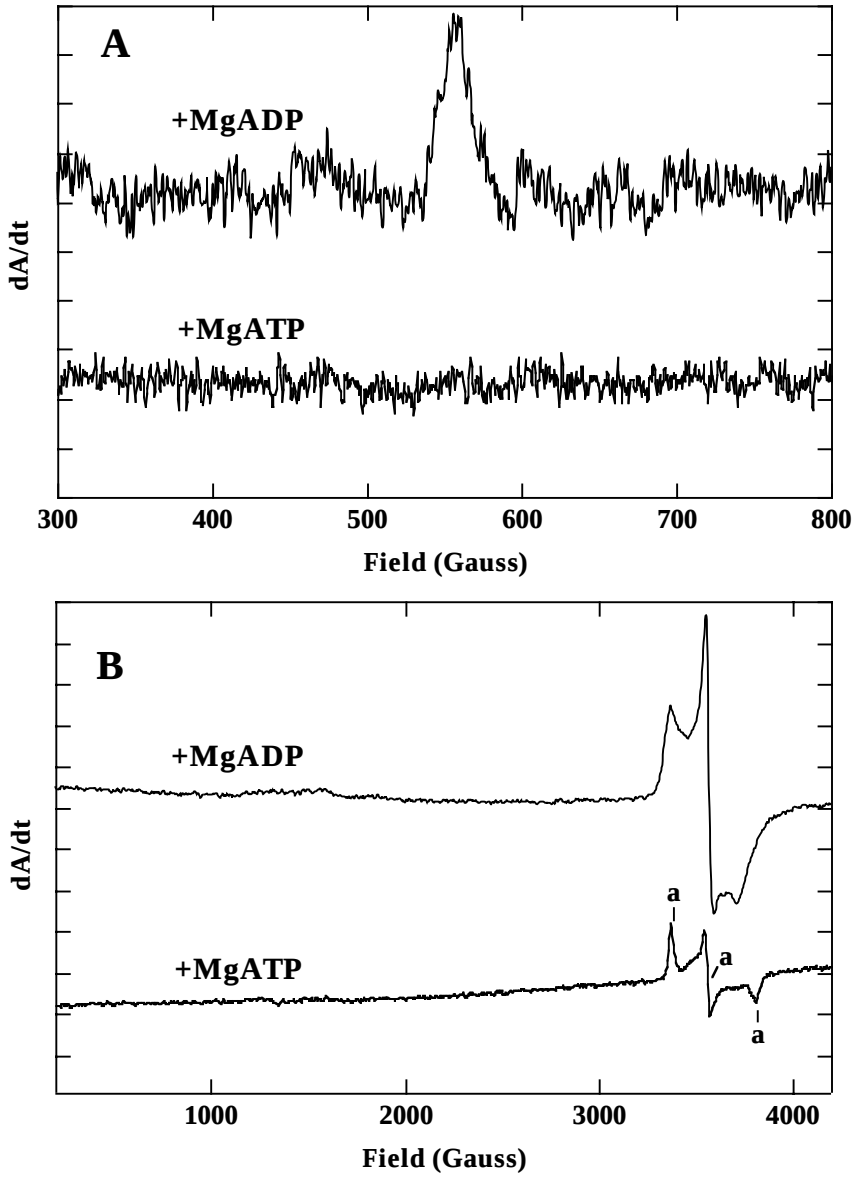

Figure 8: *MgATP dependent electron transfer from the Fe protein to the apo-MoFe protein.* (*Panel A*) Parallel mode EPR for IDS-oxidized apo-MoFe protein with reduced, Na dithionite free, Fe protein with the addition of MgADP (*top*) or MgATP (*bottom*). (*Panel B*) Perpendicular mode EPR for the same samples in Panel A with the addition of MgADP (*top*) or MgATP (*bottom*). As in Figure 5, the S=1/2 portion of the P^{1+} signal is indicated by 'a'.

MoFe protein - Fe protein complex (data not shown). However, as in the case of the AlF_4^--dependent complex trapping experiments described above, the interaction between the proteins was weaker than that observed for MoFe protein, as indicated by the presence of uncomplexed apo-MoFe protein even in the presence of excess ΔL127 Fe protein. All of these results indicate that, although the apo-MoFe protein is able to interact with the Fe protein, this interaction does not appear to be identical to the normal Fe protein - MoFe protein interaction.

Electron transfer from the Fe protein to the apo-MoFe protein. No apparent primary electron transfer from the reduced Fe protein to the as-isolated apo-MoFe protein could be detected by stopped flow spectrophotometry. Furthermore, there was neither a loss in the *S*=1/2 EPR signal characteristic of the reduced Fe protein nor the appearance of any new EPR signals when Fe protein and apo-MoFe were co-incubated under turnover conditions. In contrast, MgATP-dependent electron transfer from the Fe protein to apo-MoFe protein in the P^{2+} state was detected. Figure 8 shows the parallel and perpendicular mode EPR spectra of samples where IDS-oxidized apo-MoFe protein (P cluster in the P^{2+} state) and reduced Fe protein were co-incubated in the presence of either MgADP or MgATP. The top spectrum in Panel A of Figure 8 shows the presence of the parallel mode P^{2+} EPR signal for the oxidized apo-MoFe protein when incubated with Fe protein and MgADP, indicating that there is no electron transfer under these conditions. However, as shown in the bottom spectrum of Panel A, there is no parallel mode P^{2+} EPR signal in a sample for which MgATP was substituted for MgADP, indicating an electron transfer event has occured and the P^{2+} state has been reduced. Panel B shows the spectra of the corresponding samples run in perpendicular mode. In the top trace of Panel B the characteristic *S*=1/2 signature in the g≈2 region for the reduced Fe protein with MgADP bound [18] is evident.

In the lower trace, the sample for which MgADP has been replaced by MgATP, the signal in the g≈2 region observed in the top trace has disappeared with the attendant appearance of a new signal having g-values corresponding to the P^{1+} state of the P cluster. Thus, electron transfer from the reduced Fe protein to the IDS-oxidized apo-MoFe protein occurs only in the presence of MgATP such that the P^{2+} form of the P cluster is reduced to the P^{1+} state. Control experiments using the MoFe protein, rather than the apo-MoFe protein, gave the same results.

Discussion

Two different *A. vinelandii* strains were constructed that produce MoFe proteins having poly-histidine insertions located at, or near, their respective α-subunit C- or N-termini. Both of these modified proteins can be rapidly purified through the application of an IMAC-based procedure and yield proteins having the same catalytic, kinetic, and spectroscopic properties of the normal MoFe protein. Thus, by using the IMAC-based approach, both the heat step and the strong anion exchange chromatography step, necessary for the traditional purification of MoFe proteins [126, 127], can be avoided. By using the appropriately constructed strains and by application of the same IMAC-based purification procedure it is also possible to purify apo-MoFe protein in concentrations amenable for detailed catalytic and spectroscopic characterizations. Below, the results of the characterization of the apo-MoFe protein isolated in the present work are interpreted and discussed in light of the properties of other apo-MoFe proteins that have been previously described.

Subunit composition and activation of apo-MoFe protein. Purification of apo-MoFe protein from an *A. vinelandii nifB* mutant has been previously described [73]. There are two significant

differences between the properties of the apo-MoFe protein described here and the one previously characterized. The previously described apo-MoFe protein has an $\alpha_2\beta_2\gamma_2$ subunit organization and is reported to be 100% activatable by FeMo-cofactor addition [73], whereas the apo-MoFe protein described here does not contain the gamma subunit and is activated to 80% of the theoretical value by FeMo-cofactor addition. There is *in vitro* evidence that gamma stabilizes apo-MoFe protein and that it assists FeMo-cofactor insertion into the apo-MoFe protein [79]. It is possible that our inability to achieve 100% of the theoretical activation value could be related to the lack of the gamma protein.

There are several possibilities that could explain why there is no gamma protein associated with the apo-MoFe protein described here. One possibility is that the poly-histidine insertion located at the N-terminus of the α-subunit of apo-MoFe protein purified from DJ1143 overlaps the gamma binding site and therefore prevents complex formation between gamma and the apo-MoFe protein. This possibility was examined by isolating apo-MoFe protein from DJ1003, which carries a poly-histidine insertion near the C-terminus of the α-subunit. It was determined that this apo-MoFe protein also did not contain the gamma protein. Because the N- and C-termini of the α-subunit of the normal MoFe protein are separated by about 40 Å in the crystallographic model [12], it seems unlikely that both C- and N-terminal insertions would eliminate the ability of gamma to interact with the MoFe protein. Nevertheless, the three-dimensional structure of the apo-MoFe protein is not known, so this remains a reasonable explanation. A second possibility is that the high salt concentration (0.5 M NaCl) present in the early stages of the apo-MoFe protein purification described here, and not present in the previously described purification protocol [73], might prevent the interaction of apo-MoFe protein and gamma. A final possibility is that the attachment of gamma to the apo-MoFe protein

is an artifact of the previously described purification procedure. In this context it is noted that expression of gamma is not *nif*-regulated nor does it dissociate from the apo-MoFe protein upon activation [73]. These possibilities will only be resolved once purified gamma is available in large quantities and the gene encoding gamma can be inactivated *in vivo*. Whatever the reason for our inability to fully reconstitute the apo-MoFe protein described here, it is clear from the high level of activation that is achieved, and the appearance of a normal *S*=3/2 EPR signal upon FeMo-cofactor addition, that activation of apo-MoFe protein can be accomplished by the simple addition of isolated FeMo-cofactor and without the presence of the gamma subunit. Also, because the parallel mode P^{2+} EPR signal evoked by IDS oxidation of the apo-MoFe protein shows the same intensity when compared to IDS-oxidized MoFe protein (when adjusted for protein concentration), it is not likely that the apo-MoFe protein we have purified consists of a significant amount of unactivatable species.

There is also an $\alpha_2\beta_2\gamma_2$ subunit organization in the case of apo-MoFe protein produced by *Klebsiella pneumoniae nifB*-mutants [57, 78, 80]. However, in this organism the γ subunit has been identified as the product of the *nifY* gene, and it does dissociate from the complex upon FeMo-cofactor insertion[78, 80], in contrast with the stable hexameric form previously reported for *A. vinelandii*[73]. There is also a *nifY* gene in *A. vinelandii*, but the function of the *nifY* product in this organism is not yet known, nor is there any phenotype associated with its inactivation[81]. Even if the *nifY* gene product from *A. vinelandii* is capable of forming a complex with the apo-MoFe protein, it is unlikely that such a complex would be identified in the present work because, on the basis of northern analyses and gene fusion experiments ([[152]], our unpublished work), the expression of *nifY* is much lower than expression of the genes that encode the MoFe protein subunits. As in the case of the gamma protein, the potential

involvement of the *A. vinelandii nifY* gene product in FeMo-cofactor insertion or stabilization of the apo-MoFe protein will require the purified protein.

Spectroscopic features of the apo-MoFe protein. The EPR spectrum of the as-isolated apo-MoFe protein is featureless except for a minor S=1/2 signal in the g≈2 region that has lineshape, g-values and temperature dependence very similar to typical [4Fe-4S] clusters (Figure 4, [[153, 154]]). This signal, which integrates to only 0.05 spins per MoFe protein, disappears upon oxidation of the sample and reappears upon re-reduction by Na dithionite. The signal also persists even after the addition of FeMo-cofactor, although it is somewhat obscured by the contribution of FeMo-cofactor to the EPR spectrum at g=2. Considering the purity of the protein sample, it is unlikely that the observed S=1/2 signal arises from a contaminating protein. A similar S=1/2 EPR signal attributed to a damaged P cluster or a P cluster precursor has been reported previously [57, 155]. This same signal is also present at 0.1 to 0.3 spins per mole in an apo-MoFe protein produced by a *nifH*-deletion mutant[156]. In related work we have purified an apo-MoFe protein form produced by a *nifH* deletion strain using the IMAC-based approach and confirm a previous report that it is different from apo-MoFe protein in that it contains a more significant S=1/2 EPR signal (0.5 spins per mole of apo-MoFe protein) and that it cannot be activated by the simple addition of isolated FeMo-cofactor[74, 157]. We also find that neither the P^{1+} nor P^{2+} EPR signals can be elicited by IDS oxidation of apo-MoFe protein isolated from a *nifH* deletion strain. On the basis of these observations, we find the proposal that intact P clusters might be formed in a pathway that involves the fusion of two [4Fe-4S] cubanes an attractive one[155], and suggest that the species giving rise to the S=1/2 signal from apo-MoFe

proteins produced from either *nifH*- or *nifB*-deletion backgrounds represent either incompletely processed or damaged P clusters.

The MoFe protein P clusters have been prepared in five different oxidation states at pH 8.0, as illustrated below ([[6]], Scheme 2).

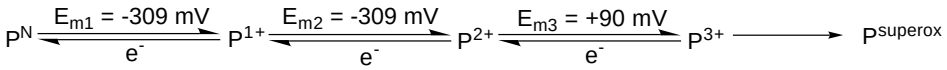

All eight iron atoms present in the P cluster in the as-isolated MoFe protein are believed to be in the Fe^{2+} oxidation state, and this form of the P cluster is often referred to as P^N (the N designation refers to the Native or as-isolated form [[156]]). There is no direct evidence that the P cluster can be reduced to a lower oxidation state. The P^N state of the P cluster can be reversibly oxidized by up to three electron equivalents to respectively yield the oxidation states designated P^{1+}, P^{2+} and P^{3+} in scheme 2. The P cluster can be further oxidized beyond the P^{3+} state but oxidation to such "superoxidized" states is not reversible[6]. The P^N state is diamagnetic and therefore EPR silent, whereas both the P^{1+} and P^{2+} states are paramagnetic and have EPR signals. The P^{1+} state has a mixed spin system (S=1/2 and 5/2) with perpendicular mode signals in the g≈2 and 5 regions[151]. The P^{2+} state has an integer spin system (S≥3) with a parallel mode EPR signal at g≈11.8[125, 136, 137]. The midpoint potentials for both E_{m1} and E_{m2} (Scheme 2) have been determined to be -309 mV at pH 8.0 and, therefore, at pH 8.0 the EPR signal for the P^{1+} oxidation state cannot be observed[136]. However, the redox couple between P^{1+} and P^{2+} is pH-dependent[24, 151], so the P^{1+} state can be readily identified in a sample that has been IDS-oxidized at pH 7.4.

If the apo-MoFe protein has intact P clusters that are structurally and electronically similar to the P clusters present in the MoFe protein, then it should be possible to elicit the P^{1+} and P^{2+} EPR signals by IDS-oxidation of apo-MoFe protein. Panel A in Figure 5 shows the P^{2+} state (parallel mode EPR signal at g≈11.8) for both the MoFe protein (trace 1) and the apo-MoFe protein (trace 2) by IDS-mediated oxidation at pH 8.0. Panel B in Figure 5 shows the P^{1+} state (perpendicular mode signal in the g≈2 region) for both the MoFe protein (trace 1) and the apo-MoFe protein (trace 2) by IDS-mediated oxidation at pH 7.4. These observations confirm and extend the work of Robinson *et al*. [158], who concluded from comparative MCD spectroscopy that P clusters present in mature MoFe protein and an apo-MoFe protein produced from a *K. pneumoniae nifB*-mutant are electronically very similar or identical to each other[158]. Nevertheless, comparisons between the present work and that involving the corresponding *K. pneumoniae* proteins must be considered in light of differences between the respective apo-MoFe proteins. For example, the apo-MoFe protein isolated from *K. pneumoniae* contained molybdenum, had an associated γ subunit, and could only be activated to a very low level.

In the present work it is shown that the respective midpoint potentials for the P^N/P^{2+} redox couple for MoFe protein and apo-MoFe protein are significantly different (-314 mV vs -377 mV, see Figure 6). Thus, there is a detectable difference in the electronic properties of P clusters from the apo-MoFe protein versus the MoFe protein. It is likely that such differences are the result of modest structural changes in the P cluster polypeptide environment rather than an alternate form of the P cluster. Other evidence that there are some differences in the global structure of apo-MoFe protein when compared to MoFe protein is that certain cysteine thiol groups from the apo-MoFe are susceptible to alkylation whereas the corresponding residues in the mature apo-MoFe protein are not ([[147]], Figure 2). Also, based on AlF_4^--dependent

complex formation, and the ΔL127 Fe protein complex formation experiments, interactions between the Fe protein and apo-MoFe protein do not appear to be as effective as interactions between the Fe protein and MoFe protein. However, whatever the differences in the folding pattern between the MoFe protein and apo-MoFe protein, perturbations at the psuedosymmetric αβ-subunit interface are likely to be minimal. This conclusion is based on the observation that Fe protein and apo-MoFe protein are able to interact in a such a way that a high rate of MgATP hydrolysis capability is maintained. In this context it is noted that the three dimensional model of the MoFe-protein/Fe protein complex shows that the Fe protein contacts the MoFe protein at its αβ-subunit interface and in the closest possible proximity to the P cluster[37, 38, 159].

Electron transfer to the apo-MoFe protein. Because apo-MoFe protein is able to catalyze a high level of Fe protein-dependent MgATP hydrolysis, and because we were able to elicit the P^{1+} and P^{2+} oxidation states within the apo-MoFe protein, it was of interest to determine if nucleotide-dependent electron transfer from the Fe protein to the apo-MoFe protein could also occur. Figure 8 shows that the oxidized apo-MoFe protein is able to accept an electron from the Fe protein in a MgATP-dependent manner. In these experiments apo-MoFe protein in the P^{2+} state was prepared and mixed with reduced Fe protein and either MgADP or MgATP. In the presence of MgADP the P^{2+} parallel mode g≈ 11.8 EPR is apparent (Figure 8A) as is the S=1/2 perpendicular mode EPR signal characteristic of the reduced Fe protein (Figure 8B). However, in the presence of MgATP, the P^{2+} parallel mode signal disappears (Figure 8A), the S=1/2 perpendicular mode EPR signal of the Fe protein also disappears (as it becomes oxidized to the diamagnetic state), and the P^{1+} S=1/2 perpendicular mode signal becomes apparent as the P cluster is reduced from the P^{2+} state to the P^{1+} state.

Relevance of the UV-visible spectrum of as-isolated and oxidized apo-MoFe protein. In the normal nitrogenase reaction the reduced- and MgATP-bound Fe protein complexes with the MoFe protein followed by an intercomponent electron transfer event that is intimately associated with nucleotide hydrolysis. The rate of oxidation of the Fe protein that occurs during these events can be followed in real-time by monitoring the increase in the A_{430} by stopped-flow spectroscopy. Similarly, the rate of dissociation of the component proteins can be measured by the decrease in the A_{430} that occurs when the oxidized Fe protein is released from the complex and becomes reduced. An example of the latter type of experiment is shown in Figure 7. In these experiments it is shown that the Fe protein dissociates from the apo-MoFe protein at a rate that is only modestly faster than the Fe protein-MoFe protein dissociation. By using this type of analysis Lowe and Thorneley have developed a kinetic model for nitrogenase catalysis and have shown that the rate-limiting step under optimum turnover conditions is the dissociation of the component proteins[139]. Although stopped-flow determination of the rate constant of primary electron transfer is straightforward, the smaller, kinetically complex absorbance changes that occur after primary electron transfer have not yet been adequately explained. As an example, a small increase in the absorbance at A_{430} that occurs in stopped-flow experiments after about 0.5 seconds has been proposed to be the result of P cluster oxidation[94]. Although, oxidation of the P clusters might occur at this stage, our finding that the UV-visible spectrum of the apo-MoFe protein does not change upon IDS-oxidization does not support the possibility that any absorbance changes that occur in stopped flow experiments can be attributed to oxidation of the P cluster to the P^{2+} state. However, the previous investigation [94] suggested that the changes in the P cluster A_{430} are most likely arising from the P^{3+} oxidation state [136, 160] of the P cluster

which was not examined in the present work. Furthermore, the previous studies [94] examined EPR samples flash frozen after ~5 s, whereas the stopped-flow experiments examined time domains of less than one second, so the possibility of a kinetic rearrangement of the P cluster that might give rise to a change in the A_{430} cannot be discounted.

In summary, a method has been developed for the large scale purification of an apo-MoFe protein that contains intact P clusters and that can be activated by the simple addition of FeMo-cofactor. The availablity of such apo-MoFe protein can now be used to advance studies aimed at determining the role of P clusters in the nitrogenase catalytic mechanism.

Acknowledgments

The authors thank Jeannine Chan for experimental assistance and for critically reading this manuscript. We also thank Matthew Ryle for critically reading the manuscript.

CHAPTER III

Initial Characterization of a NifEN Bound FeMo-cofactor Precursor and an Interaction between NifEN and NifX.

Summary

Iron-molybdenum cofactor (FeMo-cofactor) biosynthesis requires the involvement of the NifEN complex. The NifEN complex is an $\alpha_2\beta_2$ tetramer that is believed to be a processing site for FeMo-cofactor biosynthesis. Previous work involving the use of gene fusion and immobilized metal-affinity chromatography (IMAC) was used to overproduce and purify NifEN in sufficient quantities amenable for spectroscopic characterization. The NifEN complex was shown to contain two [4Fe-4S] clusters per NifEN tetramer. Current work involves the preliminary investigation of FeMo-cofactor precursors bound to the NifEN complex. Metal analysis of NifEN routinely yields the presence of more Fe than is necessary for the formation of two [4Fe-4S] clusters. It is possible that this extra Fe represents an FeMo-cofactor precursor bound to the NifEN complex. Electron paramagnetic resonance (EPR) spectroscopy and variable-temperature magnetic circular dichroism (VTMCD) were used to investigate the presence of a FeMo-cofactor precursor bound to NifEN. Oxidation of NifEN indicates the presence of a novel EPR signal that is thought to arise from a bound precursor. This represents the first spectroscopic evidence of an FeMo-cofactor precursor. VTMCD also confirmed the presence of a paramagnetic signal on oxidized-NifEN. Current work reported here also examines the interaction of NifX with the NifEN complex. NifX is capable of binding a chromophore, perhaps the bound precursor, from the NifEN complex. Additional experiments detail the initial characterization of NifX and its interaction with NifB-cofactor and FeMo-

cofactor. Based on this data, the involvement of NifX in FeMo-cofactor biosynthesis is discussed.

Introduction

Biological nitrogen fixation involves the MgATP dependent reduction of atmospheric dinitrogen to ammonia by the metalloenzyme nitrogenase. The nitrogenase enzyme complex is composed of two component proteins, the iron (Fe) protein and the molybdenum-iron (MoFe) protein [7]. During catalysis the Fe protein transfers electrons, one at a time, to the MoFe protein in a process involving component protein association, MgATP hydrolysis, and complex dissociation [6, 47]. The Fe protein is a 64 kD γ_2 homodimer that contains a single [4Fe-4S] cluster bridging the two subunits [9, 161]. Besides being the obligate electron donor to the MoFe protein, the Fe protein also provides the site of MgATP binding and hydrolysis. The MoFe protein is a 250 kD $\alpha_2\beta_2$ heterotetramer that contains two pairs of metal clusters, termed P-clusters [23] and iron-molybdenum (FeMo) cofactors [28]. The site of substrate binding and reduction is the FeMo-cofactor that is composed of a homocitrate-$MoFe_3S_3$ subcluster bridged by three inorganic sulfides to a Fe_4S_3 subcluster [28]. Although X-ray crystal structures exist for the Fe protein [9, 162] and MoFe protein [12, 23], the nature of the biosynthesis and subsequent insertion of the metal centers of nitrogenase is still not fully understood.

A number of *nif*-specific gene products have been implicated in the process of FeMo-cofactor formation and insertion [7]. This process involves the products of the *nif*H, *nif*B, *nif*E, *nif*N, *nif*V, *nif*X, and *nif*Q genes. The nitrogenase Fe protein, the product of *nif*H, is required for both the formation and the insertion of FeMo-cofactor [64, 70]. Although the specific function of Fe protein in these processes is not known, neither its MgATP-binding and hydrolysis

properties nor its ability to transfer electrons seem necessary [76, 98, 163]. Biochemical complementation experiments have shown that FeMo-cofactor is separately synthesized and then inserted into an apo-form of the MoFe protein, which contains intact P clusters, but lacks FeMo-cofactor [63]. At least a portion of the biosynthetic process occurs within a complex of the *nif*EN products. The *nif*EN gene products bear primary sequence similarity to the products of the *nif*DK structural genes, respectively [65]. The NifEN complex is an $\alpha_2\beta_2$ heterotetramer of the *nif*EN products and serves as a molecular scaffold for FeMo-cofactor assembly [66]. The product of the *nif*B gene catalyzes the formation of an FeMo-cofactor precursor called NifB-cofactor [58]. NifB-cofactor is thought to provide the Fe-S cage necessary for FeMo-cofactor construction. NifB-cofactor is thought to be inserted into the NifEN complex at an intermediate stage in FeMo-cofactor formation [59, 60]. The *nif*V gene catalyzes the condensation of acetyl-CoA and a-ketoglutarate to form homocitrate, the organic constituent of FeMo-cofactor [67, 164]. The *nif*Q gene product appears to have a role in the mobilization of molybdenum (Mo) required for FeMo-cofactor, but its exact role in this process is not known [84]. Recent work involving the *in vitro* FeMo-cofactor biosynthetic assay has shown that NifX is required for FeMo-cofactor synthesis [83], however, the exact function of NifX in cofactor synthesis remains unknown.

Previously, we have reported a gene fusion approach for the overproduction of the NifEN complex in *A. vinelandii*, as well as the application of immobilized metal-affinity chromatography for the purification of poly-histidine tagged NifEN [165]. This gene fusion/IMAC approach provided a means that allowed the purification of NifEN in quantities amenable for detail spectroscopic characterization. NifEN produced and purified in this manner is apparently unaltered in either its *in vivo* or *in vitro* activities [165]. Biophysical analyses have

been used to show that NifEN contains two identical [4Fe-4S] clusters, which are completely ligated by cysteine residues. Muchmore *et al.* [62] have previously developed a homology model for the three-dimensional structure of the NifEN complex that is based on the crystallographically solved MoFe protein structure [12]. This model places four cysteine residues in a geometry appropriate for forming the [4Fe-4S] cluster of NifEN, which is consistent with our experimental findings. In addition to the conservation of the cluster ligands, NifEN contains a conserved cysteine residue, E-250^{Cys}, that is analogous to the FeMo-cofactor cysteine ligand, D-275^{Cys} [62, 65]. Site directed mutagenesis studies have shown that E-250^{Cys} is required for FeMo-cofactor biosynthesis [166] and that D-275^{Cys} is required for MoFe protein catalytic activity [167, 168]. The role of the E-250^{Cys} ligand may be to bind FeMo-cofactor precursors during their assembly on the NifEN complex.

We speculate that NifEN complex present in a genetic background deficient for the nitrogenase structural genes (*nif*HDK) might trap a precursor to the FeMo-cofactor because the final destination for FeMo-cofactor has been deleted. Metal analysis of the NifEN complex routinely results in the presence of more Fe than is necessary to support the formation of the two [4Fe-4S] cluster (12 –15 Fe atoms per NifEN tetramer). Roll *et. al.,* [60] have previously shown that NifEN can exist in a charged or discharged form, dependent on the presence of NifB-cofactor. We believe that our preparations of the NifEN complex contain a portion of precursor-charged NifEN. The identity of this precursor is most likely NifB-cofactor or a processed form of NifB-cofactor.

In addition to identifying precursors on NifEN, recent work has been directed towards identifying additional *nif* proteins that may be involved in precursor binding/release with the NifEN complex. In *A. vinelandii*, NifY and NifX bear significant primary sequence identity

when compared to one another, as well as being associated with the transcriptional units of the MoFe protein and NifEN, respectively [81]. Based on these considerations, and on the likely structural similarity between the MoFe protein and the NifEN complex [62], we propose that NifY and NifX have related functions. The involvement of NifY in apo-MoFe protein maturation in *K. pneumoniae* suggests NifX may have a role in the mobilization of FeMo-cofactor precursor associated with NifEN.

Current work examines the involvement of FeMo-cofactor precursors on NifEN by EPR and MCD and the interactions between the NifEN complex and NifX by size exclusion chromatography.

Experimental Procedures

Overproduction of NifX in *Escherichia coli*. Overproduction of NifX in *E. coli* was accomplished by constructing a *nif*X gene cartridge *in vitro* and cloning this cartridge into the pT_7-7 plasmid such that *nif*X gene expression was controlled by the T_7 phage transcriptional and translational regulatory elements[169]. The *nif*X gene cartridge was constructed by using an isolated 1.3 kb DNA fragment, that was generated by BamHI restriction enzyme digestion of the hybrid plasmid pDB166, as a template for polymerase chain reaction (PCR) amplification of the *nif*X coding sequence. PCR amplification of *nif*X was performed essentially as recommended by the suppliers of Amplitaq (Perkin-Elmer, Norwalk, CT). Cycling temperatures for PCR amplification of *nif*X were as follows: 95°C for 1 min., 60°C for 2 min., and 72°C for 3 min. The two PCR primers used for *nif*X amplification had the following sequences: 5' CATGCATATGTCCAGCCCGACCCGA 3' and 5' CTACGGATCCTCGCTGAAAAAGTGG 3'. The amino terminal coding region for NifX is underlined in the first primer sequence shown above.

Following *nif*X amplification, the gene cartridge was digested with the restriction enzymes *NdeI* and *BamHI* and ligated to *NdeI*- and *BamHI*-digested pT_7-7 DNA. Proper orientation of *nif*X within the resulting hybrid plasmid (pDB553) such that the T_7 gene-10 promoter directs *nif*X transcription was confirmed by restriction enzyme digestion of isolated plasmid DNA. For overproduction of NifX in *E.coli*, pDB553 was transformed into the host strain BL21 (DE3) and the transformed cells were maintained on LB media supplemented with 100 µg/ml ampicillin. Cells were grown in 500-ml batches in LBA media at 30°C and were induced for NifX production at approximately 160 Klett units (red filter) by the addition of lactose to 1% final concentration. Following addition of lactose, cells were cultured for an additional 2 hours, and after this induction period cells were harvested by centrifugation and frozen at -80° C.

Purification of NifX. NifX was purified anaerobically under a purified argon atmosphere. Crude extracts were prepared by resuspending cells in 25 mM Tris-HCl, pH 7.4 (2.0 ml of buffer per gram weight of cells) and disruption by sonication. Following sonication, solid streptomycin sulfate was added to the disrupted cells at 1% w/v and incubated at ambient temperature for 5 min. The disrupted cells were then subjected to centrifugation at 35,000 rpm for 1 hour in a Beckman Type 45 rotor at 4°C. Contaminating proteins were then precipitated from the streptomycin treated crude extract by bringing the supernatent to 40% saturation with solid ammonium sulfate and allowing this solution to incubate at ambient temperature for 5 min, followed by centrifugation at 35,000 rpm for 30 min. at 4°C. NifX was then precipitated from the 40% ammonium sulfate supernatant by the addition of solid ammonium sulfate to 50% saturation. NifX precipitated in this way was collected by centrifugation at 25,000 rpm for 30 min. and resuspended in buffer (25 mM Tris-HCl, pH 7.4), containing 1 mM dithiothreitol, to a

volume equal to the original supernatant volume. The sample was then loaded onto a 1.5 cm x 15 cm (30 ml of resin) Q-Sepharose column (Pharmacia, Piscataway, NJ) using a peristaltic pump and eluted using a 200 ml 0.1-0.6M linear NaCl gradient controlled by FPLC pumps. NifX eluted between 0.3 and 0.4M NaCl. NifX was collected and concentrated using an Amicon concentrator (Beverly, MA) fitted with a YM10 membrane. Using an FPLC, concentrated NifX was further purified by passing it over a 3.0 cm x 30 cm (80 ml of resin) Sephacryl S300HR size exclusion column (Pharmacia, Piscataway, NJ) that was equilibrated in degassed buffer (25 mM Tris-HCl, pH 7.4, 200 mM NaCl and 1 mM sodium dithionite). Elution of NifX from both columns was monitored by the A_{280} of the eluent. After the Sephacryl S300HR column, NifX was concentrated using an Amicon concentrator (Beverly, MA) fitted with a YM10 membrane. Protein was quantified by a modified biuret method using bovine serum albumin as the standard [130], and protein purity was monitored by SDS-PAGE [131]. The final purified product was stored as frozen pellets in liquid nitrogen until used.

NifEN Complex Purification. The NifEN complex was purified as previously described [165].

Metal Analysis. Fe was quantitated by the α,α' bipyridyl method [107].

NifB-cofactor and FeMo-cofactor Purification. NifB-cofactor was generously donated by V.K. Shah [58]. FeMo-cofactor was extracted purified MoFe protein [56] into NMF and concentrated as previously reported [11].

Size Exclusion Chromatography. High-resolution, analytical size exclusion chromatography was performed using a ZORBAX GF-250 (9.4 mm x 250 mm) HPLC column (Hewlett Packard, Wilmington, DE) equilibrated in degassed 200 mM potassium phosphate buffer, pH 7.3 and 0.5 mM sodium dithionite. The HPLC control unit used for these experiments was a Beckman System Gold equipped with a 126NM solvent module, a 168NM diode array detector and a 100µl sample loop. Column eluent was monitored from 200 nm to 800 nm and data was collected and processed using Beckman System Gold software. Prior to injection onto the HPLC column, samples were incubated for 5 min. at ambient temperature in degassed 200 mM potassium phosphate buffer, pH 7.3, and 0.5 mM sodium dithionite. Protein concentrations for each HPLC run were as follows: NifEN complex, 35µM; NifX, 400 µM (assuming NifX is a monomer with molecular mass of 17,000 predicted by the deduced primary sequence). Metallocluster concentration (given in total concentration of Fe/sample) for each HPLC run was as follows: NifB-cofactor, 220µM; FeMo-cofactor, 250µM.

Biophysical Characterization Methods. The sample concentrations given in the figure captions are based on the quantitation of the purified protein solution by the BCA method [106]. Spectroscopic results were quantified per αβ−heterodimer. Variable-temperature magnetic circular dichroism (VTMCD) spectra were recorded on samples containing 55% (v/v) glycerol in 1-mm cuvettes using an Oxford Instruments Spectromag 4000 (0-7 T) split coil superconducting magnet (1.5-30 K) mated to a Jasco J-715C spectropolarimeter. Experimental protocols used for VTMCD studies were performed as previously described [108, 109]. X-band (~9.6 GHz) Electron Paramagnetic Resonance (EPR) spectra were recorded on a Bruker ESP-300E EPR spectrometer equipped with a dual mode ER-4116 cavity and an Oxford Instruments ESR-9 flow

cryostat. Frequencies were measured with a Systron-Donner 6054B frequency counter, and the magnetic field was calibrated with a Bruker ER035M gaussmeter. Spin quantitations were carried out under non-saturating conditions with 1mM Cu(II)EDTA as the standard, using the procedures outlined by Aasa and Vänngård [110].

Results

Purification of NifEN complex and NifX. Purification of NifEN has been discussed in detail in Chapter I of this dissertation [165]. Purification of NifX was accomplished through heterologous overproduction in *E.coli* and standard protein chromatography methods. The purification of NifX was monitored by sodium dodecylsulfate polyacrylamide gel electrophoresis (SDS-PAGE). Purification of NifX involved ammonium sulfate precipitation, Q-Sepharose ion-exchange chromatography and size exclusion chromatography, and was monitored by A_{280}. Figure 1 shows a SDS-PAGE of purified NifEN complex and purified NifX. NifEN (Fig. 1, lane 1) purified as previously reported [165] and NifX (Fig.1, lane 2) results in a single band with an apparent $M_r \approx$ 15,000, as determined by SDS-PAGE.

Size exclusion Chromatography. Figure 2 shows the elution patterns of the NifEN complex and NifX resulting from size exclusion chromatography. The patterns of the NifEN complex and NifX as monitored at 280 nm (Fig. 2A, trace1 and 2, respectively) result in single absorption peaks as is expected for the purified proteins. However, when NifEN complex and NifX are incubated together (Fig. 2A, trace 3), it appears as if there is a third unresolved peak (indicated by an arrow) which migrates at the position of NifX. This unresolved peak is better observed when the elution profiles are monitored at 405 nm (Fig. 2B). The 405 nm elution profile of the

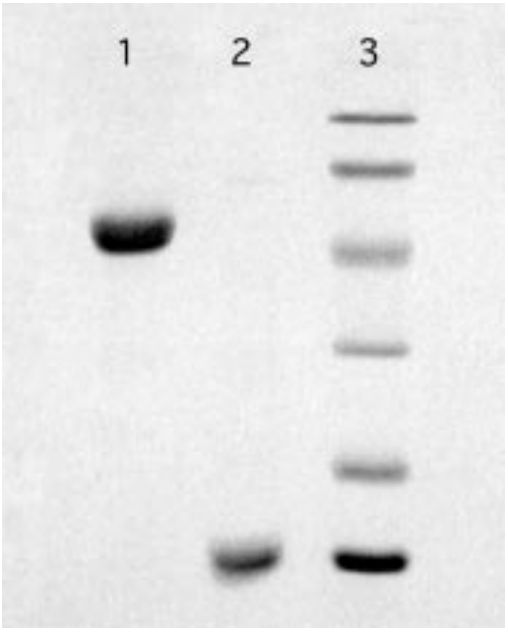

Figure 1. SDS-PAGE for purified NifEN complex and NifX. Proteins were separated using a 4% stacking gel and a 20% separating gel and then stained with Coomassie brilliant blue: lane 1, 10 µg of purified NifEN complex; lane 2, 10 µg of purified NifX; lane 3, M_r standards, (from top: phosphorylase b, 97,400; serum albumin, 66,200; carbonic anhydrase, 31,000; soybean trypsin inhibitor, 21,500; lysozyme, 14,400).

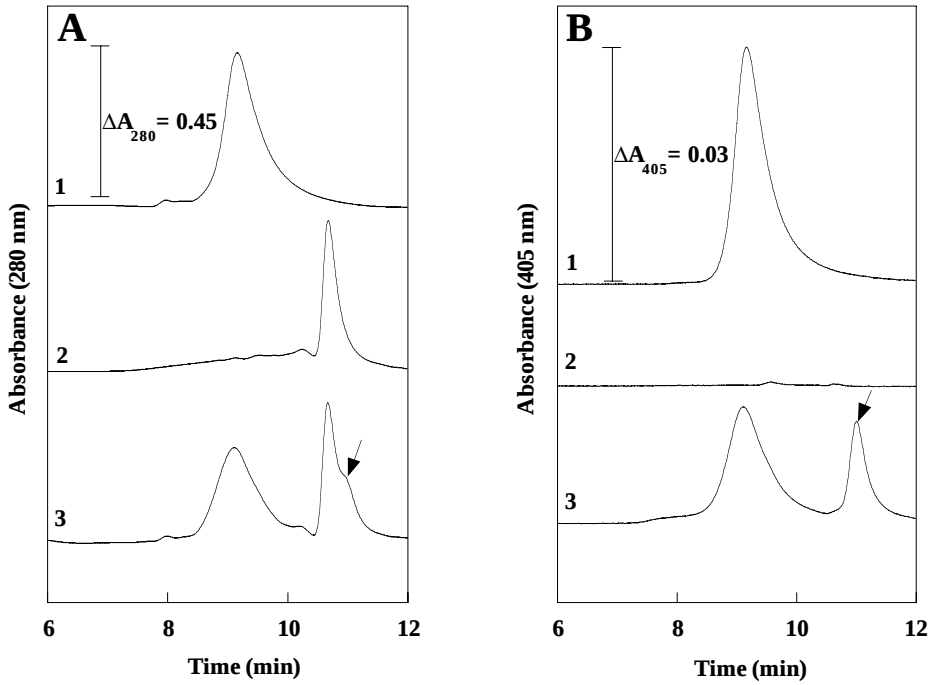

Figure 2. Interaction of NifEN and NifX monitored by size-exclusion HPLC. Column eluent was monitored at 280 nm (A) and 405 nm (B). Trace for both graph A and B are as follows: trace 1, 35 µM NifEN complex; trace 2, 400 µM NifX; trace 3, 35 µM NifEN complex + 400 µM NifX. The sample for trace 3 was prepared by incubating purified NifEN and purified NifX for 5 min. prior to injection onto the size exclusion column.

NifEN complex results in a single peak (Fig. 2B, trace 1), which is primarily due to the presence of the [4Fe-4S] clusters of NifEN. As-isolated NifX has no absorbance in the visible region and results in a trace with no apparent peaks (Fig. 2B, trace 2). When the NifEN complex and NifX (Fig. 2B, trace 3) are incubated together, two peaks are seen as monitored at 405 nm. One peak migrates at the position of NifEN and the other at the position of NifX. Additionally, the NifEN complex peak has a decreased absorbance. This decrease in absorbance is associated with a proportional increased absorbance in the peak that migrates at the position of NifX, which gives rise to the unresolved peak in Fig. 2A, trace 3. It appears that NifX is able to bind a chromophore that has been released from the NifEN complex. This chromophore may be NifB-cofactor or a processed form of NifB-cofactor, which is bound to the NifEN complex.

The interaction of NifX with NifB-cofactor and FeMo-cofactor are shown in Figure 3. Elution profiles of pure NifX (Fig. 3, trace 1), NifB-cofactor (data not shown) and FeMo-cofactor (data not shown) result in a featureless profile monitored at 405 nm. NifX is a colorless protein and so would not be detected at 405nm. However, NifB-cofactor and FeMo-cofactor are dark, brown-green in color, and should absorb in the visible region. It is known that NifB-cofactor and FeMo-cofactor are not stable in an aqueous environment, resulting in the destruction of these metalloclusters. When NifX is incubated with either NifB-cofactor or FeMo-cofactor, the elution profile contains a single peak (Fig. 3, trace 2 or 3, respectively). Upon binding of NifB-cofactor and FeMo-cofactor to NifX, these unstable metallocluster may become protected from damage by the aqueous solvent. When comparing the peaks associated with NifX-NifB-cofactor (Fig. 3, trace 2) and NifX-FeMo-cofactor (Fig. 3, trace 3) with the NifX bound to the chromophore from NifEN (Fig. 3, trace 4), it appears that the NifX-NifB-cofactor and NifX-chromophore migrate in a similar position to one another. The similarity in

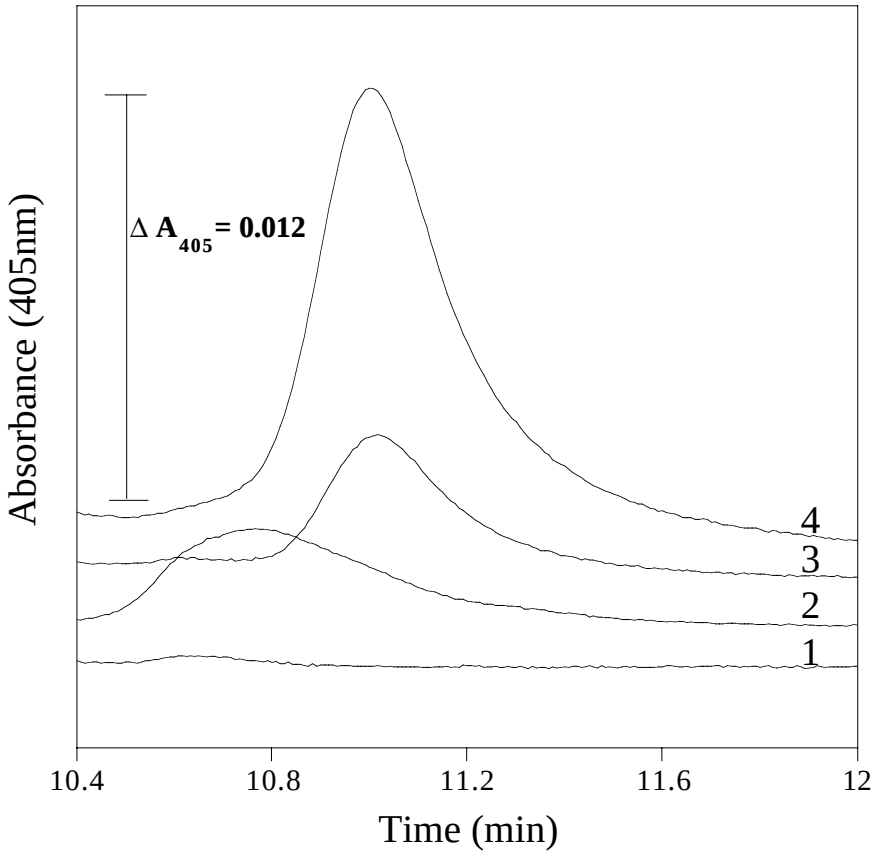

Figure 3. Interaction of NifX with NifB-cofactor and FeMo-cofactor as monitored by size-exclusion HPLC. Protein and protein-metallocluster mixtures were separated by HPLC monitored at 405 nm. Trace 1, NifX; trace 2, NifX + FeMo-cofactor; trace 3, NifX + NifB-cofactor; trace 4, NifEN + NifX. Protein and metallocluster concentrations are given in the Experimental Procedures.

the migration of these peaks infers that the chromophore released from NifEN and bound to NifX may be NifB-cofactor, or more alike NifB-cofactor than FeMo-cofactor.

EPR and VTMCD

NifEN purified by two different protocals was examined by EPR. Purification involved IMAC and anion exchange chromatography or IMAC only. A representative EPR spectrum of thionin-oxidized NifEN purified by IMAC and anion exchange is shown in Figure 4, panel A. The EPR spectrum of IDS-oxidized NifEN purified by IMAC alone is shown in Figure 4, panel B. This resonance accounts for 0.5 spins per NifEN tetramer with no evidence of additional $S > 1/2$ resonances in the low field region**.** The obvious difference between panel A and B is that the spectrum in panel B is representative of two EPR signals that are magnetically coupled. The g-values (1.98, 1.95, and 1.89) and line shape of the EPR signal are unlike any signal previously reported. Both oxidized-NifEN spectra are only discernable at temperatures below 30 K, suggesting they do not originate from a radical species.

VTMCD of thionin-oxidized NifEN results in a spectrum derived from a paramagnetic center on NifEN (Figure 5). Temperature–dependent MCD bands are observed through the 400-700 nm region in the VTMCD spectrum of thionin-oxidized NifEN. The patterns of these bands are not characteristic of any characterized cluster orientation (Agar, J.N. and Johnson, M.K., personal communication). Further information regarding this spectrum is not available at this time.

Discussion

For many years investigators have tried to identify and characterize FeMo-cofactor intermediates. Various biophysical approaches have been used to study the FeMo-cofactor

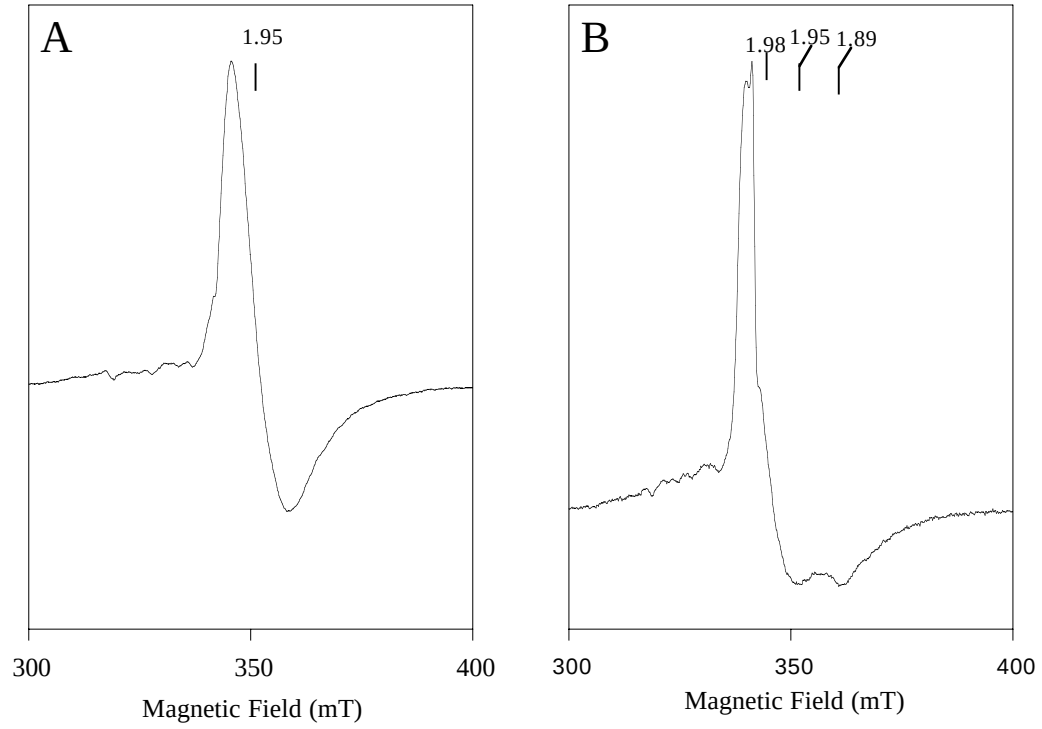

Figure 4. X-Band EPR spectra of oxidized NifEN. Panel A corresponds to NifEN oxidized with thionin and purified as previously described [165]. Panel B corresponds to a partially pure fraction of NifEN from IMAC oxidized with IDS. The samples (70 µM) were in 25 mM Tris-HCl, pH 7.9 with excess oxidant present. Conditions for measurement: microwave frequency, 9.64 GHz; microwave amplitude, 0.64 mT; microwave power, 0.5 mW; and temperature, 12K. Each trace represents the average of 100 scans.

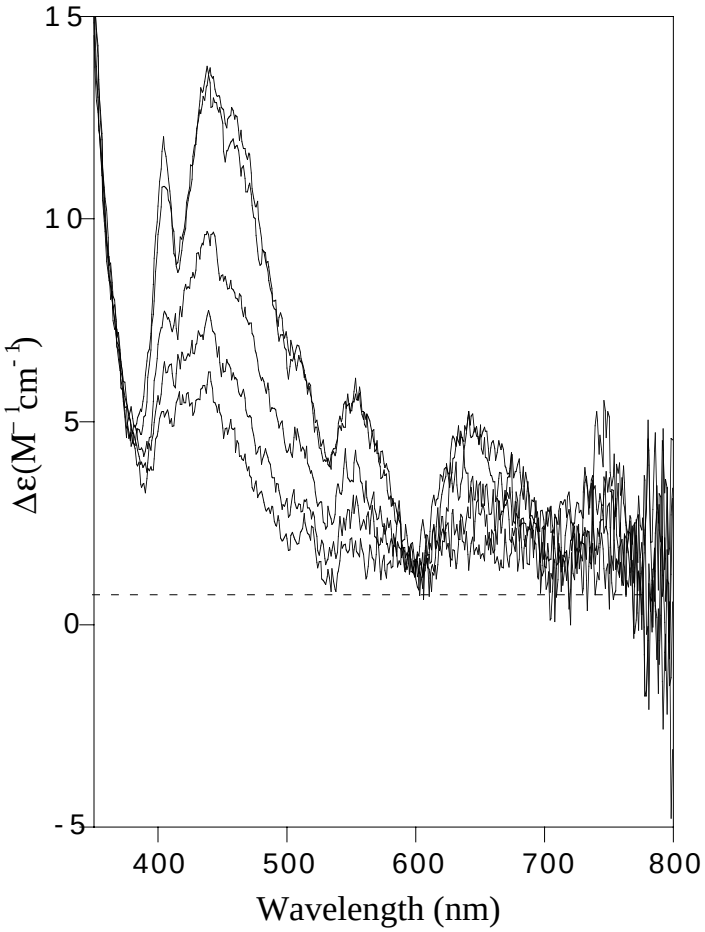

Figure 5. VTMCD spectra of thionin –oxidized NifEN. The sample (50µM) was in 25 mM Tris-HCl, pH 7.9 with excess oxidant present and 55% glycerol. The MCD spectra were recorded in a 1mm cuvette with a magnetic field of 6.0 T, at 2.0, 4.0, 10.0, 20.0, and 35 K. Each trace is the average of 50 scans. All bands increase in intensity with decreasing temperature.

precursor, NifB-cofactor. These examinations, however, have been unsuccessful, resulting in the existence of no known spectroscopic signature for NifB-cofactor (V.K. Shah, personal communication). During FeMo-cofactor biosynthesis, NifB-cofactor is bound to the NifEN complex and processed along the pathway to FeMo-cofactor [59, 60]. Based on this work, it is believed NifEN can exist in a charged or discharged state, depending on the presence or absence of NifB-cofactor. When NifEN is examined in extracts produced by mutants with *nif*B deletions, the discharged form of NifEN accumulates. This discharged form can be converted to the charged form by the addition of NifB-cofactor to the extract [60]. It has long been a goal to purify a form of the NifEN complex with bound NifB-cofactor. It is thought that perhaps NifB-cofactor in a polypeptide environment might exhibit a spectroscopic signal, permitting its characterization.

The NifEN complex has been overproduced and purified by the use of gene fusion and immobilized metal-affinity chromatography. NifEN purified in this manner was subjected to detailed biophysical characterization and found to contain two [4Fe-4S] clusters within each NifEN tetramer [165]. Metal analysis of overproduced NifEN consistently resulted in high values, yielding 12-15 Fe atoms per NifEN tetramer. These data suggest that there is more Fe present within NifEN than is required for two [4Fe-4S] clusters. It is possible that this extra Fe is organized into an FeMo-cofactor precursor bound to the NifEN complex. Because the structural genes for the MoFe protein are deleted in the strain used for the NifEN overproduction system, an obstruction of the FeMo-cofactor biosynthetic machinery would occur. A result of this obstruction would be the persistent binding of FeMo-cofactor precursors to biosynthetic proteins, such as the NifEN complex. The presence of extra Fe on the NifEN complex and the

possibility that it may be an FeMo-cofactor precursor has driven the current course of my research.

Upon oxidation, the [4Fe-4S] clusters of NifEN go from a paramagnetic, EPR active state to a diamagnetic, EPR silent state. However, oxidation of NifEN, with either indigodisulfonate (IDS) or thionin, exhibits the appearance of an EPR signal. Thionin-oxidized NifEN results in an axial EPR spectrum with a g_{AV} value of 1.95. The line shape and g_{AV} of this signal is unlike any spectrum previously seen in the nitrogenase system (Agar, J.N. and Johnson, M.K., personal communication). It is possible that this spectrum is derived from an FeMo-cofactor precursor bound on NifEN. During the purification of NifEN, protein collected on the metal-affinity column is a dark brown-green in color, characteristic of isolated FeMo-cofactor [11]. The subsequent step of purification, DEAE anion-exchange chromatography, removes this color from NifEN. Based on this observation, it is thought that NifEN accumulates in a charged, precursor-bound state *in vivo*, however, this precursor is lost during the subsequent step of the NifEN purification process (DEAE anion-exchange). In an attempt to purify and characterize a fully charged form of NifEN, NifEN was collected after the IMAC step and oxidized with IDS. IDS-oxidation of NifEN results in an EPR resonance that seems to be the product of two magnetically coupled S=1/2 signals. The line shape and g-values of this spectrum is also unique to the nitrogenase system. To date, these data represent the first spectroscopic evidence for an FeMo-cofactor precursor. In addition to the EPR data, VTMCD data was also collected on thionin-oxidized NifEN purified by IMAC and anion exchange chromatography. The resulting MCD spectra indicates the presence of a paramagnetic center, which has a number of temperature dependent MCD bands. Though MCD has not shed any light as to the nature of this paramagnetic center, it does support the presence of the paramagnetic signals observed with

EPR. Characterization of this potential precursor signal has been hindered by the availability of precursor-charged NifEN. In an attempt to isolate a fully charged form of the NifEN complex, a plasmid-based overproduction system for NifEN has been developed and is discussed in Appendix VI to this dissertation. With the application of this plasmid system for overproduction of NifEN and the application of IMAC, it should be possible to purify a fully charged form of NifEN to be used for detailed biophysical characterization .

Recent work involving the *in vitro* FeMo-cofactor biosynthesis assay has implicated the necessity of NifX [83]. This system involves mixing purified components of the FeMo-cofactor synthesis assay in order to determine which components are absolutely essential. From this work, Shah and coworkers [83] have found that the FeMo-cofactor synthesis *in vitro* requires the following: NifEN, NifB-cofactor, molybdenum, homocitrate, Fe protein, MgATP, sodium dithionite, NifX and a final unknown component. Despite the lack of direct evidence, it is possible that the unknown component is NifS, a cysteine desulfurase that activates sulfur for Fe-S cluster synthesis[51, 170]. Though it is known that NifX is required for *in vitro* FeMo-cofactor synthesis, the exact function of NifX in this process is not known. However, since a *nif*X deletion has no effect on nitrogenase activity *in vivo*, there exists a possibility for a gene product that has a general "housekeeping" function, which takes the place of NifX in FeMo-cofactor synthesis. A number of intriguing features are apparent upon inspection of the *nif*-specific gene organization in *A. vinelandii*. The *nifY* gene is contained within the same transcriptional unit that encodes the nitrogenase structural genes and the region encoding *nifE* and *nifN* also contains *nifX* [81]. It has been shown in *Klebsiella pneumoniae* that NifY is involved in the maturation of the apo-MoFe protein [78, 80]. In *A. vinelandii*, NifY and NifX bear significant primary sequence identity when compared to one another [81]. Based on these considerations, and on the likely

structural similarity between the MoFe protein and the NifEN complex [62], we propose that NifY and NifX probably have related functions. This proposed model is also attractive based on primary sequence conservation between NifX and NifB in *Rhodobacter capsulatus*, which suggests NifX may be able to bind and process FeMo-cofactor precursors [82]. The conservation of cysteine residues between NifX and NifB is also seen in *A. vinelandii* and *K. pneumnoniae*, as well as primary sequence conservation among the NifX proteins from these various organisms. The presence of conserved cysteine residues within NifX may provide the ligands necessary to bind a FeMo-cofactor precursor or the FeMo-cofactor. It is also possible that NifX may function to stabilize the NifEN complex for NifB-cofactor insertion, and/or serve to shuttle NifB-cofactor to the NifEN-complex from NifB.

To study the possible functions of NifX in FeMo-cofactor synthesis we examined protein-protein interaction by means of size exclusion chromatography. Incubation of NifEN and NifX resulted in the transfer of a chromophore from NifEN to NifX. The exact nature of the interaction is not certain, however, binding of the chromophore by NifX results in a decrease in the visible absorbance (A_{405}) associated with NifEN. This result taken in consideration with the biophysical data, suggests that NifX can remove the bound precursor on NifEN. To determine the nature of NifX interaction with nitrogenase metalloclusters, we examined the ability of NifX to bind NifB-cofactor and FeMo-cofactor. Preliminary data from this experiment suggest that NifX can bind both NifB-cofactor and FeMo-cofactor. It appears that the chromophore that NifX can remove from NifEN more closely resembles NifB-cofactor. This conclusion is based on the lack of detectable Mo on NifEN [165] and the similarity of the elution profiles of NifX-NifB-cofactor and NifX-chromophore. The exact nature of metallocluster binding by NifX

remains to be seen, however, NifX appears to has the ability to bind the NifB-cofactor, a cofactor precursor from NifEN, and the FeMo-cofactor.

Based on these data, I propose that NifX may function in FeMo-cofactor biosynthesis by mobilizing metalloclusters for FeMo-cofactor synthesis. NifX may act to bind NifB-cofactor from NifB and then transfer this precursor to the NifEN complex. The observation that NifX binds a precursor from NifEN suggests this action may be and equilibrium dependent process or a mechanism to remove damaged precursor from NifEN, preventing unproductive cofactor synthesis. In order to fully understand the nature of NifX's interaction with NifEN a fully charged form of NifEN must be available. After NifX functions to donate NifB-cofactor to NifEN, NifB-cofactor is then processed along the path to FeMo-cofactor. NifX may also be involved with binding the fully formed FeMo-cofactor and donating it to later steps in cofactor synthesis or to apo-MoFe protein directly, based on the observation that NifX can bind the FeMo-cofactor. It may be possible to purify a form of NifX that contains bound FeMo-cofactor precursor by means of a plasmid-based overproduction system in *A. vinelandii* (as described in Appendix VI). In a genetic background deficient in the genes encoding the MoFe protein and NifEN, FeMo-cofactor precursor would become bound to biosynthesis proteins that act at the stage prior to NifEN involvement. Based on data presented in this chapter, NifX would possibly contain bound precursor. Purification of NifX from this genetic background would permit the direct characterization of FeMo-cofactor precursors bound to NifX and help further the understanding of cofactor synthesis.

Acknowledgements

I thank Jeff Agar and Prof. Michael Johnson at the Univ. of Georgia, Center for Metalloenzyme Studies for performing the biophysical characterizations presented in this chapter. I also thank Dr. Jason Christiansen for help with all experiments performed within this chapter.

CHAPTER IV

Preliminary Investigations of the Interaction between the Nitrogenase Fe protein and the NifEN complex

Summary

The Fe protein has three major functions in the nitrogenase enzyme system. Besides serving as the obligate electron donor to the MoFe protein during nitrogenase turnover, the Fe protein is required for the biosynthesis of the iron-molybdenum cofactor (FeMo-cofactor) and for the maturation of $\alpha_2\beta_2$ apo-MoFe protein to the $\alpha_2\beta_2\gamma_2$ form (apo-MoFe protein maturation). The roles played by the Fe protein in FeMo-cofactor biosynthesis and apo-MoFe protein maturation are not well understood. In an attempt to understand the role of the Fe protein in FeMo-cofactor biosynthesis, an altered form of the Fe protein that contains a deletion of leucine 127, L127Δ, was employed to study possible interactions with the NifEN complex. This altered form of the Fe protein does not permit substrate reduction in the nitrogenase system because it binds to the MoFe protein, forming an irreversible protein complex. Based on the structural similarities between the MoFe protein and the NifEN complex, it is possible that L127Δ Fe protein may also bind irreversibly with NifEN. The formation of a of L127Δ Fe protein - NifEN complex has been investigated by size exclusion chromatography. We report here, the formation of a complex between L127Δ Fe protein and the NifEN complex. In addition, preliminary data obtained by stopped-flow spectrophotometry indicate that the Fe protein is capable of transferring an electron to NifEN. This electron transfer event is MgATP dependent and is accompanied by a decrease in the g = 1.95 EPR feature of a NifEN bound FeMo-cofactor precursor. The implications of these results are discussed with respect to the role of the Fe protein in FeMo-cofactor biosynthesis.

Introduction

Nitrogenase catalyzes the conversion of dinitrogen to ammonium during biological nitrogen fixation and is composed of two component metalloproteins, the molybdenum-iron (MoFe) protein and the iron (Fe) protein [171]. The Fe protein, a homodimer of the *nif*H gene product [171], contains two nucleotide binding sites and one [4Fe-4S] cluster bridged between the two identical subunits, ligated by cysteines 97 and 132 [9, 14]. During nitrogenase catalysis, the Fe protein serves as the specific reductant of the MoFe protein, delivering electrons one at a time, in a process involving component protein association-dissociation and MgATP hydrolysis [6]. The MoFe protein is an $\alpha_2\beta_2$ heterotetramer encoded by the *nif*D and *nif*K gene products [171]. To function in nitrogenase turnover, the MoFe protein employs two metalloclusters: the P cluster [23] and the iron-molybdenum (FeMo) cofactor [11, 28]. The P cluster acts in electron processing, mediating the electron flow from the [4Fe-4S] cluster of the Fe protein to the FeMo-cofactor [7]. The FeMo-cofactor provides the site of substrate binding and reduction during nitrogenase catalysis [11, 172, 173].

The Fe protein shares a high degree of structural and functional homology to a family of GTP-binding proteins, termed G-proteins [26] . Two regions of sequence and structural similarity exist between the G-proteins and the Fe protein, these are the P-loop (residues 9 to 16 in the Fe protein), which is involved in the binding of nucleotide (ATP) and the Switch II region (residues 125 to 132 in the Fe protein) involved in the coordination of Mg^{2+} [9, 38]. Though the nucleotide binding site in the Fe protein is approximately 19 Å away from the [4Fe-4S] cluster [9], changes in this cluster have been observed upon MgATP binding. These changes include the exposure of the [4Fe-4S] cluster to iron chelators like α-α'-bipyridyl [17], a decrease in the cluster's mid-point redox potential [18] and changes in the line shape of the electron paramagnetic resonance (EPR) spectrum [19]. These changes are thought to originate from the movement of the α-carbon backbone of the Fe protein in the vicinity of the P-loop and the switch II regions [47].

In addition to its indispensable role in nitrogenase catalysis, the Fe protein is involved in the biosynthesis of FeMo-cofactor [72] and in the maturation of the $\alpha_2\beta_2$ apo-MoFe protein to the $\alpha_2\beta_2\gamma_2$ form [22, 72]. It is believed that the role of the Fe protein in apo-MoFe protein maturation is to catalyze the association of γ (gamma) to the tetrameric form of apo-MoFe protein [22]. Gamma is a non-*nif* protein that is thought to donate FeMo-cofactor to apo-MoFe protein during the formation of holo-MoFe protein [79]. It has recently been shown that an *A. vinelandii*, poly-histidine tagged, apo-MoFe protein purified from a *nif*B deletion strain does not have gamma associated, but can be activated by the addition of preformed FeMo-cofactor [56]. Whether gamma is necessary for FeMo-cofactor insertion and activation of apo-MoFe protein is unclear. The presence of gamma could work to either facilitate the activation of apo-MoFe protein or to discern between catalytically competent FeMo-cofactor and damaged FeMo-cofactor *in vivo*.

The products of at least seven *nif* genes are known to be involved in FeMo-cofactor biosynthesis: *nif*Q, *nif*V, *nif*X, *nif*B, *nif*E, *nif*N, and *nif*H [66, 84, 174, 175]. *Azotobacter vinelandii* mutants harboring deletions in *nif*H, *nif*N, *nif*E or *nif*B produce a cofactorless form of MoFe protein, termed apo-MoFe protein. The *nif*Q gene product has been postulated to act in molybdenum processing during FeMo-cofactor biosynthesis [84]. The *nif*V gene encodes a homocitrate synthase, which provides homocitrate for FeMo-cofactor biosynthesis [67]. The *nif*X gene product has been shown to be required for *in vitro* FeMo-cofactor synthesis, though the exact role of NifX is not known [83]. Evidence suggests NifX may have a role in transport of FeMo-cofactor precursors during biosynthesis (Chapter III of this dissertation). The metabolic product of NifB is NifB-cofactor [58]. NifB-cofactor has been shown to function as a specific iron and sulfur donor to FeMo-cofactor during biosynthesis [59]. The *nif*E and *nif*N gene products together form an $\alpha_2\beta_2$ tetrameric protein [66, 165] that is able to bind NifB-cofactor [59, 60] and, in doing so, provide a scaffold for one or more steps in FeMo-cofactor biosynthesis. An absolute requirement of the *nif*H gene product in FeMo-cofactor biosynthesis has been demonstrated using the *in vitro* FeMo-cofactor synthesis system [99] and the lack of FeMo-cofactor synthesis is strains deleted for *nif*H [70]. However, the precise role(s) of the Fe protein in FeMo-cofactor

biosynthesis is not clear. *Nif*H mutant strains producing Fe protein defective in electron transfer, MgATP binding or hydrolysis accumulate MoFe protein that contains a full complement of FeMo-cofactor [76, 77]. This supports the hypothesis that the Fe protein contains distinct domains that enable it to perform each of its functions independently.

In an attempt to understand the role of the Fe protein in FeMo-cofactor synthesis, the interaction of Fe protein with NifEN has been studied. In this study we have used a site-specifically altered form of the Fe protein, L127Δ. L127Δ Fe protein has been shown to form a catalytically inactive, tight complex with the MoFe protein [95]. L127Δ Fe protein is inactive in FeMo-cofactor synthesis and inhibits FeMo-cofactor synthesis catalyzed by wild-type Fe protein (P. Rangaraj, V.K. Shah, and P.W. Ludden; personal communication). Here we report the formation of a L127Δ complex with NifEN. It is thought that this form of NifEN contains a bound FeMo-cofactor precursor, presumably NifB-cofactor (see Chapter III). This is the first compelling evidence to show the direct interaction of Fe protein with NifEN. Additionally, we report evidence of primary electron transfer from the Fe protein to the NifEN complex, monitored by stopped flow spectroscopy. In light of these data, the possible roles for Fe protein in FeMo-cofactor biosynthesis are discussed.

Experimental Procedures

Purification of L127Δ and Wild-Type Fe proteins**.** Expression and purification of L127Δ Fe protein was carried out as previously reported [135]. The wild-type and L127Δ Fe proteins were purified to > 95% purity as judged by sodium dodecyl sulfate polyacrylamide gel electrophoresis (SDS-PAGE), stained with Coomassie Brilliant blue R250.

Purification of NifEN and NifB-cofactor. The NifEN complex was purified from a NifEN overproducing strain of *A. vinelandii,* DJ1041, as previously described [165]. NifB-cofactor was

purified from an extract of *Klebsiella pneumoniae* strain UN1217 (Δ*nifE*) as previously described [58].

Association of NifEN with L127Δ Fe protein**.** High-resolution, analytical size exclusion chromatography was performed using a ZORBAX GF-250 (9.4 mm x 250 mm, 4μm) HPLC column (Hewlett Packard, Wilmington, DE) equilibrated in degassed 200 mM potassium phosphate buffer, pH 7.3, and 0.5 mM sodium dithionite. The HPLC control unit used for these experiments was a Beckman System Gold equipped with a 126NM solvent module, a 168NM diode array detector and a 100μl sample loop. Column eluent was monitored from 200 nm to 800 nm and data were collected and processed using Beckman System Gold software. Prior to injection onto the HPLC column, proteins were incubated for 5 min. at ambient temperature in degassed 200 mM potassium phosphate buffer, pH 7.3, and 0.5 mM sodium dithionite. The protein concentration of NifEN used for each HPLC run was 35 μM and that of wild type Fe protein or L127Δ Fe protein was 140 μM.

Stopped-Flow Spectrophotometry. A Hi-Tech SF-51 stopped-flow spectrophotometer (Salisbury, Wilts, U.K.) equipped with a computer controlled data acquisition and analysis kit was used to observe the pre-steady state electron transfer from Fe protein to the MoFe protein and NifEN. The SHU-61 sample handling unit was kept inside an anaerobic glove box and temperature was maintained at 22.4 ± 0.1°C with a Techne C-85D closed water circulator attached to a Techne FC-200 flow cooler (Techne Ltd., Duxford, Cambridge, U.K.). The oxidation of the Fe protein was monitored at 430 nm and the data were fitted with a single exponential function [140, 141]. In these experiments, syringe A contained 20μM NifEN, 10mM $MgCl_2$ or MgATP, and syringe B contained 80μM Fe protein. Both syringes contained 10mM sodium dithionite in 50mM HEPES buffer, pH 7.4. Identical conditions were used for experiments involving MoFe protein except that

NifEN was replaced with MoFe protein. The time progression curves for the MgATP induced oxidation of Fe protein represent the average of five experimental traces.

EPR Monitored Electron Transfer to the NifEN complex. In order to determine if the Fe protein is able to transfer electrons to the oxidized [4Fe-4S] clusters of the NifEN complex, EPR spectroscopy was used to monitor the signals from the nitrogenase metal clusters. For these experiments all proteins were exchanged into a 50 mM MOPS buffer, pH 7.0, which contained 2 mM sodium dithionite. The NifEN complex was first oxidized with indigodisulfonate (IDS), which was then removed by passing the sample over a Dowex anion exchange column equilibrated in 50 mM HEPES, pH 7.4, plus 250 mM NaCl. Sodium dithionite was removed from the Fe protein by passage over a Sephadex G-25 column equilibrated in 50 mM HEPES, pH 7.4. Proteins were prepared in an Fe protein:NifEN ratio of 2:1 in the presence of either 2.5 mM MgATP or no nucleotide. Samples of the individual NifEN complex (55 μM), together with Fe protein (110 μM) and the appropriate nucleotide, were flash-frozen in a hexane/liquid nitrogen slurry after approximately 1 minute and monitored by EPR. For perpendicular mode EPR, the spectra are the sum of 20 scans collected at 17 K with a microwave frequency of 9.64 Ghz, microwave power of 20.1 mW, modulation amplitude of 12.63 G at a modulation frequency of 100 kHz, conversion and time constants of 20.48 ms

Protein assays**.** Protein was quantitated by a modified biuret method using bovine serum albumin as the standard [130].

Metal Analysis. Iron was quantitated by the α,α' bipyridyl method as described previously [107].

Results

Complex formation of L127Δ Fe protein with the NifEN complex. Given the putative structural similarity between NifEN and the MoFe protein [62] and the fact that L127Δ Fe protein inhibits

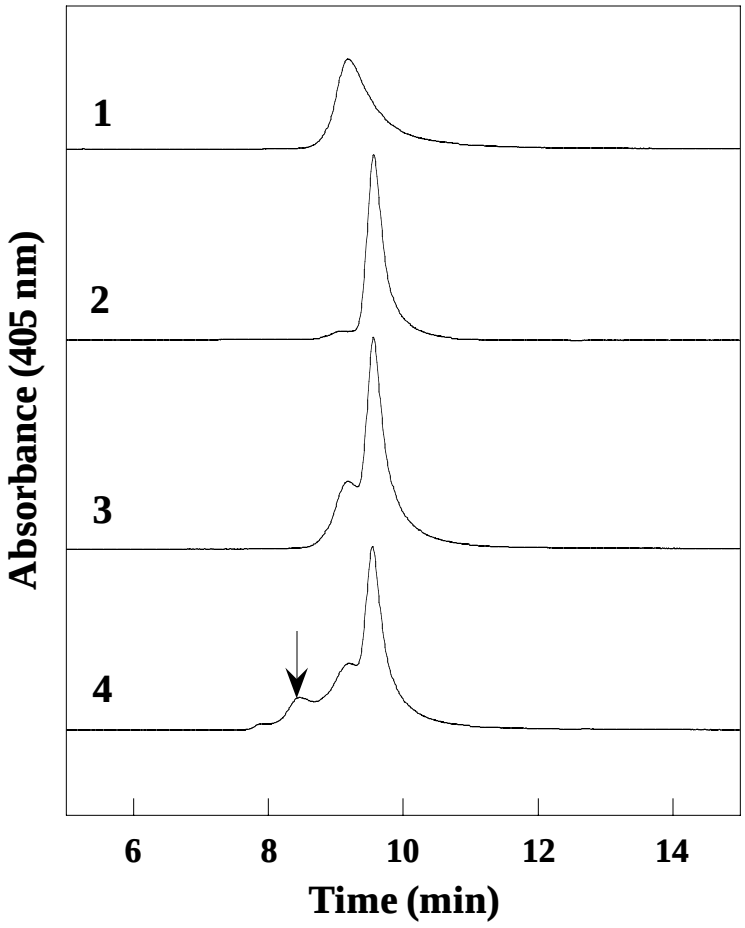

Figure 1. Interaction of NifEN and Fe protein monitored by size exclusion HPLC. Column eluent was monitored at 405 nm. The representative traces correspond to: trace 1, NifEN complex control; trace 2, Fe protein control; trace 3, NifEN complex + wild type Fe protein; trace 4, NifEN complex + L127Δ Fe protein. The arrow in trace 4 indicates the position of the proposed NifEN:L127Δ complex. Proteins were incubated for 5 min at ambient temperature prior to injection onto the column.

acetylene reduction by forming a tight complex with the MoFe protein [95], it was of interest to determine if L127Δ Fe protein could form a complex with NifEN. The association of NifEN with L127Δ Fe protein was monitored by high resolution analytical size exclusion chromatography, as described in Experimental Procedures. Figure 1 shows the elution patterns at 405 nm resulting from the interactions of NifEN and L127Δ Fe protein. The elution profile of NifEN resulted in a single peak (Fig. 1, trace 1), which is partially due to the presence of the[4Fe-4S] clusters of NifEN. Similarly, the elution profile of either the wild-type Fe protein (Fig. 1, trace 2) or L127Δ Fe protein (data not shown) also resulted in a single peak due to the presence of [4Fe-4S] clusters. When NifEN and the wild-type Fe protein were incubated together, the elution profile (Fig. 1, trace 3) resulted in two overlapping peaks that correspond to the positions of the NifEN control (Fig. 1, trace1) and the wild-type Fe protein control (Fig. 1, trace 2). However, when NifEN was incubated with the L127Δ Fe protein, the elution profile showed 3 peaks. Two of the peaks correspond to those observed with the NifEN control and the Fe protein control. The third peak (Fig. 1, trace 4-arrow) elutes at a retention time consistent with a protein that is larger in size than both NifEN and Fe protein. This third peak elutes at a similar position to that observed for the MoFe protein-L127Δ Fe protein complex (data not shown). Based on the elution profile similarities, we believe that the third peak represents a complex of NifEN and L127Δ Fe protein. Additionally, SDS-PAGE was used to confirm the co-elution of NifEN and L127Δ Fe protein (data not shown). In contrast to the complex formed between the MoFe protein and L127Δ Fe protein, the complex formation of NifEN with L127Δ Fe protein is not complete. Because the concentration of L127Δ Fe protein used in this experiment is four times that of NifEN, one would expect that all the NifEN would be complexed with L127Δ and elute at the position of the complex, as occurs with the MoFe protein. This is not the case, which can be seen clearly in Fig. 1, trace 4.

Stopped Flow Electron Transfer from the Fe protein to NifEN. Stopped-flow spectrophotometry observes electron transfer from the Fe protein by monitoring the change in absorbance at 430 nm. When the Fe protein transfers an electron, the [4Fe-4S] cluster is converted from a reduced to an

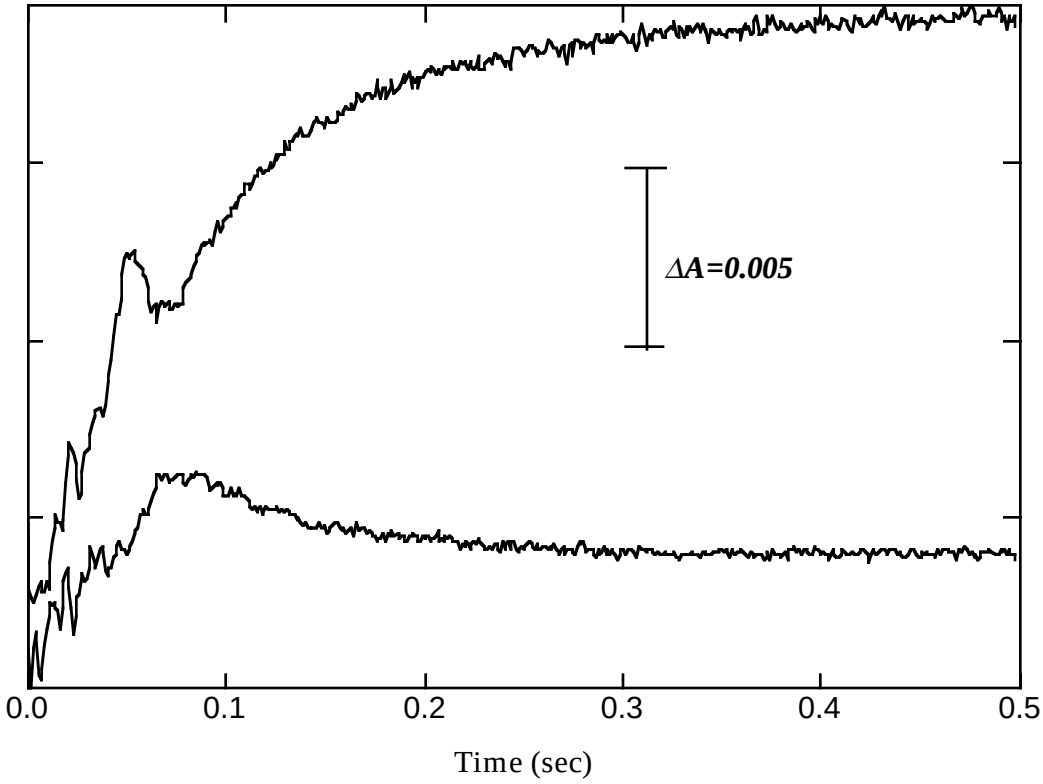

Figure 2. Primary electron transfer from the Fe protein to NifEN monitored by stopped flow spectrophotometry. The apparent first-order rate constant, k, resulted from single-exponential fits to the data. Each trace represents the change in A_{430} that occurred after mixing as described in the Experimental Procedures. The lower trace corresponds to the $MgCl_2$ control and the upper trace to the MgATP experiment.

oxidized cluster. This change in oxidation state corresponds to an increase in absorbance at 430 nm. Figure 2 depicts the primary electron transfer from the Fe protein to NifEN in the absence of MgATP (MgATP-), lower trace, and in the presence of MgATP ($MgATP^{+}$), upper trace. The $MgATP^{-}$ control trace does not show any distinct increases in intensity. Because the data from the experiments are near the limit of detection of the apparatus, there is considerable noise in the traces. In the presence of MgATP, there is an immediate increase in the stopped flow trace. This change in absorbance results from the oxidation of the Fe protein [4Fe-4S] cluster after electron transfer to NifEN. The rate constant of primary electron transfer, k, from the Fe protein to the NifEN complex, in the presence of MgATP, was determined to be $\approx 12\ sec^{-1}$, resulting from an overall change in absorbance of ≈ 0.015 units at 430nm over a 0.5 sec time span. The primary electron transfer rate from the Fe protein to the MoFe protein (data not shown) resulted in a rate constant of $140\ sec^{-1}$, with an overall absorbance change of ≈ 0.06 units at 430nm over a 0.05 sec time span.

In addition to stopped-flow spectrophotometry, electron paramagnetic resonance (EPR) spectroscopy was used to investigate electron transfer between Fe protein and NifEN (Figure 3). For these experiments, reduced Fe protein and oxidized NifEN had excess reductant or oxidant removed, as described in the Experimental Procedures. EPR spectra of reduced Fe protein and reduced Fe protein + MgATP are shown in Fig. 3, trace 1 and 2, respectively. Characteristic changes in the line shape of the EPR spectra of the [4Fe-4S] cluster can be seen on the addition of MgATP to the sample [19]. Oxidation of NifEN with indigodisulfonate (IDS) results in the oxidation of the [4Fe-4S] cluster and FeMo-cofactor precursor contained within NifEN. The oxidized [4Fe-4S] cluster is EPR silent, but oxidation of the bound precursor gives rise to a novel $S=1/2$ axial EPR signal, with a g value of 1.95 (Fig. 3, trace 3). Description of this novel EPR signal is discussed in Chapter III. By observing the behaviour of this oxidized NifEN signal, it is possible to monitor electron transfer by EPR. Incubation of reduced, dithionite-free Fe protein with oxidized NifEN did not elicit a detectable change in the oxidized EPR signal associated with

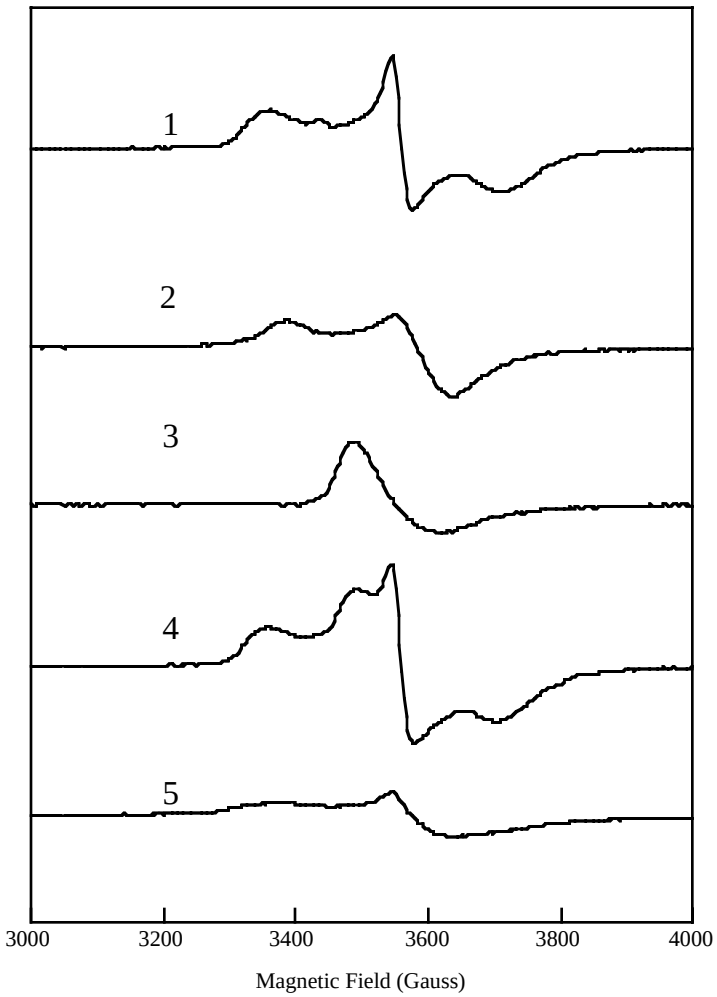

Figure 3. Electron transfer from the Fe protein to NifEN monitored by electron paramagnetic resonance (EPR) spectroscopy. EPR was used to monitor electron transfer from reduced Fe protein to oxidized NifEN complex. Protein samples were prepared as described in the Experimental Procedures. The representative traces correspond to: trace 1, reduced Fe protein; trace 2, reduced Fe protein + MgATP; trace 3, oxidized NifEN; trace 4, reduced Fe protein + oxidized NifEN, and; trace 5, reduced Fe protein + MgATP + oxidized NifEN.

NifEN (Fig. 3, trace 4), resulting in an addition EPR spectrum of reduced Fe protein + oxidized NifEN. When MgATP is added to the mixture of reduced Fe protein and oxidized NifEN, the g_{AV}=1.95 oxidized signal disappears, a result of electron transfer from the Fe protein (Fig. 3, trace 5). The resulting spectrum (Fig. 3, trace 5) from this experiment has a line shape consistent with a reduced [4Fe-4S] cluster, and could be the result of either excess reduced Fe protein with MgATP bound or reduced NifEN [4Fe-4S] cluster.

Discussion

The Fe protein is the specific reductant of the MoFe protein during nitrogenase catalysis. Besides its role in catalysis, the Fe protein plays a role in apo-MoFe protein maturation and in FeMo-cofactor biosynthesis. The role of the Fe protein in apo-MoFe protein maturation is thought to involve the processing of apo-MoFe protein to a form competent for activation by FeMo-cofactor [22, 72, 79]. The competent form of apo-MoFe protein involves the association of a third subunit provided by NifY in *K. pneumoniae* [78] and non-*nif* encoded protein, gamma, in *A. vinelandii* [79]. However, recent purification of an apo-MoFe protein produced by a *nif*B-deletion in *A. vinelandii* has shown that the third subunit, gamma, is not necessary for FeMo-cofactor activation [56]. In addition, unpublished results from our group (Christiansen, J., Goodwin, P.J. and Dean, D.R.) have indicated that apo-MoFe produced by a *nif*H deletion does not contain intact, or redox active, P clusters, in comparison to an apo-MoFe protein produced by a *nif*B deletion that does contain P clusters [56]. These data contradict a finding that shows the apo-MoFe protein produced by a *nif*H deletion in *A. vinelandii* contains intact P clusters [176]. The conflicting data include metal analysis and EPR, which shows oxidation of the Δ*nif*H apo-MoFe protein does not elicit the EPR signals characteristic of oxidized P clusters [56]. This suggests that the Fe protein may play a pivotal role early in the maturation of the MoFe protein, involving synthesis of mature P clusters.

The exact role of Fe protein in FeMo-cofactor biosynthesis is not fully understood, however, several possible functions for the Fe protein can be envisioned. Based on the potential

structural similarities between the MoFe protein and the NifEN complex [62], it is possible Fe protein may be involved with NifEN during FeMo-cofactor synthesis. Several possibilities exist for the necessity of Fe protein to complex to NifEN. The Fe protein may be required in a redox or electron transfer capacity, providing reducing equivalents during cofactor biosynthesis. This action may be required to process cofactor intermediates or promote release of processed intermediates during synthesis. It is also possible that Fe protein interaction with the NifEN complex may induce a conformational change in NifEN, which may be required for the processing of FeMo-cofactor intermediates during synthesis. Additionally, the binding of Fe protein might promote a conformational change permitting access to the FeMo-cofactor processing site within NifEN. This action could be necessary for the addition or removal of intermediates during synthesis. Although these possibilities sound intriguing, there is little evidence supporting Fe protein involvement with NifEN. In fact, certain strains that produce altered Fe proteins that are catalytically inactive still produce MoFe protein with intact FeMo-cofactor [76, 77]. Fe protein produced from a *nif*M mutant strain is inactive in substrate reduction, but can still participate in the synthesis of FeMo-cofactor [55, 75]. These studies suggest that the role of the Fe protein in FeMo-cofactor biosynthesis is different from its role in nitrogenase catalysis.

To date, experiments aimed at determining the possible interaction of Fe protein with NifEN have been unsuccessful. However, by making use of a site-specifically altered Fe protein, L127Δ, we have now been able to examine Fe protein interaction with NifEN. L127Δ Fe protein has been shown to mimic an MgATP bound state of the Fe protein [135] and forms a tight complex with the MoFe protein [95], inhibiting nitrogenase turnover. In light of the likely structural similarities between NifEN and the MoFe protein [62], it is possible that L127Δ Fe protein may form a complex with NifEN. L127Δ Fe protein was shown not to function in the *in vitro* FeMo-cofactor synthesis reaction (P. Rangaraj and P.W. Ludden, personal communication). Additionally, L127Δ Fe protein was shown to inhibit FeMo-cofactor synthesis catalyzed by wild type Fe protein. Total inhibition of FeMo-cofactor synthesis was achieved with a four-fold excess of L127Δ Fe protein over wild type Fe protein. These data suggest that L127Δ Fe protein is

sequestering vital components of FeMo-cofactor synthesis, and thus inhibiting the overall process. Two likely candidates that may interact with L127Δ Fe protein are the apo-MoFe protein and the NifEN complex. Because FeMo-cofactor synthesis is not dependent on apo-MoFe protein [63], the site of inhibition by L127Δ Fe protein is most likely NifEN. However, it does appear that MoFe protein purified from the L127Δ Fe protein strain does contain intact FeMo-cofactor (data not shown).

The NifEN complex exists in two predominant forms, a charged and an discharged form [60]. In the charged form, it is believed that NifEN contains bound NifB-cofactor, an FeMo-cofactor precursor. In extracts containing a deletion in *nif*H, this is the predominant form of NifEN that accumulates [60]. When NifEN is examined in extracts produced by *nif*B deletions, the discharged form of NifEN accumulates. This discharged form can be converted to the charged form by the addition of NifB-cofactor to the extract [60]. Because the charged form of NifEN accumulates in a *nif*H deletion, it has been proposed that the Fe protein involvement in FeMo-cofactor synthesis occurs after the binding of NifB-cofactor to NifEN [60]. Based on work presented in Chapter III of this dissertation, NifEN appears to be primarily in the discharged state due to the loss of precursor during the purification of NifEN. Though most NifEN is discharged, a population does exist that is in the charged, NifB-cofactor bound, state. Thus, it would be likely that only a small portion of NifEN would be able to complex with L127Δ Fe protein, which is consistent with the data presented here.

In this study, we examined the possible interaction of NifEN and Fe protein using size exclusion chromatography. Control experiments that examined the interaction of wild type Fe protein and NifEN did not yield complex formation. When NifEN was incubated with L127Δ Fe protein and subjected to size exclusion chromatography, it appeared as if a complex was formed. The complex formed with NifEN and L127Δ Fe protein is different from that complex formed between L127Δ Fe protein and MoFe protein. When excess L127Δ Fe protein is incubated with MoFe protein, all available MoFe protein becomes complexed with L127Δ Fe protein, however, when excess L127Δ Fe protein is incubated with NifEN only a small fraction of NifEN forms a

complex. This partial complex formation is thought to be the result of the NifEN existing as a mixed species of charged and discharged forms. If only NifEN with bound NifB-cofactor can complex with L127Δ Fe protein, and only a small population of charged NifEN exists, then only a small fraction of NifEN would complex with L127Δ Fe protein. These data are also consistent with unpublished work at the University of Wisconsin (P. Rangaraj, V.K. Shah, and P.W. Ludden), which finds that complex formation between L127Δ Fe protein and NifEN is dependent on the addition of NifB-cofactor. These results suggest that involvement of the Fe protein in FeMo-cofactor biosynthesis occur at the stage of NifEN involvement, after NifEN has bound the FeMo-cofactor precursor, NifB-cofactor. However, the observed complex of NifEN and L127Δ Fe protein may be a result of an equilibrium between of Fe protein and NifEN. Considering the conservation of primary sequence between the MoFe protein and NifEN [62], it is likely that NifEN is the product of a gene duplication event early in the evolution of nitrogenase. Based on this fact, the association of the Fe protein with the NifEN complex may only be a function of sequence conservation.

We also examined the possibility of electron transfer from the Fe protein to NifEN as monitored by stopped flow spectrophotometry. The stopped flow experiment monitors primary electron transfer from the Fe protein to the NifEN complex. Data from the primary electron transfer experiment suggest that the Fe protein can transfer an electron to the NifEN complex only when MgATP is present. Though it is possible to calculate kinetic constant for the Fe protein-NifEN complex electron transfer reaction, these values may not be accurate. Because NifEN exists as a heterogeneous mixture of charged and discharged NifEN, determination of the kinetic rate constant for electron transfer becomes difficult. Therefore, it is better to discuss the primary electron transfer data in a qualitative light, rather than quantitative. The rate of electron transfer from the Fe protein to NifEN is approximately 10% that of transfer to the MoFe protein, with an amplitude approximately 25% that of the MoFe protein. These results may be accurate, however, until sufficient quantities of a homogeneous sample of NifEN can be obtained, full kinetic characterization of NifEN will remain undetermined. Additionally, limited quantities of NifEN

prevented the completion of a number of critical control experiments. The Fe protein undergoes a conformational change associated with the binding of either MgATP or MgADP. This conformational change results in the lowering of the midpoint potential of the [4Fe-4S] cluster of the Fe protein. It is therefore possible that the primary electron transfer from the Fe protein to NifEN could be the result of the lowering of the redox potential of the [4Fe-4S] cluster and not the specific MgATP hydrolysis-dependent transfer of electrons. To date, efforts to detect MgATP hydrolysis in a mixture of NifEN and Fe protein has not been successful. However, it should be noted that Fe protein and NifEN form a complex when incubated with MgATP and AlF_4^- (data not shown). AlF_4^- has been shown to inhibit nitrogenase catalysis by the formation of a MgADP-AlF_4^- analogue in the Fe protein-MoFe protein docked complex [39, 40]. This MgADP-AlF_4^- analogue acts as a MgATP transition state analogue, preventing the dissociation of the Fe protein and MoFe protein. Because AlF_4^- treatment also causes the Fe protein and NifEN to complex, this suggests that the Fe protein-NifEN complex is capable of hydrolyzing MgATP, since the action of AlF_4^- is thought to occur after MgATP hydrolysis.

Electron transfer from the Fe protein to NifEN was also investigated using EPR spectroscopy. In this set of experiments, a novel EPR signal of a NifEN bound FeMo-cofactor precursor was used to monitor electron transfer. The initial discussion of this novel EPR signal is contained within Chapter III of this dissertation. The signal is an axial S=1/2 EPR signal with a g_{AV} value of 1.95. The line shape and g value of this signal is unlike any other EPR signal previously reported. The presence of this signal, which for the content of discussion will be called ENox, permitted the investigation of EPR monitored electron transfer. The data from these experiments indicated that reduced Fe protein, which was free of excess dithionite, was capable to transferring electrons to NifEN when MgATP is present. The MgATP dependent electron transfer is monitored by the disappearance of the ENox signal in the EPR spectra. Control experiments that did not contain any nucleotide did not result in electron transfer to the ENox signal. However, incubation of oxidized NifEN and reduced Fe protein with MgADP did result in electron transfer and loss of the EN_{ox} EPR signal. It is possible that either the MgADP stock was contaminated

with MgATP, or the Fe protein functions as a non-specific reductant by the lowering of its [4Fe-4S] cluster upon nucleotide binding. Both the EPR and stopped flow data support a function of the Fe protein involving the transfer of electrons to the NifEN complex.

The work presented in this chapter is not definitive. Further study of the interaction between the Fe protein and NifEN is necessary to understand the role of Fe protein during FeMo-cofactor biosynthesis. It appears that the Fe protein can only interact with NifEN if NifEN is in the charged, or NifB-cofactor-bound state. Therefore, the population of charged NifEN dictates its participation with the Fe protein. Until homogenous samples of charged and discharged NifEN can be prepared, deciphering this interaction will be difficult. It is possible that the role of the Fe protein in biosynthesis is to transmit a signal by binding to NifEN. This signal could be to simply inform the FeMo-cofactor biosynthetic machinery that the Fe protein is present, and to proceed with the maturation of the MoFe protein. This suggestion makes sense since there is no need to mature the MoFe protein if the Fe protein is not present to participate in catalysis. From this study, it appears that the Fe protein can form a complex with the NifEN complex that contains bound NifB-cofactor. Whether or not this Fe protein interaction induces modification of NifB-cofactor on NifEN is not known at this time. It could be that this interaction is the signal for the NifEN-NifB-cofactor complex to bind Mo and homocitrate and finish the process of FeMo-cofactor synthesis. Mature FeMo-cofactor could then be transferred to a transport protein, prior to insertion into apo-MoFe protein. A likely candidate for the transport protein is NifX, which has the ability to bind both NifB-cofactor and FeMo-cofactor (see Chapter III). The role of NifX in FeMo-cofactor biosynthesis is not clear, though the requirement for this protein has been demonstrated by the *in vitro* FeMo-cofactor synthesis reaction [83].

Acknowledgements

I thank Prof. Lance Seefeldt at Utah State University for supplying the L127Δ Fe protein and permitting a portion of this work to be completed in his laboratory. I thank Dr. Jason Christiansen for help with all of the experiments performed in this chapter.

CHAPTER V

Summary and Outlook

The research contained within this dissertation concerns the biosynthesis of the FeMo-cofactor of nitrogenase, particularly involvement of the NifEN complex. The current state of understanding regarding FeMo-cofactor biosynthesis is as follows. Fe and S are most likely mobilized by the action of NifU and NifS, respectively. Fe and S mobilized in this manner are then donated to NifB, which catalyzes the formation of an FeMo-cofactor precursor that is called NifB-cofactor. NifB-cofactor is then transferred to the NifEN complex, which functions as an assembly point for FeMo-cofactor synthesis. After the formation of the NifEN-NifB-cofactor complex, it is processed in an unknown manner by the action of the Fe protein of nitrogenase. The following steps of FeMo-cofactor synthesis are unclear. It is thought that after the Fe protein interacts with the NifEN-NifB-cofactor complex, that the system is ready for the incorporation of molybdenum (Mo) and homocitrate. Whether FeMo-cofactor synthesis is completed on the NifEN complex is still unknown. After the biosynthetic cycle is completed, fully formed FeMo-cofactor is available for apo-MoFe protein maturation. How FeMo-cofactor is mobilized to apo-MoFe protein maturation is also unknown.

The purpose of my dissertation was to shed light on this biosynthetic pathway, particularly steps within this process involving the NifEN complex. The NifEN complex is an $\alpha_2\beta_2$ tetramer that functions as an assembly site during an FeMo-cofactor biosynthesis. Until recently, work involving the characterization of NifEN was hindered by the lack of available protein. My initial work involved a gene fusion approach for overproduction of the NifEN complex in *A. vinelandii* and the application of immobilized metal-affinity chromatography for

NifEN complex purification. This approach provided a system that allowed the purification of NifEN in quantities necessary for biophysical and biochemical characterizations. Biophysical characterization determined that the NifEN complex contained two identical [4Fe-4S] clusters per NifEN tetramer. Further biophysical analysis was also used to perform the initial characterization of FeMo-cofactor precursors bound to the NifEN complex. Biochemical studies involved the interaction of the NifEN complex with other proteins required for FeMo-cofactor biosynthesis. Preliminary findings indicate that the NifEN complex interacts with NifX and the Fe protein of nitrogenase.

Future studies of NifEN would involve characterization of the preliminary findings reported in this dissertation. To facilitate overproduction of the NifEN complex, a plasmid-based overproduction system has been devised. Not only will this plasmid system be useful for overproduction of NifEN, but site specifically altered forms of NifEN will be easier to generate and purify. The ability to generate and purify site specifically altered forms will be useful in deciphering the interaction of NifEN and other biosynthetic proteins, such as NifX and the Fe protein.

LITERATURE CITED

1. Burns, R.C. and R.W.F. Hardy, *Nitrogen Fixation in Bacteria and Higher Plants*. 1975, New York: Springer-Verlag.
2. Newton, W.E. and W.H. Orme-Johnson, *Nitrogen Fixation*. 1980, Baltimore: University Park Press.
3. Bishop, P.E. and R. Premakumar, *Alternative Nitrogen Fixation Systems*, in *Biological Nitrogen Fixation*, G. Stacey, R.H. Burris, and H.J. Evans, Editors. 1992, Chapman & Hall: New York. p. 736-762.
4. Eady, R.R., *Structure-Function Relationships of Alternative Nitrogenases.* Chem. Rev., 1996. 96: p. 3013-3030.
5. Ribbe, M., Gadkari, D. and Meyer, O., *N2 fixation by Streptomyces thermoautotrophicus involves a molybdenum- dinitrogenase and a manganese-superoxide oxidoreductase that couple N2 reduction to the oxidation of superoxide produced from O2 by a molybdenum-CO dehydrogenase.* J Biol Chem, 1997. 272(42): p. 26627-33.
6. Burgess, B.K. and D.J. Lowe, *Mechanism of Molybdenum Nitrogenase.* Chem. Rev., 1996. 96: p. 2983-3011.
7. Dean, D.R., J.T. Bolin, and L. Zheng, *Nitrogenase metallclusters: Structures, organization, and synthesis.* J. Bacteriol., 1993. 175: p. 6737-6744.
8. Mortenson, L.E., J.A. Morris, and D.Y. Yeng, *Purification, Metal Composition and Properties of molybdenum ferredoxin and azoferredozin, two of the*

components of the nitrogen-fixing system of Clostridium pasteurianum. BBA, 1967. 141: p. 516-22.

9. Georgiadis, M.M., H. Komiya, P. Chakrabarti, D. Woo, J.J. Kornuc, and D.C. Rees, *Crystallographic structure of the nitrogenase iron protein from Azotobacter vinelandii.* Science, 1992. 257: p. 1653-1659.

10. Mortenson, L.E., M.N. Walker, and G.A. Walker, *Effect of Magnesium Adenosine Di and Triphosphates on the Structure and Electron Transport Function of the Components of Clostridial Nitrogenase*, in *Nitrogen Fixation*. 1976, Washington State University Press. p. 117-49.

11. Shah, V.K. and W.J. Brill, *Isolation of an Iron-Molybdenum Cofactor from nitrogenase.* Proc. Natl. Acad. Sci. (USA), 1977. 74(8): p. 3249-3253.

12. Kim, J. and D.C. Rees, *Crystallographic structure and functional implications of the nitrogenase molybdenum iron protein from Azotobacter vinelandii.* Nature, 1992. 360: p. 553-560.

13. Hageman, R.V. and R.H. Burris, *Nitrogenase and nitrogenase reductase associate and dissociate with each catalytic cycle.* Proc. Natl. Acad. Sci. USA, 1978. 75: p. 2699-2702.

14. Hausinger, R.P. and J.B. Howard, *Thiol Reactivity of the Nitrogenase Fe-Protein from Azotobacter vinelandii*. J. Biol. Chem., 1983. 258(22): p. 13486-92.

15. Walker, J.E., M. Saraste, M.J. Runswick, and N.J. Gay, *Distantly related sequences in the α- and β-subunits of ATP synthase, myosin, kinases and other ATP-requiring enzymes and a common nucleotide binding fold.* EMBO J., 1982. 1: p. 945-951.

16. Robson, R.L., *Identification of possible adenine nucleotide binding sites in nitrogenase Fe- and MoFe-proteins by amino acid sequence comparison.* FEBS Lett., 1984. 173: p. 394-398.

17. Walker, G.A. and L.E. Mortenson, *Effect of magnesium adenosine 5'-triphosphate on the accessibility of the iron of clostridial azoferredoxin, a component of nitrogenase.* Biochemistry, 1974. 13: p. 2382-2388.

18. Zumft, W.G., L.E. Mortenson, and G. Palmer, *Electron-paramagnetic-resonance studies on nitrogenase. Investigation of the oxidation-reduction behaviour of azoferredoxin and molybdoferredoxin and potentiometric and rapid-freeze techniques.* Eur. J. Biochem., 1974. 46: p. 525-535.

19. Morgan, T.V., R.C. Prince, and L.E. Mortenson, *Electrochemical titration of the S=3/2 and S=1/2 states of the iron protein of nitrogenase.* FEBS Lett., 1986. 206: p. 4-8.

20. Seefeldt, L.C., T.V. Morgan, D.R. Dean, and L.E. Mortenson, *Mapping the sites of MgATP and MgADP interactions with the nitrogenase of Azotobacter vinelandii: Lysine 15 of the iron protein plays a major role in MgATP interaction.* J. Biol. Chem., 1992. 267: p. 6680-6688.

21. Moustafa, E. and L.E. Mortenson, *Acetylene reduction by nitrogen-fixing extractes of Clostridium pasteurianum: ATP requirement and inhibition by ADP.* Nature, 1967. 216: p. 1241-1242.

22. Allen, R.M., M.J. Homer, R. Chatterjee, P.W. Ludden, G.P. Roberts, and V.K. Shah, *Dinitrogenase reductase-dependent and MgATP-dependent maturation of*

apodinitrogenase from Azotobacter-vinelandii. J. Biol. Chem., 1993. 268(31): p. 23670-23674.

23. Peters, J.W., M.H.B. Stowell, S.M. Soltis, M.G. Finnegan, M.K. Johnston, and D.C. Rees, *Redox-Dependent Structural Changes in the Nitrogenase P-Cluster.* Biochemistry, 1997. 36(6): p. 1181-1187.

24. Lanzilotta, W.N., J. Christiansen, D.R. Dean, and L.C. Seefeldt, *Evidence for Coupled Electron and Proton Transfer in the [8Fe-7S] Cluster of Nitrogenase.* Biochemistry, 1998. 37(32): p. 11376-84.

25. Peters, J.W., K. Fisher, W.E. Newton, and D.R. Dean, *Involvement of the P cluster in intramolecular electron transfer within the nitrogenase MoFe protein.* J. Biol. Chem., 1995. 270: p. 27007-27013.

26. Howard, J.B. and D.C. Rees, *Nitrogenase: A nucleotide -dependent molecular switch.* Annu. Rev. Biochem., 1994. 63: p. 235-264.

27. Chan, J.M., Christiansen, J., Dean, D.R. and Seefeldt, L.C., *Spectroscopic Evidence for Changes in the Redox State of the Nitrogenase P-Cluster during Turnover.* Biochemistry, 1999.

28. Kim, J. and D.C. Rees, *Structural models for the metal centers in the nitrogenase molybdenum-iron protein.* Science, 1992. 257: p. 1677-1682.

29. Hawkes, T.R., P.A. McLean, and B.E. Smith, *Nitrogenase from nifV mutants of Klebsiella pneumoniae contains an altered form of the iron-molybdenum cofactor.* Biochem. J., 1984. 217: p. 317-321.

30. Liang, J., M. Madden, V.K. Shah, and R.H. Burris, *Citrate substitutes for homocitrate in nitrogenase of a nifV mutant of Klebsiella pneumoniae.* Biochemistry, 1990. 29: p. 8577-8581.

31. Scott, D.J., H.D. May, W.E. Newton, K.E. Brigle, and D.R. Dean, *Role for the nitrogenase MoFe protein α-subunit in FeMo-cofactor binding and catalysis.* Nature, 1990. 343: p. 188-190.

32. Dance, I., *Theoretical Investigations of the Mechanism of Biological Nitrogen Fixation at the FeMo Cluster Site.* J. Bioinorg. Chem., 1996. 1: p. 581-586.

33. Hughes, D.L., S.K. Ibrahim, C.J. Pickett, G. Querne, A. Lauoenan, J. Talarmin, A. Queiros, and A. Fonesca, *On Carboxylate as a Leaving Group at the Active Site of Mo Nitrogenase.* Polyhedron, 1994. 13: p. 3341-3348.

34. Thorneley, R.N.F., G.A. Ashby, C. Julius, J.L. Hunter, and M.R. Webb, *Nitrogenase of Klebsiella pneumoniae: Reversibility of the reductant-independent MgATP-cleavage reaction is shown by MgADP catalysed phosphate/water oxygen exchange.* Biochem. J., 1991. 277: p. 735-741.

35. Deits, T.L. and J.B. Howard, *Effects of salts on Azotobacter vinelandii nitrogenase activities.* J. Biol. Chem., 1990. 265: p. 3859-3867.

36. Willing, A.H., M.M. Georgiadis, D.C. Rees, and J.B. Howard, *Cross-linking of nitrogenase components.* J. Biol. Chem., 1989. 264: p. 8499-8503.

37. Howard, J.B., *Protein component complex formation and adenosine triphosphate hydrolysis in nitrogenase*, in *Molybdenum Enzymes, Cofactors, and Model Systems*, E.I. Stiefel, D. Coucouvanis, and W.E. Newton, Editors. 1993, American Chemical Society: Washington DC. p. 271-289.

38. Schindelin, H., C. Kisker, J.L. Schlessman, J.B. Howard, and D.C. Rees, *Structure of ADP•AlF4- stabilized nitrogenase complex and its implications fro signal transduction.* Nature, 1997. 387: p. 370-376.

39. Duyvis, M.G., H. Wassink, and H. Haaker, *Formation and characterization of a transition state complex of Azotobacter vinelandii nitrogenase.* FEBS Lett., 1996. 380: p. 233-236.

40. Renner, K.A. and J.B. Howard, *Aluminum Fluoride Inhibition of Nitrogenase: Stabilization of a Nucleotide•Fe-Protein•MoFe-Protein Complex.* Biochemistry, 1996. 35(17): p. 5353-5358.

41. Lowe, D.J. and R.N.F. Thorneley, *The mechanism of Klebsiella pneumoniae nitrogenase action: The determination of rate constants required for the simulation of the kinetics of N_2 reduction and H_2 evolution.* Biochem. J., 1984. 224: p. 903-909.

42. Simpson, F.B. and R.H. Burris, *A Nitrogen Pressure of 50 Atmoshperes Does Not Prevent Evolution of Hydrogen by Nitrogenase.* Science, 1984. 224: p. 1095-1097.

43. Dilworth, M.J., *Acetylene reduction by nitrogen-fixing prepartions from Clostridium pasteurianum.* Biochim. Biophys. Acta, 1966. 127: p. 285-294.

44. Scott, D.J., D.R. Dean, and W.E. Newton, *Nitrogenase-catalyzed ethane production and CO-sensitive hydrogen evolution from MoFe proteins having amino acid substitutions in an α-subunit FeMo cofactor-binding domain.* J. Biol. Chem., 1992. 267: p. 20002-20010.

45. Dilworth, M.J., R.R. Eady, and R.L. Robson, *Ethane formation from acetylene as a potential test for vanadium nitrogenase in vivo.* Nature, 1987. 327(14): p. 167-8.

46. Dilworth, M.J., R.R. Eady, and M.E. Eldridge, *The vanadium nitrogenase of Azotobacter chroococcum: Reduction of acetylene and ethylene to ethane.* Biochem. J., 1988. 249: p. 745-751.

47. Seefeldt, L.C. and D.R. Dean, *Role of Nucleotides in Nitrogenase Catalysis.* Acc. Chem. Res., 1997. 30: p. 260-266.

48. Lowe, D.J., K. Fisher, and R.N.F. Thorneley, *Klebsiella pneumoniae nitrogenase. Mechanism of acetylene reduction and its inhibition by carbon monoxide.* Biochem. J., 1990. 272(3): p. 621-625.

49. Howard, K.S., P.A. McLean, F.B. Hansen, P.V. Lemley, K.S. Koblan, and W.H. Orme-Johnson, *The Klebsiella pneumoniae nifM gene product is required for stabilization and activation of nitrogenase iron protein in Escherichia coli.* J. Biol. Chem., 1986. 261: p. 772-778.

50. Rudd, K.E., Sofia, H.J., Koonin, E.V., Plunkett, G., Lazar, S., and Rouviere, P.E., *A new family of peptidyl-prolyl isomerases.* Trends Biochem. Sci., 1995. 20: p. 12-14.

51. Zheng, L. and D.R. Dean, *Catalytic formation of a nitrogenase iron-sulfur cluster.* J. Biol. Chem., 1994. 269: p. 18723-18726.

52. St. John, R.T., H.M. Johnson, C. Seidman, D. Gerfinkel, J.K. Gordon, V.K. Shah, and W.J. Brill, *Biochemistry and genetics of Klebsiella pneumoniae mutant strains unable to fix N2.* J. Bacteriol., 1975. 121: p. 759-765.

53. MacNeil, T., D. MacNeil, G.P. Roberts, M.A. Supiano, and B.W. J., *Fine-Structure mapping and Complementation Analysis of nif (Nitrogen Fixation) Genes in Klebsiella pnuemoniae.* J. Bacteriol., 1978. 136(1): p. 253-66.

54. Merrick, M., Filser, M., Dixon, R.A., Elmerich, C., Sibold, L., and Houmard, J., *The use of translocatable genetic elements to construct a fine- structure map of the Klebsiella pneumoniae nitrogen fixation (nif) gene cluster.* J. Gen. Microbiol., 1980. 117: p. 509-520.

55. Roberts, G.P., t. McNeil, D. MacNeil, and W.J. Brill, *Regulation and Characterization of Protein Products Coded by the nif (Nitrogen Fixation) Genes of Klebsiella pnuemoniae.* J. Bact., 1978. 136(1): p. 267-79.

56. Christiansen, J., P.J. Goodwin, W.N. Lanzilotta, L.C. Seefeldt, and D.R. Dean, *Catalytic and Biophysical Properties of a Nitrogenase Apo-MoFe Protein Produced by a nifB-Deletion Mutant of Azotobacter vinelandii.* Biochemistry, 1998. 37(36): p. 12611-23.

57. Hawkes, T.R. and B.E. Smith, *Purification and Characterization of the Inactive MoFe Protein (NifB-Kp1) of the Nitrogenase from nifB mutants of Klebsiella pneumoniae.* Biochem. J., 1983. 209: p. 43-50.

58. Shah, V.K., J.R. Allen, N.J. Spangler, and P.W. Ludden, *In vitro synthesis of the iron-molybdenum cofactor of nitrogenase. Purification and characterization of NifB cofactor, the product of the NifB protein.* J. Biol. Chem., 1994. 269: p. 1154-1158.

59. Allen, R.M., R. Chatterjee, P.W. Ludden, and V.K. Shah, *Incorporation of iron and sulfur from NifB cofactor into the iron-molybdenum cofactor of dinitrogenase.* J. Biol. Chem., 1995. 270: p. 26890-26896.

60. Roll, J.T., V.K. Shah, D.R. Dean, and G.P. Roberts, *Characteristics of NIFNE in Azotobacter vinelandii strains. Implications for the synthesis of the iron-molybdenum cofactor of dinitrogenase.* J. Biol. Chem., 1995. 270: p. 4432-4437.

61. Dean, D.R. and M.R. Jacobson, *Biochemical genetics of nitrogenase*, in *Biological Nitrogen Fixation*, G. Stacey, R.H. Burris, and H.J. Evans, Editors. 1992. p. 763-834.

62. Muchmore, S.W., R.F. Jack, and D.R. Dean, *Developments in the analysis of nitrogenase FeMo-cofactor biosynthesis*, in *Mechanisms of Metallocenter Assembly*, R.P. Hausinger, G.L. Eichhorn, and L.G. Marzilli, Editors. 1996, VCH Publishers, Inc.: New York. p. 111-132.

63. Ugalde, R.A., J. Imperial, V.K. Shah, and W.J. Brill, *Biosynthesis of iron-molybdenum cofactor in the absence of nitrogenase.* J. Bacteriol., 1984. 159: p. 888-893.

64. Robinson, A.C., B.K. Burgess, and D.R. Dean, *Activity, Reconstitution, and Accumulation of Nitrogenase Components in Azotobacter vinelandii Mutant Strains Containing Defined Deletions within the Nitrogenase Structural Gene Cluster.* J. Bacteriol., 1986. 166(1): p. 180-6.

65. Brigle, K.E., M.C. Weiss, W.E. Newton, and D.R. Dean, *Products of the Iron-Molybdenum Cofactor-Specific Biosynthetic Genes, nifE and nifN, Are*

Structurally Homologous to the Products of the Nitrogenase Molybdenum -Iron Protein Genes, nifD and nifK. J. Bacteriol., 1987. 169: p. 1547-1553.

66. Paustian, T.D., V.K. Shah, and G.P. Roberts, *Purification and characterization of the nifN and nifE gene products from Azotobacter vinelandii mutant UW45.* Proc. Natl. Acad. Sci. USA, 1989. 86: p. 6082-6086.

67. Zheng, L., R.H. White, and D.R. Dean, *Purification of the Azotobacter vinelandii nifV-Encoded Homocitrate Synthase.* J. Bacteriol., 1997. 179: p. 5963-5966.

68. McLean, P.A. and R.A. Dixon, *Requirement of nifV gene for production of wild-type nitrogenase enzyme in Klebsiella pneumoniae.* Nature, 1981. 292(5824): p. 655-6.

69. McLean, P.A., B.E. Smith, and R.A. Dixon, *Nitrogenase of Klebsiella pneumoniae nifV mutants.* Biochem J, 1983. 211(3): p. 589-97.

70. Filler, W.A., R.M. Kemp, J.C. Ng, T.R. Hawkes, R.A. Dixon, and B.E. Smith, *The nifH gene product is required for the synthesis or stability of the iron-molybdenum cofactor of nitrogenase from Klebsiella pneumoniae.* Eur J Biochem, 1986. 160(2): p. 371-7.

71. Robinson, A.C., D.R. Dean, and B.K. Burgess, *Iron-molybdenum cofactor biosynthesis in Azotobacter vinelandii requires the iron proteins of nitrogenase.* J. Biol. Chem., 1987. 262: p. 14327-14332.

72. Robinson, A.C., T.W. Chun, J.-G. Li, and B.K. Burgess, *Iron-molybdenum cofactor insertion into the Apo-MoFe protein of nitrogenase involves the iron protein-MgATP complex.* J. Biol. Chem., 1989. 264: p. 10088-10095.

73. Paustian, T.D., Shah, V. K., and Roberts, G.P., *Aponitrogenase: Purification, Association with a 20-Kilodalton Protein, and Activation by the Iron-Molybdenum Cofactor in the Absence of Dinitrogenase Reductase.* Biochemistry, 1990. 29: p. 3515-3522.

74. Tal, S., T.W. Chun, N. Gavini, and B.K. Burgess, *The ΔnifB (or ΔnifE) FeMo Cofactor-deficient MoFe Protein Is Different from the ΔnifH Protein.* J. Biol. Chem., 1991. 266(16): p. 10654-657.

75. Jacobson, M.R., V.L. Cash, M.C. Weiss, N.F. Laird, W.E. Newton, and D.R. Dean, *Biochemical and genetic analysis of the nifUSVWZM cluster from Azotobacter vinelandii.* Mol Gen Genet, 1989. 219(1-2): p. 49-57.

76. Gavini, N. and B.K. Burgess, *FeMo Cofactor Synthesis by a nifH Mutant with Altered MgATP Reactivity.* J. Biol. Chem., 1992. 267: p. 21179-21186.

77. Wolle, D., D.R. Dean, and J.B. Howard, *Nucleotide iron-sulfur cluster signal transduction in the nitrogenase iron-protein-the role of asp(125).* Science, 1992. 258: p. 992-995.

78. Homer, M.J., T.D. Paustian, V.K. Shah, and G.P. Roberts, *The nifY Product of Klebsiella pneumoniae Is Associated with Apodinitrogenase and Dissociates upon Activation with the Iron-Molybdenum Cofactor.* J. Bacteriol., 1993. 175: p. 4907-4910.

79. Homer, M.J., D.R. Dean, and G.P. Roberts, *Characterization of the γ protein and its involvement in the metallocluster assembly and maturation of dinitrogenase from Azotobacter vinelandii.* J. Biol. Chem., 1995. 270: p. 24745-24752.

80. White, T.C., G.S. Harris, and W.H. Orme-Johnson, *Electrophoretic studies on the Assembly of the Nitrogenase Molybdenum-Iron Protein from the Klebsiella pneumoniae nifD and nifK gene products.* J. Biol. Chem., 1992. 267: p. 24007-24016.

81. Jacobson, M.R., K.E. Brigle, L.T. Bennett, R.A. Setterquist, M.S. Wilson, V.L. Cash, J. Beynon, W.E. Newton, and D.R. Dean, *Physical and genetic map of the major nif gene cluster from Azotobacter vinelandii.* J Bacteriol, 1989. 171(2): p. 1017-27.

82. Moreno-Vivian, C., M. Schmehl, B. Masepohl, W. Arnold, and W. Klipp, *DNA sequence and genetic analysis of the Rhodobacter capsulatus nifENX gene region: Homology between NifX and NifB suggests involvement of NifX in processing of the iron-molybdenum cofactor.* Mol. Gen. Gent., 1989. 216: p. 353-363.

83. Shah, V.K., P. Rangaraj, R. Chatterjee, R.M. Allen, J.T. Roll, G.P. Roberts, and P.W. Ludden, *Requirement of NifX and Other nif Proteins for In Vitro Biosynthesis of the Iron-Molybdenum Cofactor of Nitrogenase.* J Bacteriol, 1999. 181(9): p. 2797-2801.

84. Imperial, J., R.A. Ugalde, V.K. Shah, and W.J. Brill, *Role of the nifQ gene product in the incorporation of molybdenum into nitrogenase in Klebsiella pneumoniae.* J. Bacteriol., 1984. 158: p. 187-194.

85. Joerger, R.D. and P.E. Bishop, *Nucleotide Sequence and Genetic Analysis of the nifB-nifQ Region from Azotobacter vinelandii.* J. Bacteriol., 1988. 170: p. 1475-1487.

86. Ugalde, R.A., Imperial, J., Shah, V.K., and Brill, W.J., *Biosynthesis of the iron-molybdenum cofactor and the molybdenum cofactor in Klebsiella pneumonia: effect of sulfur source.* J. Bacteriol., 1985. 164: p. 1081-1087.

87. Imperial, J., R.A. Ulgalde, V.K. Shah, and W.J. Brill, *Mol- mutants of Klebsiella pneumoniae requiring high levels of molybdate for nitrogenase activity.* J. Bacteriol., 1985. 163: p. 1285-1287.

88. Fu, W., R.F. Jack, T.V. Morgan, D.R. Dean, and M.K. Johnson, *nifU Gene Product from Azotobacter vinelandii Is a Homodimer that Contains Two Identical [2Fe-2S] Clusters.* Biochemistry, 1994. 33: p. 13455-463.

89. Agar, J.N., Yuvaniyama, P., Jack, R.F., Cash, V.L., Dean, D.R. and Johnson, M.K., *Modular Organization and Identification of a Second Iron-Binding Site Within the NifU Protein.* J. Biol. Chem., 1999. submitted.

90. Flint, D.H., *Escherichia coli contains a protein that is homologous in function and N-terminal sequence to the protein encoded by the nifS gene of Azotobacter vinelandii and that can participate in the synthesis of the Fe-S cluster of dihydroxy-acid dehydratase.* J. Biol. Chem., 1996. 271: p. 16068-16074.

91. Kim, S. and B.K. Burgess, *Purification and Characterization of Nitrogenase from a dnifW Strain of Azotobacter vinelandii.* J. Bio. Chem., 1994. 269(6): p. 4215-4220.

92. Paul, W. and M. Merrick, *The roles of the nifW, nifZ, and nifM genes of Klebsiella pnuemoniae.* Eur. J. Biochem., 1989. 178: p. 675-82.

93. Peters, J.W., K. Fisher, and D.R. Dean, *Nitrogenase structure and function: A biochemical-genetic perspective.* Ann. Rev. Microbiol., 1995. 49: p. 335-366.

94. Lowe, D.J., K. Fisher, and R.N.F. Thorneley, *Klebsiella pneumoniae nitrogenase: Pre-Steady State Absorbance Changes Show That Redox Changes Occur in the MoFe Protein that Depend on Substrate and Component Protein Ratio; A Role for P-Centres in Reducing Nitrogen ?* Biochem. J., 1993. 292: p. 93-98.

95. Lanzilotta, W.N., K. Fisher, and L.C. Seefeldt, *Evidence for Electron Transfer from the Iron Protein to the Molybdenum Iron Protein Without MgATP Hydrolysis: Characterization of a Tight Protein-Protein Complex.* Biochemistry, 1996. 35(22): p. 7188-7196.

96. Ludden, P.W., Shah, V.K., Roberts, G.P., Ruttiman-Johnson, C., Rangaraj, P., Foulger, T., Allen, R.M., Homer, M., Roll, J.T., Zhang, X., and Chatterjee, R., *Biosynthesis of the Iron-Molybdenum and Iron-Vanadium Cofactors*, in *Biological Nitrogen Fixation for the 21st Century,* C. Elmerich, Kondorosi, A., and Newton, W.E., Editor. 1998, Kluwer Academic Publishers: Dordrecht, the Netherlands. p. 33-38.

97. Hoover, T.R., J. Imperial, P.W. Ludden, and V.K. Shah, *Homocitrate is a component of the iron-molybdenum cofactor of nitrogenase.* Biochemistry, 1989. 28: p. 2768-2771.

98. Rangaraj, P., V.K. Shah, and P.W. Ludden, *ApoNifH functions in iron-molybdenum cofactor synthesis and apodinitrogenase maturation.* Proc. Natl. Acad. Sci. U.S.A., 1997. 94: p. 11250-11255.

99. Shah, V.K., J. Imperial, R.A. Ugalde, and P.W. Ludden, *In vitro synthesis of the iron-molybdenum cofactor of nitrogenase.* Proc. Natl. Acad. Sci. USA, 1986. 83: p. 1636-1640.

100. Dean, D.R. and K.E. Brigle, *Azotobacter vinelandii nifD- and nifE-encoded polypeptides share structural homology.* Proc. Natl. Acad. Sci., 1985. 82: p. 5720-5723.

101. Page, W.J. and M. von Tigerstrom, *Optimal conditions for transformation of Azotobacter vinelandii.* J. Bacteriol., 1979. 139: p. 1058-1061.

102. Vieira, J. and J. Messing, *The pUC plasmids, an M13mp7-derived system for insertion mutagenesis and sequencing with synthetic universal primers.* Gene, 1982. 19: p. 259-268.

103. Thomas, U., M.G. Kalyanpur, and C.M. Stevens, *The absolute configuration of homocitric acid (2-Hydroxy-1,2,4-butanetricarboxylic acid), an intermediate in lysine biosynthesis.* Biochemistry, 1966. 5: p. 2513-2516.

104. Strandberg, G.W. and P.W. Wilson, *Formation of the nitrogen-fixing enzyme system in Azotobacter vinelandii.* Can. J. Microbiol., 1968. 14: p. 25-31.

105. Shah, V.K., L.C. Davis, and W.J. Brill, *Nitrogenase. I. Repression and derepression of the iron-molybdenum and iron proteins of nitrogenase in Azotobacter vinelandii.* Biochim. Biophys. Acta, 1972. 256: p. 498-511.

106. Smith, P.K., R.L. Krohn, G.T. Hermanson, A.K. Mallia, F.H. Gartner, M.D. Provenzano, E.K. Fujimoto, N.M. Goeke, B.J. Olson, and D.C. Klenk, *Measurement of protein using bicinchoninic acid.* Meth. Enzymol., 1985. 226: p. 199-232.

107. Fortune, W.B. and M.G. Mellon, *Determination of Iron with o-Phenanthroline.* Ind. Eng. Chem. Anal. Ed., 1938. 10: p. 61-64.

108. Johnson, M.K., *Variable-Temperature Magnetic Circular Dichroism Studies of Metalloproteins*, in *ACS Symposium Series*, L. Que, Editor. 1988: Washington, D.C. p. 326-342.

109. Thomson, A.J., M.R. Cheeseman, and S.J. George, *Variable-temperature magnetic circular dichroism.* Meth. Enzymol., 1993. 226: p. 199-232.

110. Aasa, R. and T. Vänngård, *EPR Signal Intensity and Powder Shapes: A Reexamination.* J. Magn. Reson., 1975. 19: p. 308-315.

111. Drozdzewski, P.M. and M.K. Johnson, Appl. Spectros., 1988. 42: p. 1575-1577.

112. Johnson, M.K., A.E. Robinson, and A.J. Thomson, *Low-Temperature Magnetic Circular Dichroism Studies of Iron-Sulfur Proteins*, in *Iron-sulfur Proteins*, T.G. Spiro, Editor. 1982, Wiley-Intersceince: New York. p. 367-406.

113. Onate, Y.A., M.G. Finnegan, B.J. Hales, and M.K. Johnson, *Variable temperature magnetic circular dichroism studies of reduced nitrogenase iron proteins and [4Fe-4S]+ synthetic analog clusters.* Biochem. Biophys. Acta., 1993. 1164: p. 113-123.

114. Conover, R.C., A.T. Kowal, W. Fu, J.B. Park, S. Aono, M.W.W. Adams, and M.K. Johnson, *Spectroscopic characterization of the novel iron-sulfur cluster in Pyrococcus furiosus ferredoxin.* J. Biol. Chem., 1990. 265: p. 8533-8541.

115. Conover, R.C., J.B. Park, M.W.W. Adams, and M.K. Johnson, *Exogenous Ligand Binding to the [Fe4-S4] Cluster in Pyrococus furiosus Ferredoxin.* J. Am. Chem. Soc., 1991. 113: p. 2799-2800.

116. Spiro, T.G., J. Hare, B. Yachandra, A. Gewirth, M.K. Johnson, and E. Remsen, in *Iron-sulfur Proteins*, T.G. Spiro, Editor. 1982, Wiley-Interscience: New York. p. 407-423.

117. Spiro, T.G., R.S. Czernuszewicz, and S. Han, *Iron-Sulfur Proteins and Analog Complexes*, in *Resonance Raman Spectra of Heme and Metalloproteins*, T.G. Spiro, Editor. 1988, John Wiley & Sons: New York. p. 523-554.

118. Duin, E.C., M.E. Lafferty, B.R. Crouse, R.M. Allen, I. Sanyal, D.H. Flint, and M.K. Johnson, *[2Fe-2S] to [4Fe-4S] cluster conversion in Escherichia coli biotin synthase.* Biochemistry, 1997. 36: p. 11811-11820.

119. Czernuszewicz, R.S., K.A. Macor, M.K. Johnson, A. Gewirth, and T.G. Spiro, *Vibrational Mode Structure and Symmetry in Proteins and Analogues Containing Fe4S4 Clusters: Resonance Raman Evidence fro Different Degrees of Distortion in HiPIP and Ferredoxin.* J. Am. Chem. Soc., 1987. 109: p. 7178-7187.

120. Fu, W., T.V. Morgan, L.E. Mortenson, and M.K. Johnson, *Resonance Raman studies of the [4Fe-4S] to [2Fe-2S] cluster conversion in the iron protein of ntirogenase.* FEBS Lett., 1991. 284: p. 165-168.

121. Kilpatrick, L.K., M.C. Kennedy, H. Beinert, R.S. Czernuszewicz, D. Qui, and T.G. Spiro, *Cluster Structure and H-Bonding in Native, Substrate-Bound, and 3Fe Forms of Aconitase as Determined by Resonance Raman Spectroscopy.* J. Am. Chem. Soc., 1994. 116: p. 4053-4061.

122. Roberts, G.P. and W.J. Brill, *Gene-Product Relationships of the nif Regulon of Klebsiella pnuemoniae.* J. Biol. Chem., 1980. 144(1): p. 210-16.

123. Dean, D.R., R.A. Setterquist, K.E. Brigle, D.J. Scott, N.F. Laird, and W.E. Newton, *Evidence that conserved residues Cys-62 and Cys-154 within the Azotobacter vinelandii nitrogenase MoFe protein a-subunit are essential for nitrogenase activity but conserved residues His-38 and Cys-88 are not.* Mol. Microbiol., 1990. 4(9): p. 1505-12.

124. Burgess, B.K., *The Iron-Molybdenum Cofactor of Nitrogenase.* Chemical Reviews, 1990. 90: p. 1377-1406.

125. Surerus, K.K., M.P. Hendrich, P.D. Christie, D. Rottgardt, W.H. Orme-Johnson, and E. Münck, *Mössbauer and integer-spin EPR of the oxidized P-clusters of nitrogenae: P^{OX} is a non-Kramers system with a nearly degenerate ground doublet.* J. Am. Chem. Soc., 1992. 114: p. 8579-8590.

126. Burgess, B.K., D.B. Jacobs, and E.I. Steifel, *Large-Scale Purification of High Activity Azotobacter vinelandii Nitrogenase.* Biochim. Biophys. Acta, 1980. 614: p. 196-209.

127. Kim, C.-H., W.E. Newton, and D.R. Dean, *Role of the MoFe protein α-subunit histidine-195 residue in FeMo-cofactor binding and nitrogenase catalysis.* Biochemistry, 1995. 34: p. 2798-2808.

128. Brigle, K.E., W.E. Newton, and D.R. Dean, *Complete Nucleotide Sequence of the Azotobacter vinelandii Nitrogenase Structural Gene Cluster.* Gene, 1985. 37: p. 37-44.

129. Vieira, J. and J. Messing, *Production of single-stranded plasmid DNA.* Methods Enzymol., 1987. 153: p. 3-11.

130. Chromy, V., J. Fischer, and V. Kulhanek, *Re-evaluation of EDTA-chelated biuret reagent.* Clin. Chem., 1974. 20: p. 1362-1363.

131. Laemmli, U.K., *Cleavage of structural proteins during the assembly of the head of bacteriophage T4.* Nature, 1970. 227: p. 680-685.

132. Peters, J.W., K. Fisher, and D.R. Dean, *Identification of a Nitrogenase Protein-Protein Interaction Site Defined by Residues 59 Through 67 within the Azotobacter vinelandii Fe Protein.* J. Biol. Chem., 1994. 269: p. 28076-28083.

133. Ennor, A.H., *Determination and Preparation of N-Phosphates of Biological Origin.* Methods Enzymol., 1957. 3: p. 850-856.

134. Seefeldt, L.C. and S.A. Ensign, *A Continuous, Spectrophotometric Activity Assay for Nitrogenase Using the Redudtant Titanium (III) Citrate.* Anal. Biochem., 1994. 221: p. 379-386.

135. Ryle, M. and L. Seefeldt, *Elucidation of a MgATP signal transduction pathway in the nitrogenase iron protein: Formation of a conformation resmbling the MgATP-bound state by protein engineering.* Biochemistry, 1996. 35(15): p. 4766-4775.

136. Pierik, J., H. Wassink, H. Haaker, and R. Hagen, *Redox properties and EPR spectroscopy of the P clusters of Azotobacter vinelandii MoFe protein.* Eur. J. Biochem., 1993. 212: p. 51-61.

137. Hagen, W.R., in *Advances in Inorganic Chemistry*, A.G. Sykes and R. Cammack, Editors. 1992, Academic Press: New York. p. 165-222.

138. Dutton, P.L., *Redox Potentiometry: Determination of Midpoint Potential of Oxidation-Reduction Components of Biological Electron-Transfer Systems.* Methods Enzymol., 1978. 54: p. 411-35.

139. Thorneley, R.N.F. and D.J. Lowe, *Nitrogenase of Klebsiella pnuemoniae.* Biochem. J., 1983. 215: p. 393-403.

140. Thorneley, R.N.F., *Nitrogenase of Klebsiella pneumoniae. A stopped-flow study of magnesium- adenosine triphosphate-induce electron transfer between the compeonent proteins.* Biochem. J., 1975. 145: p. 391-396.

141. Fisher, K., D.J. Lowe, and R.N.F. Thorneley, *Klebsiella pneumonia nitrogenase: The pre-steady state kinetics of MoFe-protein reduction and hydrogen evolution under conditions of limiting electron flux show that the rates of association with the Fe-protein and electron transfer are independent of the oxidation level of the MoFe-protein.* Biochem. J., 1991. 279: p. 81-85.

142. Li, J.-G., S. Tal, A.C. Robinson, V. Dang, and B.K. Burgess, *Analysis of Azotobacter vinelandii Strians Containing Defined Deletions in the nifD and nifK Genes.* J. Bacteriol., 1990. 172(10): p. 5884-91.

143. Orme-Johnson, W.H., W.D. Hamilton, T.L. Jones, M.Y.W. Tso, R.H. Burris, V.K. Shah, and W.J. Brill, *Electron paramagnetic resonance of nitrogenase and nitrogenase components from Clostridium pasteurianum W5 and Azotobacter vinelandii OP.* Proc. Natl. Acad. Sci. USA, 1972. 69: p. 3142-3145.

144. Imam, S. and R.R. Eady, *Nitrogenase of Klebsiella pneumoniae: reductant-independent ATP hydrolysis and the effect of pH on the efficiency of coupling of ATP hydrolysis to substrate reduction.* FEBS Letters, 1980. 110: p. 35-38.

145. Jeng, D.Y., J.A. Morris, and L.E. Mortenson, *The effect of reductant in inorganic phosphate release from adenosine 5'-triphosphate by purified nitrogenase of Clostridium pasteurianum.* J. Biol. Chem., 1970. 245: p. 2809-2813.

146. Watt, G.D., W.A. Bulen, A. Burns, and K.L. Hadfield, *Stoichiometry, ATP/2e values, and energy requirements for reactions catalyzed by nitrogenase from Azotobacter vinelandii.* Biochemistry, 1975. 14: p. 4266-4272.

147. Magnuson, J.K., T.D. Paustian, V.K. Shah, D.R. Dean, G.P. Roberts, D.C. Rees, and J.B. Howard, *Nitrogenase Iron-Molybdenum Cofactor Binding Site: Protein Conformational Changes Associated With Cofactor Binding.* Tetrahedron, 1997. 53: p. 11971-11984.

148. Watt, G.D. and Z.-C. Wang, *Protein Interaction with and Higher Oxidation States of the Nitrogenase MoFe Protein from Azotobacter vinelandii.* Biochemistry, 1989. 28: p. 1844-1850.

149. Watt, G.D. and Z.C. Wang, *Further redox Reactions of Metal Clusters in the Molybdenum-Iron Protein of Azotobacter vinelandii Nitrogenase.* Biochemistry, 1986. 25(18): p. 5196-5202.

150. Rawlings, J., V.K. Shah, J.R. Chisnell, W.J. Brill, R. Zimmermann, E. Munck, and W.H. Orme-Johnson, *Novel metal cluster in the iron-molybdenum cofactor of nitrogenase.* J. Biol. Chem., 1978. 253: p. 1001-1004.

151. Tittsworth, R.C. and B.J. Hales, *Detection of EPR Signals Assigned to the 1-equiv-Oxidized P-Clusters of the Nitrogenase MoFe Protein from Azotobacter vinelandii.* J. Am. Chem. Soc., 1993. 115: p. 9763-9767.

152. Jacobson, M.R., Z.R. Premakumar, and P.E. Bishop, *Transcriptional Regulation of Nitrogen Fixation by Molybdenum in Azotobacter vinelandii.* J. Bact., 1986. 167: p. 480-6.

153. Orme-Johnson, W.H. and R.H. Sands, *Probing Iron-Sulfur Proteins with EPR and ENDOR Spectroscopy*, in *Iron Sulfur Proteins*, W. Lovenberg, Editor. 1973, Academic Press: New York. p. 195-238.

154. Rupp, H., K.K. Rao, D.O. Hall, and R. Cammack, *Electron Spin Relaxation of Iron-Sulfur Proteins Studied by Microwave Power Saturation.* Biochim. Biophys. Acta, 1978. 537: p. 255-269.

155. Blanchard, C.Z. and B.J. Hales, *Isolation of Two Forms of the Nitrogenase VFe Protein from Azotobacter vinelandii.* Biochemistry, 1996. 35: p. 472-478.

156. Zimmerman, R., E. Münck, W.J. Brill, V.K. Shah, M.T. Henzl, J. Rawlings, and W.H. Orme-Johnson, *Nitrogenase X: Mossbauer and EPR Studies on Reversibly Oxidized MoFe Protein from Azotobacter vinelandii OP.* Biochem. Biophys. Acta, 1978. 537: p. 185-207.

157. Gavini, N., L. Ma, G.D. Watt, and B.K. Burgess, *Purification and Characterization of a FeMo Cofactor-Deficient MoFe Protein.* Biochemistry, 1994. 33: p. 11842-11849.

158. Robinson, A.E., A.J.M. Richards, A.J. Thomson, T.R. Hawkes, and B.E. Smith, *Low Temperature Magnetic Circular Dichroism Spectroscopy of the Iron-Molybdenum Cofactor and the Complementary Cofactor-less MoFe Protein of Klebsiella pneumoniae.* Biochem. J., 1984. 219: p. 495-503.

159. Rees, D.C., H. Schindelin, C. Kisker, J. Schlessman, J.W. Peters, L.C. Seefeldt, and J.B. Howard, *Complex Structures of Nitrogenase,* in *Biological Nitrogen Fixation for the 21st Century*, C. Elmerich, A. Kondorosi, and W.E. Newton, Editors. 1998, Kluwer Academic Publishers: Dordrecht. p. 11-16.

160. Hagen, W.R., H. Wassink, R.R. Eady, B.E. Smith, and H. Haaker, *Quantitative EPR of an S=7/2 System in Thionine-Oxidized MoFe Proteins of Nitrogenase.* Eur. J. Biochem., 1987. 169: p. 457-465.

161. Howard, J.B. and D.C. Rees, *Structural Basis of Biological Nitrogen Fixation.* Chem. Rev., 1996. 96: p. 2965-2982.

162. Schlessman, J.L., D. Woo, L. Joshua-Tor, J.B. Howard, and D.C. Rees, *Conformational variability in structures of the nitrogenase iron proteins from Azotobacter vinelandii and Clostridium pasteurianum.* J Mol Biol, 1998. 280(4): p. 669-85.

163. Wolle, D., C.-H. Kim, D. Dean, and J.B. Howard, *Ionic interactions in the nitrogenase complex: Properties of Fe-protein containing substitutions for Arg-100.* J. Biol. Chem., 1992. 267: p. 3667-3673.

164. Hoover, T.R., A.D. Robertson, R.L. Cerny, R.N. Hayes, J. Imperial, V.K. Shah, and P.W. Ludden, *Identification of the V factor needed for synthesis of the iron-molybdenum cofactor of nitrogenase as homocitrate.* Nature, 1987. 329(6142): p. 855-7.

165. Goodwin, P.J., J.N. Agar, J.T. Roll, G.P. Roberts, M.K. Johnson, and D.R. Dean, *The Azotobacter vinelandii NifEN complex contains two identical [4Fe- 4S] clusters.* Biochemistry, 1998. 37(29): p. 10420-8.

166. Wilson, M., Setterquist, R., Weiss, M., Newton, W., and Dean, D., *Analysis of the nifE and nifN genes from Azotobacter vinelandii,* in *Nitrogen Fixation: Hundred Years After*, H. Bothe, de Bruijn, F.J., and Newton, W.E., Editor. 1988, Gustav Fischer: New York, N.Y. p. 325-332.

167. Brigle, K.E., R.A. Setterquist, D.R. Dean, J.S. Cantwell, and M.C. Weiss, *Site-directed mutagenesis of the MoFe protein of Azotobacter vinelandii.* Proc. Natl. Acad. Sci (USA), 1987. 84: p. 7066-69.

168. Kent, H.M., I. Ioannidis, C. Gormal, B.E. Smith, and M. Buck, *Site-directed mutagenesis of the Klebsiella pneumoniae nitrogenase. Effects of modifying conserved cysteine residues in the α and β-subunits.* Biochem. J., 1989. 264: p. 257-264.

169. Tabor, S. and C.C. Richardson, *A bacteriophage T7 RNA polymerase/promoter system for controlled exclusive expression of specific genes.* Proc. Natl. Acad. U.S.A., 1985. 82: p. 1074-1078.

170. Zheng, L., R.H. White, V.L. Cash, R.F. Jack, and D.R. Dean, *Cysteine desulfurase activity indicates a role for NIFS in metallocluster biosynthesis.* Proc. Natl. Acad. Sci. USA, 1993. 90: p. 2754-2758.

171. Burris, R.H., *Nitrogenase.* J. Biol. Chem., 1991. 266: p. 9339-9342.

172. Madden, M.S., N.D. kindon, P.W. Ludden, and V.K. Shah, *Diastereomer-dependent substrate reduction properties of a dinitrogenase containg 1-flourohomocitrate in the iron-molybdenum cofactor.* Proc. Natl. Sci. (USA), 1990. 87: p. 6517-21.

173. Imperial, J., T.R. Hoover, M.S. Madden, P.W. Ludden, and V.K. Shah, *Substrate Reduction Properties of Dinitrogenase Activated in Vitro Are Dependent upon the Presence of Homocitrate or Its Analogues during iron-0Molybdenum Cofactor Synthesis.* Biochemistry, 1989. 28: p. 7796-99.

174. Hoover, T.R. and P.W. Ludden, *Derepression of Nitrogenase by addition of Malate to Cultures of Rhodospirillum rubrum Grown with Glutamate as the Carbon and Nitrogen Source.* J. Bact., 1984. 159(1): p. 400-3.

175. Shah, V.K., T.R. Hoover, J. Imperial, T.D. Paustian, G.P. Roberts, and P.W. Ludden. *Role of nif gene products and homocitrate in the biosynthesis of the iron-molybdenum cofactor.* in *Nitrogen Fixation: Hundred Years After*. 1988. Cologne: Gustav Fischer.

176. Musgrave, K.B., Lui, H.I., Ma, L., Burgess, B.K., Watt, G., Hedman, B., and Hodgson, K.O., *EXAFS Studies of the Pn and Pox States of the P-cluster of Nitrogenase.* J. Bio. Inorg. Chem., 1998. 3: p. 344-352.

APPENDIX I: 150L Fermentor Procedure

This appendix represents the fermentation procedure for *Azotobacter vinelandii* employed by the Dean laboratory. The fermentor used is a custom built WB Moore 150 liter IF Series Pilot Plant, located in the fermentation facilities of the Fralin Biotechnology Center. Individuals who plan to use this fermentor should be trained and certified by a qualified operator and should read the operations manual for the fermentor. Before using the fermentor, operators should be trained and proficient with aseptic microbiological techniques and the media used in the growth of *A. vinelandii.* The growth of *A. vinelandii* is a very simple task, however, its importance to the overall research effort is incalculable. This appendix should be used in conjunction with the operators manual supplied by WB Moore.

System Tour

As complicated as the 150 liter fermentor may look to a new user, it is a fairly simple instrument to understand and operate. The fermentor consists of a large, jacketed vessel that contains an agitation impellar, gas (air) input and addition/harvest ports. The system is equipped with simple gauges and valves for operation. More difficult tasks, such as temperature control, are controlled by a computer located on the upper right-hand side of the machine.

Growth of *A. vinelandii* in the 150L fermentor is a 3 day process. The first day consists of media preparation and inoculation of the intial *A. vinelandii* starter cultures. Day 2 involves the sterilization of the fermentor and the inoculation of additional bacterial cultures for fermentor inoculation. Day 3 inolves the growth, derepression and harvesting of the bacteria growing in the fermentor.

Day 1

1. Prepare 8-12 1xPO_4 starter cultures by adding 5 ml 100xPO_4 and 450 ml dH_2O to a 2L flask. Cover with aluminum foil and autoclave on the Liquid 20 cylce.
2. Prepare 10xSALT in 50ml aliquots, according to the A. vinelandii media protocal located in the Dean Lab. Autoclave on the Liquid 20 cycle.
3. Prepare 6M Urea and filter-sterilize into 200ml aliquots.
4. Prepare 600xPO_4 solution.
5. When media is sterile and cool, prepare two starter cultures aseptically. Starter cultures consist of a 1xPO_4 starter culture and 50ml aliquot of 10xSALT, plus 2.5ml of 2M sterile Urea. Inoculate this starter with 1/2 to a full loop of the bacterial strain of interest.
6. Place the inoculated culture in the floor shaker set at 30°C and 300 rpm agitation. Allow to incubate for 10-12 hours.

Day 2

1. After 10-12 hours the culture should be turbid with bacteria (160-180 Klett units; a light brown hazy culture). Prepare six additional starter cultures as required by step 4, Day 1.
2. Inoculate the six starters with 20-30ml of the strongest initial growth culture using sterile pipets.
3. Allow to incubate for 8-10 hours in the shaking incubator. During this time autoclave the fermentor using the protocal provided below. Media for the fermentor includes:
    1. 2400g of sugar
    2. 10.8g of $CaCl_2$

3. 24g of $MgSO_4$
4. 13ml of 10mM Mo-solution

4. After the fermentor has cooled to 30°C it is ready to inoculate with the bacerial starter cultures.
5. Inoculuate the fermentor following the procedure listed below with:
    1. Six starter cultures
    2. 200ml of 6M Urea
    3. 200ml of 600xPO_4
    4. 6ml of 300mM Fe-citrate solution (provided in Dean Lab, make as necessary)
6. Set agitation at 125 rpm and air flow to 80L per minute. Allow to grow for 10-12 hours. Bacteria will be ready to derpress at 180-220 Klett units.

Day 3

1. Follow the concentrator protocal for the derepression and harvesting of the bacterial growth (see Appendix II).
2. Clean up any mess.

Note: If multiple growths are to be run back to back, on Day 2 one must begin the Day 1 procedure and see it through to Day 3.

150L Fermentor System Operation

Initial Start-up and Inspection

1. Confirm that all valves are in the closed position.
2. Confirm that all power and control switches are set to 'OFF'.
3. Open the three service valves (air/steam/water) at the rear of the unit (S1, S2 and S3)

4. Check and adjust service pressures:
5. Water pressure on WPG3 set to 20-30 psig
6. Steam pressure set on SPG3 set to 25-30 psig
7. Air pressure on APG2 set to 30 psig.
8. Examine the gauges before and after each of the input filters for pressure drop. If the differential is greater than 20 psig for water, or 10 psig for steam, the filters must be disassembled and replaced/cleaned.
9. Check the water traps for the air inputs and drain if necessary.
10. Perform a complete visual inspection of all components for leakage, excessive dirt, etc.
11. Examine interior of vessel for any dirt or contaminants leftover from a previous run.

Start-Up

1. Secure all fittings and plugs on the vessel assembly.
2. Check all electrical connections.
3. Make sure the temperature sensor is in the thermowell with some mineral oil for contact.
4. Turn on the main power switch.
5. Fill vessel with media through the fillport on the vessel headplate. The working volume of 120L is accomplished by filling the vessel to the midpoint of the top viewport.
6. Open the blue needle valve TV4 ~2 turns.
7. Open yellow needle valve TV3 ~4 turns.

8. Adjust BPCV-2 (at the bottom of the vessel, to the rear) until the gauge reads 10-20 psig. During the run, frequently check this gauge to make sure that it is within the recommended operating range.
9. Turn on the agitation power switch.
10. Adjust the agitation using the knob and reading the display on the bottom of the control box. (125 RPM for *A. vinelandii*)

Vessel Pressure Test

1. Open black valve A8.
2. Open the air flow control valve, AF1, 4 to 5 turns.
3. Open air flow valve A1 to start sparging air into the vessel.
4. Adjust R5 to read 60 psig. This will adjust the backpressure valve to the closed position allowing pressure to build up in the vessel. Carefully monitor the vessel backpressure gauge.
5. Allow vessel to reach 20 psig, then shut off valve A8.
6. Hold vessel at this pressure for several minutes. If the pressure drops, there is a leak in the vessel somewhere that needs to be fixed.
7. Adjust R5 to read 0 psig, pressure in the vessel will be released.
8. Close valve A1.
9. Close valve A8 and valve AF1.

Sterilization Cycle

1. Open valve T8 to allow the vessel jacket to drain, wait 5 minutes before continuing.

2. Close blue needle valve TV4.
3. Open green valve EC4.
4. Confirm that blue needle valve H9 is closed.
5. Confirm that valves T6 and T7 are closed.
6. Confirm that the addition, sample and harvest ports are all closed.
7. Open the steam input (red) and drain (green) on each of the addition, sample and harvest ports. (there are four pairs of these valves total)
8. **Caution:** These lines will heat up fast, do not touch. Care needs to be used throughout the sterilization cycle to avoid burns.
9. Confirm valves A8 and AF1 are closed.
10. Confirm valve A1 is closed.
11. Adjust R5 to read 60 psig.
12. Open red valve S5.
13. Open red valve S6 3-4 turns.
14. Open green filter condensate valve.
15. Confirm agitation rate and adjust if necessary.
16. Place the temperature control switch into the "STER" position. This will allow steam to start entering the jacket. Monitor the steam pressure on the gauge just above the jacket drain valve T8. The gauge should start with little/no pressure indicated and then rise as the jacket heats up. Be aware of any over/under pressure readings. The system will now start to warm up.

at 100°C:

1. Open valve A1. This will allow steam to sparge through the vessel/media.
2. Open the addition and sample valves for a short period of time (1-2 minutes). Do not open the harvest valve at the bottom of the vessel. Be sure these valves are closed when finished.

at 121.5°C:

1. Close valve A1.

Vessel can now be soaked at sterilization temperature for a desired time (~10 mins for *Av*). Monitor the vessel pressure gauge to make sure that vessel pressure does not go past 30 psig.

Rapid Cool Cycle

When done sterilizing:

1. Close green valve EC4.
2. Turn temperature control switch to the "OFF" position.
3. Close the red and green steam lines on the addition, sample and harvest ports.
4. Close red valves S5 and S6.
5. Open valve A8.
6. Open valve AF1 3-4 turns.
7. Open valve A1.
8. Close valve EC4. (green filter condensate valve)

Closely monitor vessel backpressure at this point, it should NEVER exceed 30 psig. If pressure continues to climb, IMMEDIATELY close valve A8 and release vessel pressure with valve R5.

9. Slowly open valve T6. (can also open valve H9 here to speed cooling).
10. Close valve T8.
11. Open valve C9. This starts a flow of cold water through the jacket.
12. Open valve TV4 3-4 turns. Start monitoring the seal pressure gauge and adjust with BPCV-2. The reading will show a lot of fluctuation until the vessel reaches an equilibrium temperature.

The vessel will now cool down under pressure. Allow the temperature to reach 10° above your growth setpoint before switching to temperature control. If it will be a while before inoculation, the system can be put into temperature control at any time after the vessel temperature has reached ~70°C.

<u>Temperature Control Mode</u>

1. Adjust R5 to 0 psig.
2. Close valve A8.
3. Open valve T7.
4. Open needle valve TV1 1 all the way.
5. Open needle valve TV2 1 turn.
6. Close valve C9.

7. Turn temperature control switch to the “ON” position.
8. Open exhaust condenser valve H9.

Allow the vessel to approach the setpoint temperature, then move into the Growth Cycle.

Growth Cycle

1. Confirm desired growth temperature.
2. Set desired agitation rate.
3. Open valves A8 and A1, adjust the sparge rate by opening valve AF1 and monitoring the flowmeter on the front of the control box. (~75 L/min for *Av*)
4. Adjust R5 to achieve desired vessel backpressure (5-6 psig for *Av*)

Note: backpressure and airflow readings can change with temperature, so these should be checked and adjusted periodically.

5. Adjust seal pressure using BPCV2 and make sure it is set to 10-20 psig.

Once growth temperature is reached, the vessel can be inoculated. Be sure to turn off air flow and allow pressure to drop before opening fillport on top of vessel. To allow sampling during the growth, remove the steam supply line from one of the lower sample ports and attach the sampling nipple. Refer to concentrator instructions (Appendix II) when ready to harvest.

Clean-Up

1. After growth, all equipment must be thoroughly cleaned and readied for the next user. This includes rinsing out the vessel and wiping all surfaces.
2. Turn all control knobs to off (temperature, agitation).
3. Turn off the main power switch.
4. Turn off all service inputs (valves S1, S2 and S3) and allow any remaining pressure to drain. For air, this can be accomplished by opening valves A1, AF1 and A8 to sparge any remaining air through the vessel. For steam, open the red supply and green drain lines on the sample and addition ports (this will bleed out slowly).
5. Close all valves.
6. Perform a visual inspection of the area for any leaks, dirt or other problems.

APPENDIX II: Concentrator Procedure

This appendix represents the procedure for concentration of *Azotobacter vinelandii* to be used in conjunction with the 150 liter fermentor. The concentrator used is a GrandStand Pilot/Process System designed by A/G Technology Corporation specifically for use with the 150L WB Moore Fermentor. Prior to operation of the GrandStand, user must be trained by a qualified technician and must read the operation instructions provided by A/G Technologies.

System Tour

The GrandStand concentrator is best described when it is broken down into its component parts. The component which functions to concentrate the cell suspension is a A/G Technology Hollow Fiber Cartridge (size 65). This cartridge is an ultrafiltration device functioning to concentrate the feed strean by tangential flow. The feed stream that is delivered to the cartridge and is processed into either permeate or retentate. Permeate consists primarily of media and waste, and is withdrawn to a waste drain. Retentate is recirculated through the system until is has been concentrated to a desired volume. The feed stream, or cell suspension, is delivered to the concentration cartridge by a UNIBLOC pump. Feed stream can flow through the pump from either the feed tank or the process feed line. The feed tank is part of the concentrator apparatus, where as the process feed line is a detachable line which is connected to the harvest valve of the fermentor (see appendix I). The amount of cell suspension that is to be concentrated will determine if the feed stream is supplied by either the feed tank, or the process feed line. The entire plumbed system is made of stainless steel tubing which is connected by tri-clamps and gaskets. Switching the feed stream from either the feed tank, or the process feed line can be accomplished by either closing, or opening butterfly valves built into the system.

System Operation

System Draining*:* To begin derepression or harvest concentration (see appendix I) first drain the system be opening the retentate valve 100%. Next, place a bucket under the drain valve and open it (**NOTE:** Make sure the feed tank is empty before draining the system). Storage solution or water should drain from the system into the bucket. After draining the system close the drain valve.

System Priming and Concentrating*:*

1. Before concentrating, make sure the retentate outlet is directed into the feed tank. If the retentate outlet is not directed into the feed tank make it so using the available PVC tubing and plastic fitting.
2. Connect the process feed line to the fermentor harvest valve using the available PVC tubing and plastic fitting. Also make sure that the permeate waste lines are placed in the bench top drain. The system is now ready to be primed.
3. Turn off air flow into the fermentor be closing the A8 valve. As the air flow diminishes the pressure in the fermentor vessel will decrease to 0 psi. After the pressure has dropped to 0 psi, open the main addition port on the fermentor.
4. Open the fermentor harvest valve, making sure that the PVC line to the concentrator process feed line is connected. To prime the transfer line and the concentrator pump, open the process feed line valve on the concentrator (**NOTE:** If you forgot to close the concentrator drain valve you have just flooded the floor with your cells).
5. Open the feed tank valve. Upon opening this valve you should observe the cell suspension flowing into the feed tank.

6. To begin concentrating, turn on the AC invertor by touching the forward button. Adjust the forward speed with the up and down arrows to read 325 rpm. The cell suspension will begin to flow from the fermentor to the concentrator. Keep note to the level of cell suspension inside the fermentor. When the level falls below the lowest impellar, close the feed tank valve and fill the feed tank with cell suspension. When the feed tank level begins to reach full, open the feed tank valve and close the process feed line valve. This action will cycle the feed stream through the feed tank. As the level in the feed tank lowers, repeat the above filling procedure until all of the cells have been removed from the fermentor. Begin to collect the permeate from the permeate waste line in the carboy available. At this point the procedure deviates depending on whether the cells are being concentrated for a derepression or a harvest.

Derepression.

1. Concentrate cells to approximately 15 liters using the gradations on the side of the feed tank.
2. Re-inoculate the fermentor with 20 liters of cells. There should be about 15 liters in the feed tank, which can be removed through the concnetrator harvest valve. The additional 5 liters comes from the permeate that has been collected in the storage carboy.
3. After all the cells have been removed from the feed tank, fill the tank with the stored permeate. Flush the remaining cells from the cartridge using the permeate and collect for the additional five liters of inoculum.

Harvesting.

1. Concentrate the cell down to about 4 liters in the feed tank. The speed of the concentrator will have to be decreased when the volume in the feed tank falls below 10 liters (approx. 150 rpm).
2. Press the stop button on the AC Invertor.
3. Press the jog button. This will only allow the concentrator to attain a set speed (50 rpm). This speed has been set to allow for concentration of small volumes. After the jog button has been pressed, the concentrator is in jog mode, which is distinguished by the presence of a green light on the jog button.
4. Press and hold the forward button. This will begin to concentrate at a set low speed. To stop the jog concentration, release pressure from the forward button.
5. Once there is no cells left in the feed tank, remove the cells from the cartridge by opening the concentrator harvest valve, making sure you have a bucket to collect your sample. This should yield approximately 4 liters. Flush the remaining cells from the cartridge and the system using the stored permeate. Spin the cell suspension in the Beckman J6-HC centrifuge equipped with a composite rotor (6 x 1L bottle capacity) at 5,200 rpms, 10°C for 15 minutes.
6. Supernatant is poured down the drain and cell pellet is removed with a spatula and placed in ZipLoc freezer bags labeled with the storage code (strain-date-fermentor), date, strain, and operators. Cells are stored in the -80°C freezer until used.

Washing and Storing the Concentrator

1. Fill the feed tank with hot tap water.

2. Direct both the permeate lines and the retentate outlet lines into the feed tank. The feed tank valve should be open and the retentate outlet valve should be open 100%. The harvest valve should be closed, as well as the process feed line valve.
3. Cylce the hot tap water through the system at 350 rpm (forward). This action will remove excess cells from the concentrator cartridge. After 15 minutes direct the flow from the feed tank to the waste drain, making sure to decrease the speed of the AC Invertor to approximately 260 rpm.
4. Fill the feed tank 2/3 full with hot tap water. Add approximately 25g of Tergezyme to the feed tank. Follow steps 2 and 3 above.
5. Repeat steps 1 through 3.
6. Fill the feed tank with distilled water. Follow step 3. The concentrator is now ready for storage.

APPENDIX III: Osmotic Shock Procedure

This appendix represents the procedure for crude extract preparation for *Azotobacter vinelandii* using the technique of osmotic shock. The following procudure represents a modification from the original method published by Shaw *et al.*,(ref. #39, Chapter I). Before performing this techniqe individuals should be experienced in anaerobic technique and sample handling, as well as use of the Schlenk apparatus.

System Tour

The means by which *A. vinelandii* is disrupted by osmotic shock is its ability to take up glycerol. *A. vinelandii* is incubated in the presence of 4 M Glycerol buffer, during which time glycerol is absorbed. Excess glycerol is then removed by centrifugation. The bacteria are then treated with buffer that contains no glycerol, and experience an osmotic pressure effect. Through manipulation of the bacteria during this change in osmotic pressure, the bacteria rupture. Any unbroken cells or cell fragments are then removed by centrifugation. After centrifugation the resulting supernatent is treated as the cell-free crude extract.

Procedure

To begin prepare the following buffers: Buffer A – 25mM Tris-HCl, pH 8.0 + 4 M Glycerol; Buffer B – 25mM Tris-HCl, pH 8.0 + 0.2 mM Phenylmethylsulfonylflouride (PMSF). Degas Buffer A and B using the Schlenk apparatus. After the buffers have been degassed, make them 2 mM in sodium dithionite. Next, aliquot 60 g of frozen *A. vinelandii* cells into 500 ml centrifuge bottles containing five marbles. The purpose of the marbles is to aid in mixing the cell suspension and assist in cell rupture during the osmotic shock. After the cells have been placed in the bottles bring them to the bench containing the degassed buffers. Place an argon line into a bottle containing cells to flush out the air in the bottle. Next, place and argon line into

a 250 ml graduated cylinder to flush out the air in it. Rinse the cylinder with about 50 ml of degassed Buffer A. Next, resuspend the cells with 3 volumes of Buffer A (60 g cells – 180 ml Buffer A). After Buffer A has been added to the cells, fasten the lid on the bottle and shake to mix the cells and buffer. After mixing place the cell suspension on ice. Allow the cell suspension to incubate in the ice for 15 to 20 minutes. During this incubation the cells are taking up the glycerol in Buffer A and will begin to swell. After the incubation period spin the cell suspension for 20 minutes at 4°C and ≈ 12,000 x g. Discard the supernatant. Add some DnaseI to the cell pellet (enough to cover the tip of a small spatula) and loosen the cell pellet with a spatula under an argon line. Next, add 3-4 volumes of Buffer B (based on the original weight of the cells) and quickly fasten lid and shake vigorously. When the solution is shaken, one will notice if the Dnase I was not added due to the viscous nature of the suspension. As the cells begin to rupture under the osmotic pressure the suspension will become foamy and have the appearance of a freshly poured pint of Guinness beer (if you don't know what that looks like you are on your own). Place the ruptured cell suspension on ice and allow it to incubate for 20 – 30 minutes, during which time the foam will rise and the cell suspension will darken. After this incubation period transfer the cell suspension, under an argon line, to 250 ml centrifuge bottles (clear plastic ones) and spin the cell suspension for 1 hour at 4°C and ≈ 26,000 x g. The resulting supernatant is the osmotic shock crude extract.

APPENDIX IV: Western Blot Procudure

This appendix represents the procedure for performing a western blot in the laboratory of Prof. Dennis Dean. Before attempting this procedure individuals should be proficient in the application of sodium dodecyl - polyacrylamide gel electrophoresis (SDS-PAGE). If one is not familiar with the technique of SDS-PAGE, consult a member of the Dean Lab for assistance.

System Tour

The purpose of performing a western analysis is to immunologically probe for a known protein on a SDS-PAGE. After one runs a SDS-PAGE gel, the individual protein bands on the gel are electrophoretically transferred onto a nitrocellulose membrane. The nitrocellulose membrane is probed with a primary antibody (monoclonal or polyclonal) specific for the known target protein band(s). After an incubation period, the remaining primary antibody is washed away and the membrane is probed with a secondary antibody, specific to the immunoglobulin species contained in the first antibody. The secondary antibody is labeled with an enzyme(an antibody conjugate), and the specific protein band can be visualized by the addition of enzyme substrate containing a color developer. It is then possible to see where your target protein is by looking for the presence of color on the membrane.

Procedure

1. Run a SDS-PAGE on the antigen specific to the antibody to be used. Also run any controls which may be important to comparison.
2. Transfer proteins to nitrocellulose paper by electrophoretic transfer (see below). Proper transfer of proteins may be verified by staining the nitrocellulose with 0.1% Ponceau red in 1 % acetic acid. The dye is then washed off with TBST before proceeding with the Western blot.

3. Remove the membrane from the transfer apparatus and place the nitrocellulose paper in Blocking buffer (4% non-fat milk in TBST buffer) and put on a shaker at room temperature for 1 hour. The gel may be stained as usual if desired.
4. Wash the membrane 3 times for 5 minutes with 15 ml of TBST buffer to remove any excess Blocking buffer.
5. Place the nitrocellulose membrane in 20 ml of primary antibody solution (1:10,000 dilution in TBST buffer). Incubate on a shaker at room temperature for 1 hour.
6. Rinse blot 3 times for 5 minutes each in 15 ml TBST buffer on the shaker table to remove any unbound primary antibody.
7. Place the nitrocellulose in 20 ml diluted conjugate (an enzyme-linked anti-IgG) which is specific to your sample (e.g. Goat anti-Rabbit IgG-AP) at the recommended dilution (1:7,500) in TBST buffer. Incubate 1 hour at room temperature on a shaker.
8. Rinse blot 3 times for 5 minutes each in 15 ml TBST buffer on the shaker table to remove any unbound secondary antibody conjugate.
9. Develop blot with one of the following substrates(specific for the conjugate used):

   Horseradish Peroxidase (HRP)

   GIBCO BRL TMB-Blot & Slide (Cat.#5982SA)

   Alkaline Phosphatase

   GIBCO BRL BCIP/NBT Stable Mix (Cat.#5984SA)
10. Allow approximately 10 minutes for the blot to develop. To stop development, rinse with dH_2O.

Western blot Buffer Solutions

1. Electrophoresis buffer:

   20 mM Tris-HCl, do not pH

   150 mM Glycine

   20% Methanol

   0.1% sodium dodecyl sulfate

2. TBST buffer:

   50 mM Tris-HCl, pH 7.5

   150 mM NaCl

   0.05% Tween-20 (polyoxyethylenesorbitan monolaurate)

3.

Electrophoretic Transfer

1. After the SDS-PAGE has been run assemble the components of the electrophoretic transfer apparatus, consisting of:

   Electrophoretic Blotting Unit [MODEL EBU-1000 (American BioNuclear, Emeryville, CA)]

   2 pieces of Whatman paper (15 x 20 cm)

   2 pieces of 3M foam (15 x 20 cm)

   1 plastic sandwich (2 pieces of porated plastic connected with a plastic band)

2. Place enough electrophoresis buffer in a pyrex dish (21 x 21 x 5 cm) to cover 1 piece of Whatman which is lying on top of a piece of foam.

3. Remove the SDS-PAGE from the glass plates and score the upper right hand corner with a spatula.
4. Next, place the SDS-PAGE on the Whatman paper such that it has been flipped over and the scored edge is now in the upper left hand corner.
5. Very carefully place a nitrocellulose membrane (ADVANTEC MFS Inc., Pleasanton, CA; Cat. No. A045A078C; 7 x 8 cm) on top of the SDS-PAGE. Note: Once the membrane touches the gel, it will bind proteins. Moving the membrane after it has made contact will result in smears on the developed blot.
6. Wet the additional piece of Whatman paper with the excess electrophoresis buffer and place it on top of the nitrocellulose membrane. On top of the Whatman paper, place the additional piece of foam, wetted in electrophoresis buffer.
7. Next, slide the foam, Whatman, gel, and membrane stack into the plastic sandwich piece, with the membrane nearest to the plastic piece labeled with a plus sign.
8. Place the completed sandwich into the blotting unit which has been filled with electrophoresis buffer.
9. Add the electrode slabs to the blotting units, placing the positive electrode next to the plastic sandwich pieces labeled with the plus sign and the negative electrode on the opposite side of the sandwich.
10. Put the protective cover on the blotting unit and attach the electrode leads to a constant power supply.
11. Electrophoretically transfer the proteins from the SDS-PAGE to the nitrocellulose membrane at room temperature overnight at 20 volts. Note: Make sure that the

electrodes are producing bubbles to be sure that current is running through the system.

APPENDIX V: Acetylene Synthesis Procedure

This appendix represents the process by which the Dean Lab synthesizes acetylene gas. Acetylene is a very combustible gas. Caution should be used in the preparation of acetylene gas by performing all manipulations in an operating fume hood and in the absence of any ignitable substances. If you are following this procedure for the first time, ask someone who has performed this operation for assistance.

System Tour

The overall process of acetylene synthesis is very simple. Water is added to solid calcium carbide, which produces acetylene gas. The gas is then trapped and stored in a holding apparatus which has been made from spare laboratory parts. This holding apparatus is fashioned with a Suba-seal to allow acetylene gas to be withdrawn from the trapped gas reservoir. The reservoir is held under positive pressure by the aid of a water-filled funnel connected to the bottom of the gas reservoir.

Procedure

1. Clean up any unnecessary waste in the fume hood.
2. Fill the 4 L waste bucket with tap water. Fill a water bottle with dH_2O, as well as fill the acetylene holding apparatus with water. The holding apparatus is comprised of a tear-drop separatory funnel (500 ml) and a large cylindrical separatory funnel (1000 ml) connected to one another by rubber tubing. The holding apparatus is supported by two ring stands fitted with clamps, which should be positioned such that the tear-drop funnel is in a higher position relative to the cylindrical funnel. The flow of water is controlled by stopcocks, which are located on both the separatory funnels. Both stopcocks should be in the closed position after the apparatus is filled with

water. **Note:** Make sure there is no trapped air in the holding apparatus after it is filled with water. Residual air will contaminate the acetylene stock.

3. With the cylindrical funnel filled to the top, and residual air removed, place a piece of parafilm over the neck of the funnel. If any air is trapped under the parafilm seal, the procedure must be repeated. Trapped air will contaminate the acetylene.
4. Fill a plastic container is with dH_2O to approximately three-quarters full and place under the cylindrical funnel. Invert the sealed cylindrical funnel and place its neck under the water level in the container. Secure the funnel in this position with the aid of the ring stand and clamp. Once the funnel is secure and submerged, remove the parafilm seal from the neck of the funnel.
5. In a 125 ml vacuum flask place approximately 5 g of solid calcium carbide. Wear gloves when handling the calcium carbide and make sure to secure the calcium carbide canister and remove it from the immediate working area.
6. Place a piece of surgical tubing (approximately 30 cm in length) on the vacuum port of the 125 ml vacuum flask. You are now ready to make acetylene. At this point make sure that you have the following items at the ready: i) a dH_2O filled water bottle; ii) a No. 5 butyl-stopper; iii) a No. 57 Suba-Seal stopper.
7. Quickly add 5-10 ml of dH_2O to the 125 ml flask containing the calcium carbide. The acetylene reaction will immediately start, quickly place the No. 5 butyl-stopper over the opening of the 125 ml flask. The acetylene gas will be expelled through the connected surgical tubing. Allow the flow of gas to proceed for about five seconds, in order to purge any trapped air from the flask and/or the tubing. Place the tubing in the water-filled container under the opening of the cylindrical funnel. The acetylene

gas will begin to fill the cylinder and displace the water in the funnel into the container. Fill the cylinder to about three-quarters full with acetylene gas.

8. After the cylinder is filled to the desired level, remove the tubing from underneath the opening. Remove the stopper from the 125 ml flask and place the flask in the 4 L waste bucket. This action will quench the acetylene synthesis reaction after about five minutes. After this time remove the flask from the waste bucket and clean off any residual calcium carbide its sides.
9. Place the No. 57 Suba-seal in the water-filled container and remove any air bubbles that remain on its surface. Seal the gas-filled cylinder with the Supa-seal and remove the cylinder from the water-filled container. Re-invert the cylinder and remove the water container from the hood, making sure the cylinder is secure on the ring stand.
10. Open both stopcocks on the holding apparatus. Water from the upper tear-drop funnel will pressurize the gas in the lower cylindrical funnel. Remove gas with a gas tight syringe from the Suba-seal on the cylindrical funnel. When gas is removed from the lower cylindrical funnel, water from the upper tear-drop funnel replaces it. Acetylene gas can be stored up to a week. After gas is removed, remember to replace the water in the upper tear-drop funnel.

APPENDIX VI: Development of an A.*vinelandii* Plasmid-Based Protein Overproduction System

Introduction

In an attempt of overproduce *nif*-specific proteins in *A. vinelandii* a hybrid plasmid system has been devised. This system utilizes the broad-host specific (gram-negative bacteria) plasmid, pKT230 as the plasmid vector. The plasmid construct contains the protein of interest under the control of the *nif*H promoter. This powerful promoter utilizes the *A. vinelandii* transcriptional and translational host regulation machinery to overproduce specific target proteins. The pKT230 vector contains a unique BamHI cloning site located between the genes encoding streptomycin and kanamycin resistance. By digesting pKT230 with BamHI, one is able to insert a particular gene construct with the proper compatible sticky ends. This allows the use of BamHI and BglII for construction of specific gene constructs for insertion into pKT230.

The *nif*H promoter has been isolated from the *A. vinelandii* chromosome using PCR and recombinant DNA technology. The PCR amplified *nif*H promoter has engineered 5' BglII and 3' NdeI ends, and has been cloned into BglII-NdeI digested pT_7-7 vector. The Dean Lab has long been the pioneer in the use of PCR and recombinant DNA technology in the study of the *nif*-specific gene products in. In addition to the *nif*H promoter, over twenty *nif*-specific genes of *A. vinelandii* have been all been cloned, sequenced and amplified. This is a great advantage when considering the design of gene constructs for the in-house overproduction of proteins in *A. vinelandii*. Overproduction of many of the *nif*-specific gene products has been successful utilizing *E. coli* as the host source.

However, some of the more interesting *nif*-specific proteins are unable to be produced in an active form by *E. coli* overproduction. Difficulties arise in terms of protein maturation and synthesis of metalloclusters necessary for protein structure and function. However, by overproducing *nif*-specific proteins in their organism of origin, these obstacles can be overcome.

*Nif*H promoter overproduction of a poly-histidine tagged NifEN complex has been described (Chapter I). Overproduction in this manner was accomplished by altering *the A. vinelandii* chromosome by means of homologous DNA recombination. The advantages of this system place the transcriptional and translational control of NifEN under the control of the *nif*H promoter. Though this system provides a powerful tool in protein overproduction, there are some disadvantages. First, there is only a single chromosomal copy of the overproduction template. In plasmid overproduction systems, 20-50 copies of the overproduction template may be present within the host organism, yielding a possible increase in protein production by 20-50 fold. Second, use of site directed mutagenesis is hindered by the chromosomal derived overproduction system. Though it is possible to use the chromosomal overproduction system for the production of site specifically altered proteins, the complexity of the experiment to transfer and ensure that the proper change has occurred becomes laborious. On the contrary, by use of a plasmid borne overproduction system, one only has to introduce the site specific alteration by means of oligonucleotide directed mutagenesis and sequence the region to ensure the proper change occurred within the plasmid. The plasmid borne system does have a distinct disadvantage associated with it. In order to ensure that homologous DNA recombination does not occur between the host organism chromosome and the plasmid

overproduction system, the region containing chromosomal DNA homologous to the plasmid system must be removed. Recombination between the plasmid and the chromosome would result in the loss of copy number of the plasmid, and hence the strength of this system in the overproduction of target proteins. Though deletion of chromosomal DNA sounds tedious, this techniques is commonly used with in the Dean Lab.

The application of this plasmid overproduction system is of extreme interest in studying the gene products associated with the biosynthesis of the FeMo-cofactor of nitrogenase. The following instructions detail the construction of a plasmid overproduction system for a poly-histidine tagged form of NifEN. The gene construct used for this plasmid construction is the contains the same genetic arrangement as that used to construct the chromosomal poly-histidine tagged NifEN overproduction system (DJ1041; see Chapter I). An additional application of the plasmid overproduction system involves the NifX protein from A. vinelandii. Using this system it will be possible to overproduce NifX (or poly-histidine tagged NifX) in a genetic background deficient for the nitrogenase structural genes as well as the NifEN complex. Data presented in Chapter III of this dissertation shows that NifX has the ability to bind the FeMo-cofactor precursor, NifB-cofactor as well as the FeMo-cofactor itself. Additionally, NifX can bind an FeMo-cofactor precursor that is associated with the NifEN complex. Given this data, it is possible that in the absence of the nitrogenase structural genes and NifEN, NifX could become charged with an FeMo-cofactor precursor, presumably NifB-cofactor. Purification on this form of NifX could be a valuable tool in the understanding of how complex metalloclusters are mobilized, as well as synthesized.

Experimental Methods

Assembly of the NifEN Overproduction Construct. The gene construct with the *nif*H promoter controlling the synthesis of the *nif*E and N genes was constructed in the following manner. Plasmid DNA containing a poly-histidine *nif*E under the control of the *nif*H promoter, pDB867, was digested with BamHI and EcoRI. From this digestion an approximately 3.5 kb fragment of DNA containing the *nif*H promoter and 5' portion of the poly-histidine tagged *nif*E in pT_7-7 was isolated. Next, plasmid DNA containing the region from *nif*Y to orf4, pDB55, was digested with EcoRI and BamHI. A 2.1 kb fragment from this digestion was isolated, containing the 3' region of *nif*E, *nif*N, *nif*X and a portion of orf3. This 2.1 kb fragment from pDB55 was ligated into the EcoRI-BamHI digested pDB867. This ligation mixture was transformed into competent 7118 *E. coli*. Proper gene construct was determined by minipreps and restriction enzyme digests. The resulting plasmid , pDB1072, contained a poly-histidine *nif*E, *nif*N, and *nif*X under the control of the *nif*H promoter in the pT_7-7 vector. Next, pDB1072 was digested with BglII and BamHI, and a ≈ 3.8 kb fragment containing the *nif*H promoter and *nif*ENX was isolated. This fragment was then ligated into BamHI digested pKT230 and transformed into competent TB-1 *E. coli.*. Insertion of the gene construct into pKT230 was identified by restriction enzyme digest. The resulting plasmid was stored as pDB1078.

Construction of the *A. vinelandii* recipient strain. The region of *A. vinelandii* chromosome from the *nif*H promoter to orf3 was deleted by transforming wild-type *A. vinelandii* (TRANS) with pDB1074. This plasmid contains a deletion of the

chromosomal DNA from the 5' region of orf12 to the 3' region of orf3. A rif^r-congression experiment was used to transform wild-type *A. vinelandii* to nif^- with pDB1074 and the resulting strain was stored as DJ1222. Proper antibiotic screens were performed to ensure a double recombination event had occurred. The plasmid pDB1074 was constructed by ligating an approximately 5 kb XhoI-HindIII fragment of pDB37 into the 4.6 kb SalI-HindIII fragment of pDB894.

Conjugation of recipient strain with overproduction plasmid.

1. Competent E. coli strain S17-1 were transformed with pDB1078 and selected on LBK plates. Plates were incubated at 30°C overnight. Prepare FM plates (BN plate media: LB plate media mixed in a 1:1 ratio).
2. Wash a 1/4 loopful of S17-1xpDB1078 cells with 200µl of sterile 1xPO_4 buffer in a sterile 1.5 ml eppendorf tube. Repeat this process three times, aspirating the wash buffer after pelleting the cells in a microfuge.
3. Resuspend the washed S17-1xpDB1078 cells in 50µl of 1xPO_4 buffer. Place 5µl of the resuspended cells in the middle of a FM plate.
4. Take 1/4 loopful of DJ1222 cells (third generation from a BN-Mo plate) and mix into the 5µl droplet of S17-1xpDB1078 cells. Allow mixture to incubate at30° C overnight. Prepare BNK plates. The FM plates allow the growth of both *E.coli* and *A. vinelandii.*
5. Streak out the S17-1xpDB1078-DJ1222 mixture on BNK plates in order to isolate independent colonies. Plates were incubated at 30°C until colonies became apparent.

E.coli does not grow on BN media, therefore bacteria that grow are DJ1222 *A.vinelandii* that have taken up pDB1078 be conjunction.

6. Independent colonies were checked for resistance to kanamycin. The resulting strain was stored as DJ1228.

Results

A 150-L growth of DJ1228 was performed under the selective pressure of kanamycin (20µg/ml) at all points during the growth. The presence of kanamycin is critical, ensuring the presence of the plasmid overproduction system in growing bacteria. DJ1228 was derepressed at 180 Klett (red filter) and allowed to grow for an additional 2.5 hours. Samples were taken at 30 minute intervals from the time of derepression. Samples were analyzed by Western analysis (Appendix IV) and compared to DJ1041 (chromosomal overproduction system) grown in the same manner (except the presence of kanamycin). From this direct comparison (data not shown) it is apparent that the plasmid system (DJ1228) produces more NifEN than does the chromosomal system (DJ1041). Further work is necessary to purify the overproduced NifEN from DJ1228 and see if it is possible to purify larger quantities in comparison with DJ1041.

VITA

Paul Goodwin was born in Kingston, Pennsylvania on the ninth of April in the year nineteen hundred and seventy two. He was raised by his parents, Paul and Geraldine, along with his younger brother, Justin, on a small lake in northeastern Pennsylvania. After graduating from Lake-Lehman High School, Paul attended the Pennsylvania State University. At Penn State, Paul pursued a degree in Biochemistry and graduated with a Bachelor of Science in May of nineteen hundred and ninety four. He then began graduate studies at Virginia Polytechnic and State University in the laboratory of Prof. Dennis Dean. Upon completion of his Doctorate of Philosophy in Biochemistry, Paul intends to pursue a career at Life Technologies, Inc. in Frederick, MD.